WATER DESALINATION USING CARBIDE DERIVED CARBON (CDC)/MIXED MATRIX MEMBRANE

BY

ANWAR UL HAQ KHAN

A Thesis Presented to the
DEANSHIP OF GRADUATE STUDIES

KING FAHD UNIVERSITY OF PETROLEUM & MINERALS

DHAHRAN, SAUDI ARABIA

In Partial Fulfillment of the
Requirements for the Degree of

MASTER OF SCIENCE

In

CHEMICAL ENGINEERING

May 2016

WATER DESALINATION USING CARBIDE DERIVED CARBON (CDC)/MIXED MATRIX MEMBRANE

ANWAR UL HAQ KHAN

CHEMICAL ENGINEERING

May 2016

KING FAHD UNIVERSITY OF PETROLEUM & MINERALS

DHAHRAN- 31261, SAUDI ARABIA

DEANSHIP OF GRADUATE STUDIES

This thesis, written by **Anwar Ul Haq Khan** under the direction his thesis advisor and approved by his thesis committee, has been presented and accepted by the Dean of Graduate Studies, in partial fulfillment of the requirements for the degree of **MASTER OF SCIENCE IN CHEMICAL ENGINEERING.**

Dr. Mohammed Ba-Shammakh
Department Chairman

Dr. Isam Al-Jundi
(Advisor)

Dr. Salam A. Zummo
Dean of Graduate Studies

Dr. Basim Ahmed Ali Abussaud
(Member)

16/5/16
Date

Dr. Abdul-Hadi Abdallah R Al-Juhani
(Member)

To My Beloved Father and Mother

ACKNOWLEDGMENTS

All praise and glory be to Allah for his limitless help and guidance. Peace pleasing of Allah be upon his Prophet Mohammed. Without His consent this task would never have been possible. Love for my dear parents, brothers and sister for encouraging me every moment of my life. I would like to express my profound gratitude and appreciation to my advisor **Dr. Isam Al-Jundi,** committee members **Dr. Basim Ahmed Ali Abussaud** and **Dr. Abdul Hadi Abdallah R Al-juhani** for their guidance and critical help from starting this study till the end. Their encouragement, guidance and invaluable suggestions enabled me to develop an understanding of the subject.I am grateful to King Fahd university of Petroleum and Minerals and Chemical Engineering Department for providing me the good platform, opportunities and well equipped lab facilities for my research.

TABLE OF CONTENTS

LIST OF TABLES

LIST OF FIGURES

LIST OF ABBREVIATIONS

CDC	**:**	**Carbide Derived Carbon**
MMM	**:**	**Mixed Matrix Membrane**
PSF	**:**	**Polysulfone**
PA	**:**	**Polyamide**
RO	**:**	**Reverse Osmosis**
TiC-DC-TFN	**:**	**Titanium Carbide Derived Carbon Thin Film Nanocomposite**
MPD	**:**	**m-Phenylenediamine**
TMC	**:**	**Trimesoyl Chloride**
IP	**:**	**Interfacial Polymerization**
SEM	**:**	**Scanning Electron Microsopy**
TEM	**:**	**Transmission Electron Microsopy**
TGA	**:**	**Thermo Gravimetric Analysis**
AFM	**:**	**Atomic Force Microscopy**
CAM	**:**	**Contact Angle Measurements**

ABSTRACT

Full Name : Anwar Ul Haq Khan

Thesis Title : Water Desalination using Carbide Derived Carbon (CDC) / Mixed Matrix Membrane

Major Field : Chemical Engineering

Date of Degree : April 2016

Improvement of fouling-resistance of reverse osmosis (RO) membranes is still needed in the desalination industry. In this research work, we report the preparation of Carbide derived carbon (CDC)/polyamide mixed matrix membrane for the improvement of anti-fouling property of RO membranes. SEM images of the synthesized CDC nano-particle showed a faceted surface and particle structure with an apparent average size of around 0.1-0.3 µm while the images of the prepared membranes showed a typical ridge and valley structure of aromatic polyamide with obvious nano-particles on the surface. The hydrophilicity of TiC-DC-TFN membrane (M_3) surface was much higher than that of the virgin polyamide (PA) membrane (M_0). Desalination experiments showed that the permeate flux increased 51%, 45% and 38% as compared to the PA membrane under pure water conditions, brackish water conditions and fouling conditions respectively, PA membrane lost 26% of its initial flux while TiC-DC-TFN membrane (M_3) lost only 11% after 2 hours of operation. Membrane cleaning with dilute NaOH solution was able to recover 97% of the original water flux. This study showed that the CDC nanoparticles can significantly enhance the polyamide fouling resistance.

ملخص الرسالة

الاسم الكامل: أنور ماي الحق خان

أطروحة العنوان: تحلية المياه باستخدام الكربون كربيد المشتقة منها (CDC) / مختلط غشاء مصفوفة

كبير الميدان: الهندسة الكيميائية

تاريخ الدرجة العلمية: أبريل 2016

لا تزال تحتاج إلى تحسين من قاذورات المقاومة التناضح العكسي (RO) الأغشية في مجال تحلية المياه. في هذا البحث، ونحن التقرير إعداد كربيد الكربون المشتقة منها (CDC) / مادة البولي أميد مختلطة غشاء مصفوفة لتحسين المضادة للحشف الملكية الأغشية ريال عماني. وأظهرت لقطات SEM من مركز السيطرة على الأمراض نانو الجسيمات المركبة على سطح الأوجه وبنية الجسيمات مع متوسط حجم واضح من جميع أنحاء 0.1-0.3 ميكرون بينما أظهرت صور من الأغشية أعدت سلسلة من التلال وادي هيكل نموذجي من مادة البولي أميد العطرية مع واضحة نانو جزيئات على السطح. كان hydrophilicity من غشاء تك-DC-رقم الملف الضريبي السطحية (M3) أعلى بكثير من مادة البولي أميد البكر (PA) غشاء (M0). وأظهرت التجارب تحلية أن تدفق تتخلل زيادة 51٪، 45٪ و 38٪ بالمقارنة مع غشاء السلطة الفلسطينية تحت ظروف المياه النقية، وظروف المياه المالحة والشروط قاذورات على التوالي، فقد غشاء السلطة الفلسطينية 26٪ من التدفق الأولي بينما تك-DC-رقم الملف الضريبي غشاء (M3) خسر فقط 11٪ بعد 2 ساعة من العملية. كان غشاء تنظيف مع محلول هيدروكسيد الصوديوم المخفف قادرة على استرداد 97٪ من تدفق المياه الأصلي. وأظهرت هذه الدراسة أن الجسيمات النانوية CDC يمكن أن تعزز بشكل كبير من مقاومة مادة البولي أميد قاذورات.

CHAPTER 1

INTRODUCTION

1.1 Background

Water treatment has become quite essential in the era in which we are spending our lives at this time. There are detailed and specific reasons for this particular statement. It is a very obvious fact that due to increase in human activities especially regarding the advancement in technology, the mankind is on a verge to pay its price by consuming pollutants in one way or the other. Water being a very important component of life needs to be consumed in a very pure form or otherwise it will be harmful for human health [1].

If we just break down the earth's water, it can be seen that 96.5 % of all world water consist of oceans, 1 % of the other saline water and only 2.5 % consist of fresh water. This 2.5 % of fresh water is further divided by different portions in which 68.70 % of fresh water consist of ice caps and glaciers, 30.10 % ground water and 1.2 % is accessible surface fresh water. If we further divide this small percentage, we will come to know that 1.2 % of surface fresh water consists of lakes, rivers, surface moistures and water vapors etc [1]. A bar chart (Figure 1.1) shows a summarize description about world's water distribution in which we can realize that how much small quantity of actual fresh water exist.

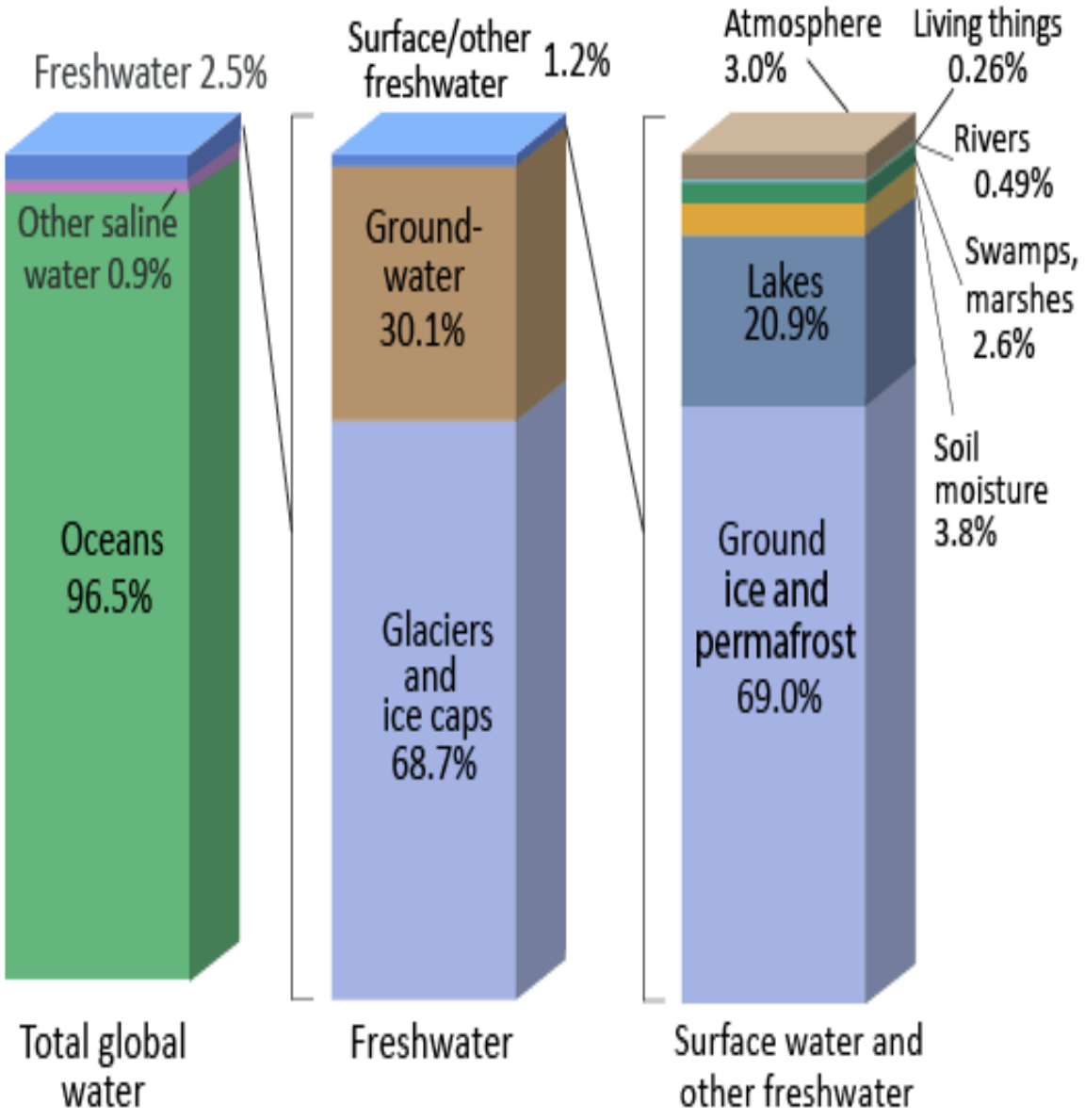

Figure 1.1 Distribution of the World's fresh water resources [1]

1.2 Significance of Study

Among 1.2 % of the earth fresh water, various activities including industrial, agricultural, municipal, etc, render water as polluted by addition of various materials that need not to be present in it specially the drinking water which has to become part of the human body

in some way. The problem is that we cannot really imagine our lives with the benefits of the above mentioned sectors as well and this is where we come across a very common phrase that to achieve something you might have to lose another[2].

Over 1 billion human beings in the world do not have access to safe water, that is, one in six people. According to United Nations, the usage of water has increased more than double the rate of population in last century. By 2025, the demand of fresh water will increase by 2/3 and 1.8 billion people will be living in such areas/countries with completely water scarcity. It is also predicted that water extraction will be enhanced by 50 % in the emergent nations and 18 % in developed nations [3], [4].

To get rid of this problem, people are moving to utilize the 96.5 % of ocean water after removing the desired salts which is known as desalination process. Depending on the type and form of energy used, desalination process can be classified into two types[5]

1. Thermal desalination
2. Membranes desalination

Thermal desalination process can be defined as the process in which heat energy is required to remove the desired salts from the saline water. The thermal desalination process consists of multi stage flash desalination (MSF), multi effect distillation (MED) as well as mechanical vapor compression (MVC). There are some other lab scale desalination processes like solar stills, humidification dehumidification and freezing etc. Thermal desalination process is more energy consuming process when compared to reverse osmosis process[5]. Reverse osmosis technique has gained more attention than all others membrane based techniques due to most energy efficient technique to date and RO

technology for desalination process is very common in world wide. Reverse osmosis is one of the best desalination technique which required low energy about 3 to 10 kWh /m^3 of fresh water from saline water [6], [7].

A membrane is a special separation technique which allows the passage of some desired constituents and retains the unwanted constituents in the process liquid. The liquid influencing the membranes is known as feed stream, the liquid that passes through the membranes is called as permeate and the liquid which cannot pass through the membrane and consist of retained constitutes is known as retentate/concentrate [8]. A basic membranes separation process is shown in Figure 1.2.

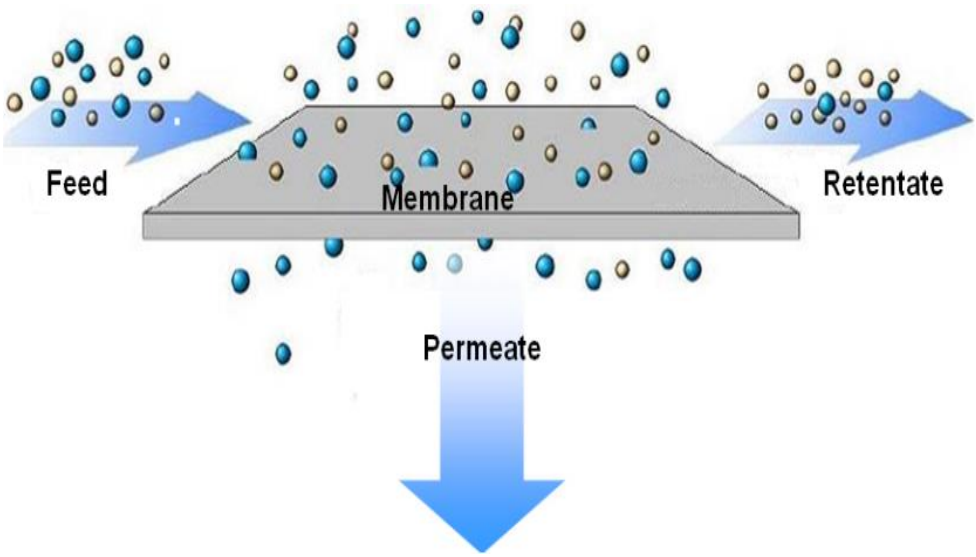

Figure 1.2 Basic separation process in membranes [9]

1.3 Problem Statement

Water desalination by using reverse osmosis membranes has been used widely to obtain pure and high quality water. Polyamide thin film composite RO membranes provide high water permeability and high salt rejection. There is a big problem while using these RO

membranes which decreases the water permeability after some time due adsorption and accumulation of organic/inorganic particles onto the membrane surface and/or within the pores of membrane which is known as membrane fouling. This fouling phenomena reduced the water flux and also salt rejection [10]. Roughly idea about different types of foulant and their adsorption style on the membranes surface is shown in Figure 1.3.

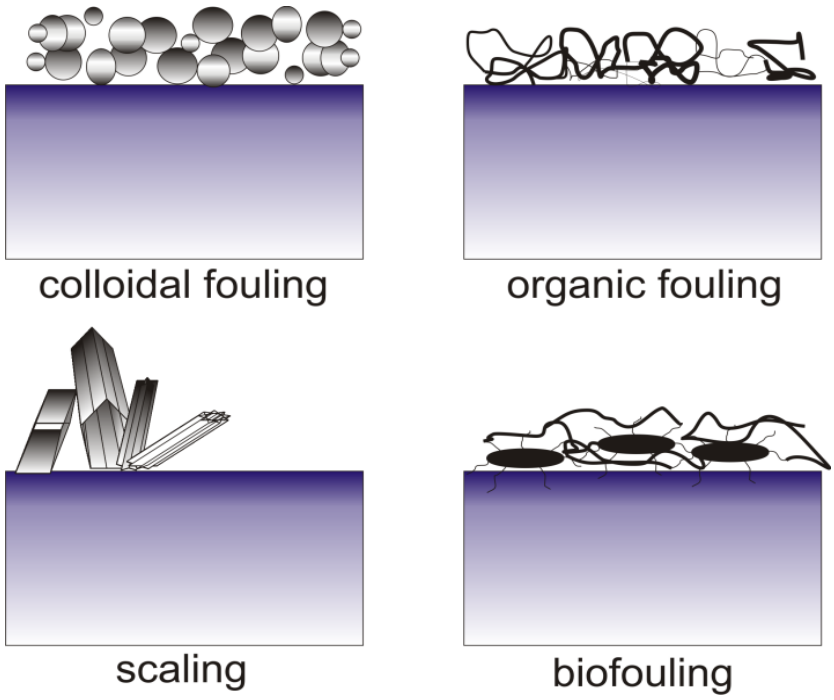

Figure 1.3 Types of foulants and their adsorption style [10]

To diminish the fouling and to enhance the water flux rate, surface modifications and nanoparticles incorporations showed an effective strategy. During the nano particles incorporations, the most important factor is cost effectiveness and environmental friendly properties. For example, the application of graphene and carbon nanotubes showed great importance in desalination process but due to high cost and unpredictability in environmental security, their applications might be limited. However, nano particles having reasonable cost and environmental friendly applications will be considered in further development of TFC RO membranes [11].

1.4 Research Objectives

The main objectives of this project is to prepare a new carbide derived carbons (CDC) / Polymer thin film nanocomposite membrane for water desalination which can

- Offer high water flux
- Improve control of selectivity
- Enhance fouling resistance

To accomplish the above discussed three points, the following steps are performed successfully

- Synthesis of the carbide derived carbons (CDCs) nanoparticles.
- Incorporation of the nanoparticles into the polymeric membrane by interfacial polymerization.
- Testing the membrane in bench scale setup to evaluate the flux, rejection and fouling.

CHAPTER 2

LITERATURE REVIEW

2.1 Introduction and History of Reverse Osmosis Membranes

Studies about the membranes phenomena can be ferret out from the scientists of 18th century. For instant, in 1748, Abbe Nolet originate the word 'osmosis' to explain water permeation through a diaphragm. There were no industrial and commercial usage of membranes through 19^{th} and early 20^{th} centuries except as laboratory tools to flourish chemical and physical theories. For instant, the membranes were used to calculate the osmotic pressure of solutions by Pfeffer and Traube in 1887 to expand the law known as limit law which describes the nature of dilute ideal solution which lead to develop van't Hoff equation [12]. A general idea about the perfectly selective semi-permeable membrane was employed by Maxwell and coworkers for the development of kinetic theory for gases[12].

Bechhold technique was improved further by Elford, Zsigmondy and Bachmann and Ferry [13] and in early 1930s the micro porous membranes were available commercially. From 1940 to 1960, the technology was spread to other polymers like cellulose acetate and at the end of Second World War, the applications of membranes were found in testing of drinking water. In early 1960, the defect free, high flux anisotropic RO membranes were developed in laboratory [14]. A notable change was seen in the development of membranes technology from 1960 to 1980[15].

Membranes can be classified according to the thin perm-selective layer: porous or dense, or according to the type of material the membrane film is made from (inorganic, organic, polymeric, metallic, etc.). Membranes are also classified according to their structure: symmetric or asymmetric. The symmetric membranes have a uniform structure and the necessary mechanical strength to withstand high pressure. However, the perm-selective thin layer sometimes cannot be self-supporting. Hence, the membrane selective layer is deposited on a support that provides the necessary mechanical stability while having negligible mass transfer resistance [12] as shown in Figure 2.1.

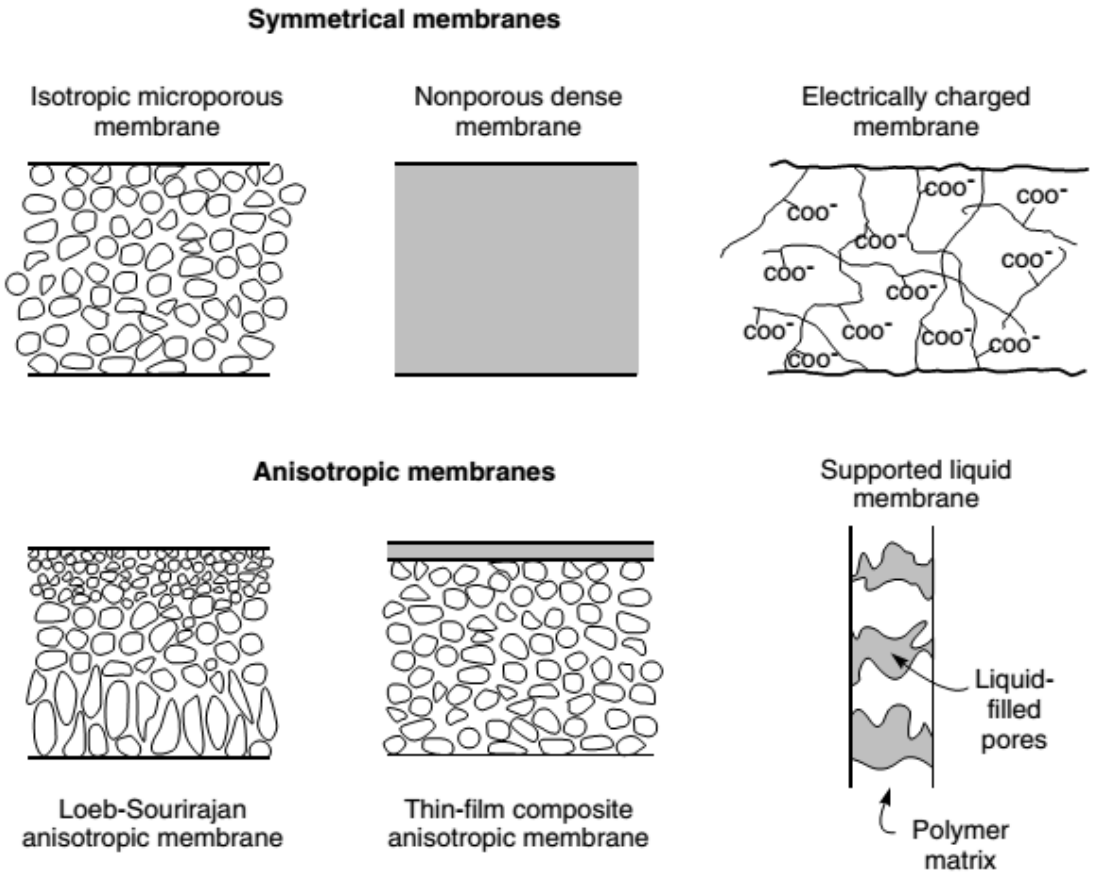

Figure 2.1 Basic types of membranes [12]

Today, reverse osmosis (RO) is an advanced technology for desalination process and it has left behind conventional thermal multi – stage flash (MSF) technology [16].

Reverse osmosis is water desalting process in which external pressure is applied, which is higher than the natural osmotic pressure, to the semipermeable membrane containing higher contaminant concentration to pushing the water to travel from the membrane from higher TDS chamber to lower one. For the first time in history, Pfeffer, Traube and other coworkers studied about this phenomena in 1850s. In 1931, this desalination method was introduced with a term known as reverse osmosis process [17]. A simple and basic working phenomena about reverse osmosis membranes is shown in Figure 2.2.

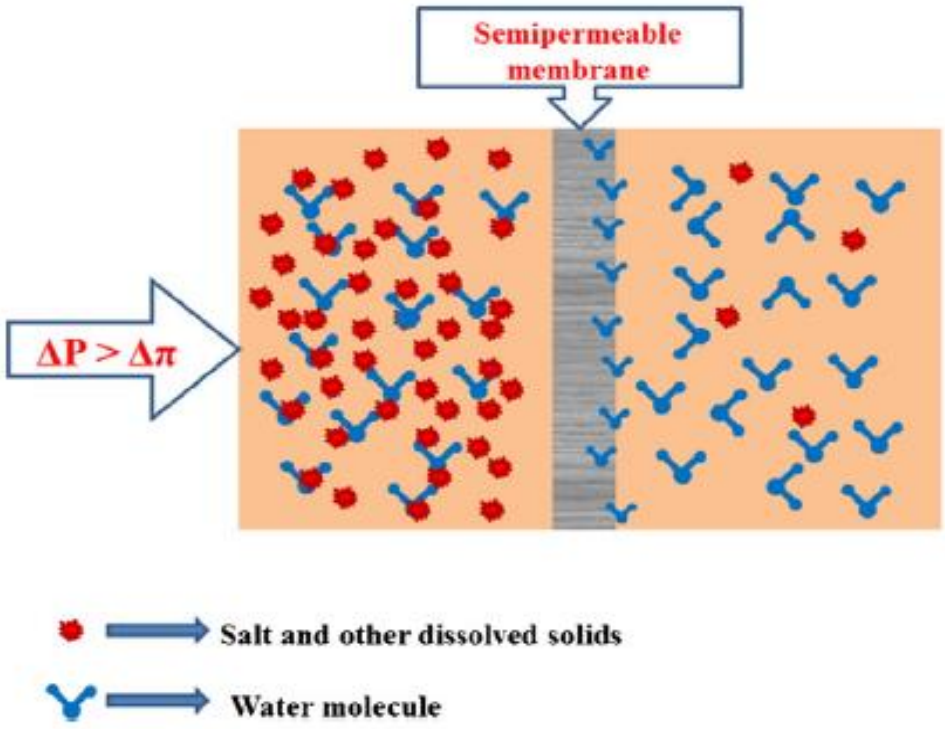

Figure 2.2 Basic concept about RO membrane working phenomena [16]

In 1959, Scientists developed cellulose acetate films having thickness 5-20 µm for desalting saline water by applying high pressure (1000 psi) to get 98 % salt rejection by scarifying the water flux [18]. From 1960 to mid of 1970s, the cellulose acetate membranes were became standard in industries for desalination process with good salt rejection but low water flux in permeate so it means people were consuming high energy.

Cadotte developed interfacial polymerization method to form composite membranes to give high salt rejection with good permeate water flux. Later on, Cadotte developed a fully aromatic interfacial composite membranes by using phenylene diamine (MPD)and trimesoyl chloride (TMC) as a basic reactants [19].

At the present time, about 1billion gal/day of water are desalted by using RO process. RO plants are equipped in the japan, Europe and USA for pure water production for industries usage. Large quantity of RO plants are also equipped in desert region like Middle East for the production of pure water. Nowadays, interfacial polymerization membranes are produced in different required shapes like flat sheet, spiral wound module form etc. Here below a charge is shown (Figure 2.3), describing the milestones in the developed of Reverse Osmosis membrane [12].

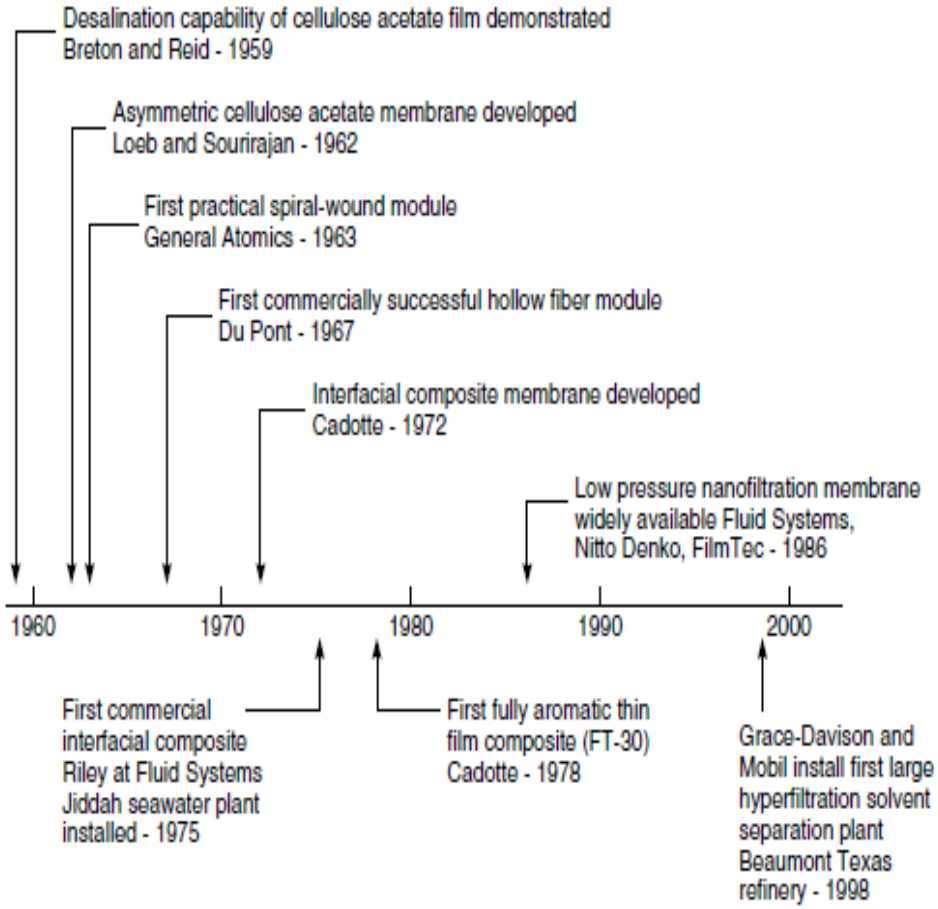

Figure 2.3 Milestones in the development of RO membranes [12]

2.2 A Brief Theoretical Background

Reverse osmosis membranes works on the principle of solution diffusion transport mechanism. There is strong link between water flux j_w and applied pressure on membrane surface and concentration gradient across the membrane. This mechanism is described by equation.

$$j_w = A(\Delta p - \Delta\pi) \qquad (2.1)$$

Where

j_w is water flux.

A is constant (water permeance, LMH/bar).

Δp is pressure difference across the membrane.

$\Delta \pi$ is osmotic pressure differential across the membrane.

According to this mathematical equation, it shows that when $\Delta p < \Delta \pi$, it means water direction is from dilute to concentrated side of the membrane due to osmosis phenomena. If the applied pressure and osmotic pressure are equal to each other ($\Delta p = \Delta \pi$) there is no flow across the membrane surface and known as osmotic equilibrium and when ($\Delta p > \Delta \pi$) it means fluid direction is from concentrated to dilute solution side which is known as reverse osmosis [12]. All these conditions are shown in Figure 2.4.

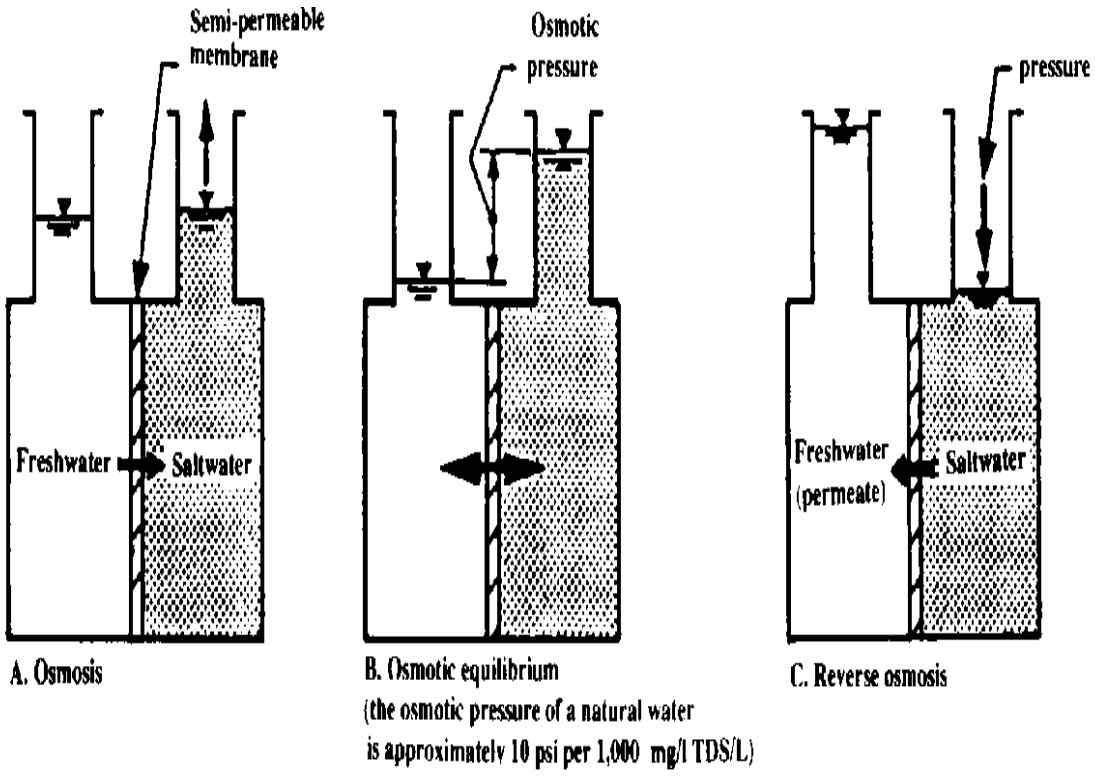

Figure 2.4 Reverse osmosis operating principles [20]

2.3 Reverse Osmosis Membranes: Developments and Challenges

Polyamide thin film composite membranes are very successful RO membranes in water desalination process because of their high salt rejection and high flux. The PA selective layer, approximately 200 nm thickness, is manufactured at the top of a porous support name as polysulfone by using interfacial polymerization method. However, there are some disadvantages in these membranes [21].

- Low resistance to fouling
- Low resistance to chlorine or hypochlorite disinfectants
- Low chemical and thermal resistance of the polysulfone support [21].

Inorganic membranes are becoming competitors to the polymeric membranes because of their higher resistance to attacks by chemicals and their excellent mechanical properties and their high tolerance to harsh environments [22]. While there are many advantages for inorganic membranes, some disadvantages are very critical and serious enough to prohibit industrial applications such as: high cost, brittleness and sealing problems [23] and it is difficult to prepare defect free large areas.

To improve the performance of RO TFC membranes, researchers are merging the porous inorganic materials in the polyamide layer in interfacial polymerization reaction [21].

To eliminate the problem, researcher developed a hybrid (organic- inorganic) membranes to modify the transport properties of membranes and take the advantages of both types of materials. This hybrid asymmetric membrane is called Thin Film Nano-composites (TFN) membrane in which the top selective layer contains a dispersed nano-filler in the polymeric matrix [24] as shown in Figure 2.5.

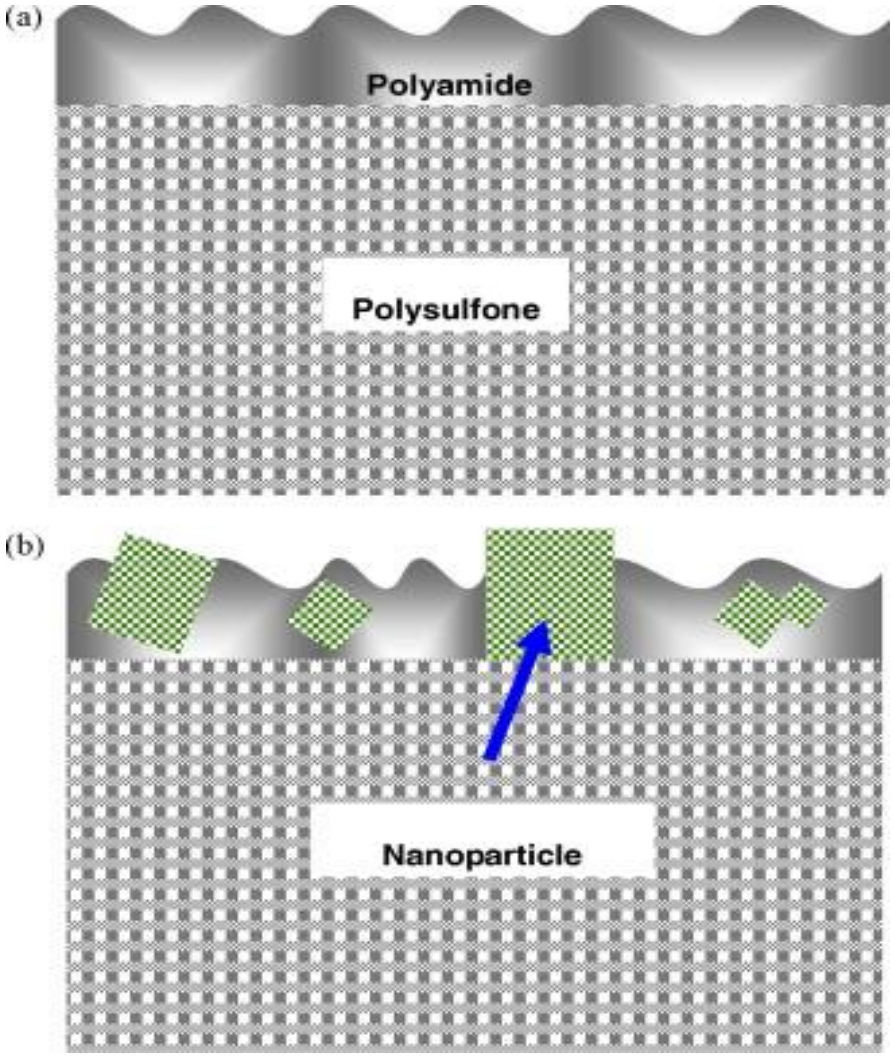

Figure 2.5 Schematic diagram of the thin film nano-composite membrane [24]

Mixed matrix membranes, also recognize as thin film composite membranes improved the characteristics of host polymer matrix by taking benefit of the characteristics offered by inorganic fillers added to them. The common adjustment relation between permeability and selectivity can be addressed by such organic-inorganic hybrid systems. The united link between the host and guest help in improving selectivity, permeability, thermal and chemical stability in addition to fouling resistance of the composites. Inorganic fillers as a host particles have been analyzed for this purpose that consist of zeolites, silica, carbon nano tubes, silver, alumina, TiO2 nanoparticles, etc [24]–[28].

Following are different methods for the preparation of thin film nanocomposite membranes (TFN):

a) Dispersion of nano particles in MPD solution during interfacial polymerization reaction.
b) Dispersion of nano particles in organic solution of TMC during crosslinking process.
c) Deposition on the surface after formation of PA film by dipping the TFC membrane in the colloidal solution of nanoparticles.

But mostly second method is more famous for interfacial polymerization reaction. Many studies on the performance of TFN membrane confirmed that they show better performance as compared to TFC [22], [29]–[31]. To check the performance and effect of nanoparticles on the TFN membranes characteristics, different studies has been done. Nanoparticles have great ability to change the membranes performance. Addition of inorganic nanoparticles have great ability to enhance the flux permeation of polymeric membrane by modifying the membrane surface properties [25]. A significant improvement was seen in flux permeation, water contact angle and surface roughness by addition of nano zeolite sand silicates in thin film composite membrane [30], [32].

Lind et al, inspected the impact of size of zeolite crystal on the properties of TFN membrane [33]. As per their results, the addition of nano zeolites built more permeable and negatively charged thicker membranes [34]. Symbolic improvement in pure water flux (29.76 LMH) without rejection loss has been associated to preferential flow channels provided by zeolite pores for water (2.7 Å). These pores are large enough to allow

passage of water molecules but are too small for solute carriage (8–9 Å). [30], [35]. Confinement of silver nanoparticles (Ag-np) onto the surface of polyamide TFC membrane is shown in Figure 2.6, which describe the whole mechanism from PSF support to addition of nanoparticles [36].

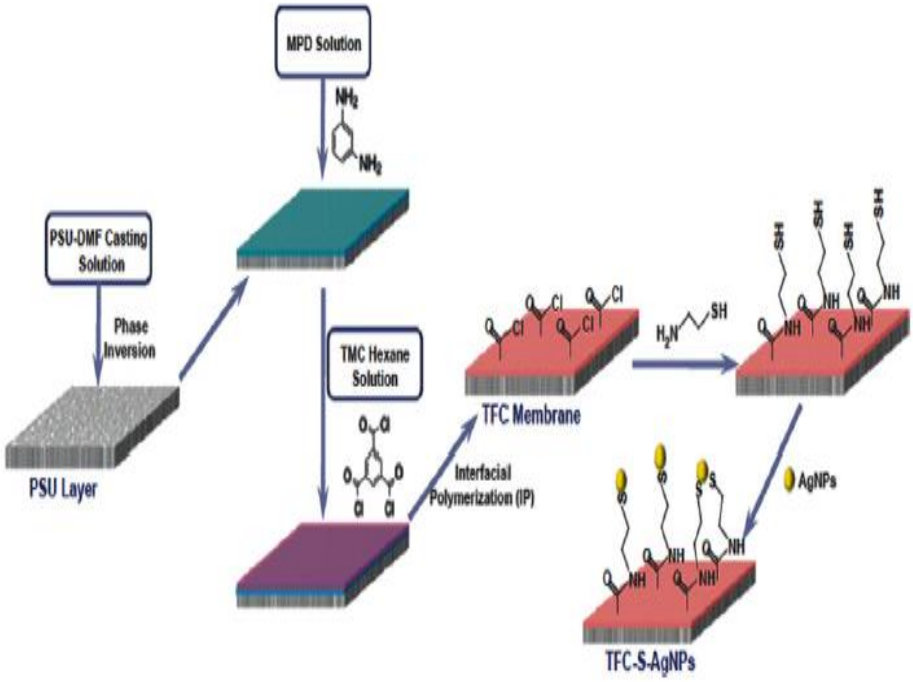

Figure 2.6 Schematic diagram of attachment of Agnps onto thin film composite membrane [36]

Kim, et al prepared polyamide TFN membrane by using hydrophilized ordered meso carbon (H-OMC) particles by interfacial polymerization method and results showed that by addition of 5 % H-OMCs loading, the membrane wettability, surface hydrophilicity and flux permeability were enhanced. It was noted that by increasing nanoparticles loading, BSA adsorption was decreased. This might be due to enhancement in membrane hydrophilicity [37]. A schematic diagram related to preparation and incorporation of H-OMCs is shown in Figure 2.7 and Figure 2.8.

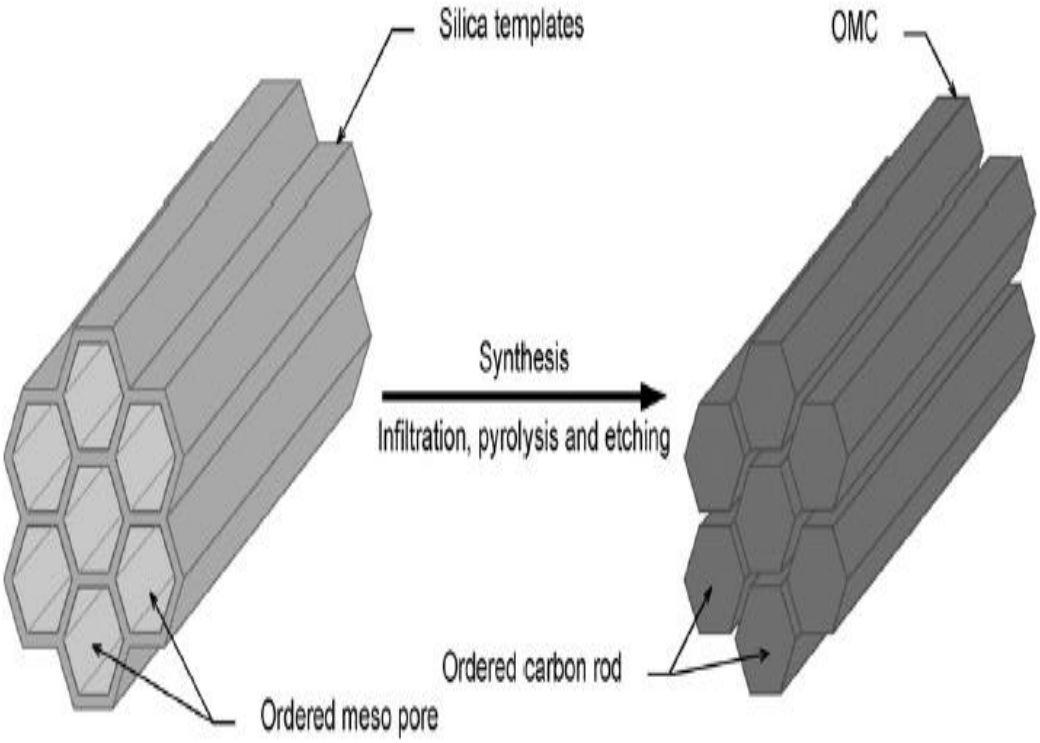

Figure 2.7 Preparation of H-OMCs from silica template [37]

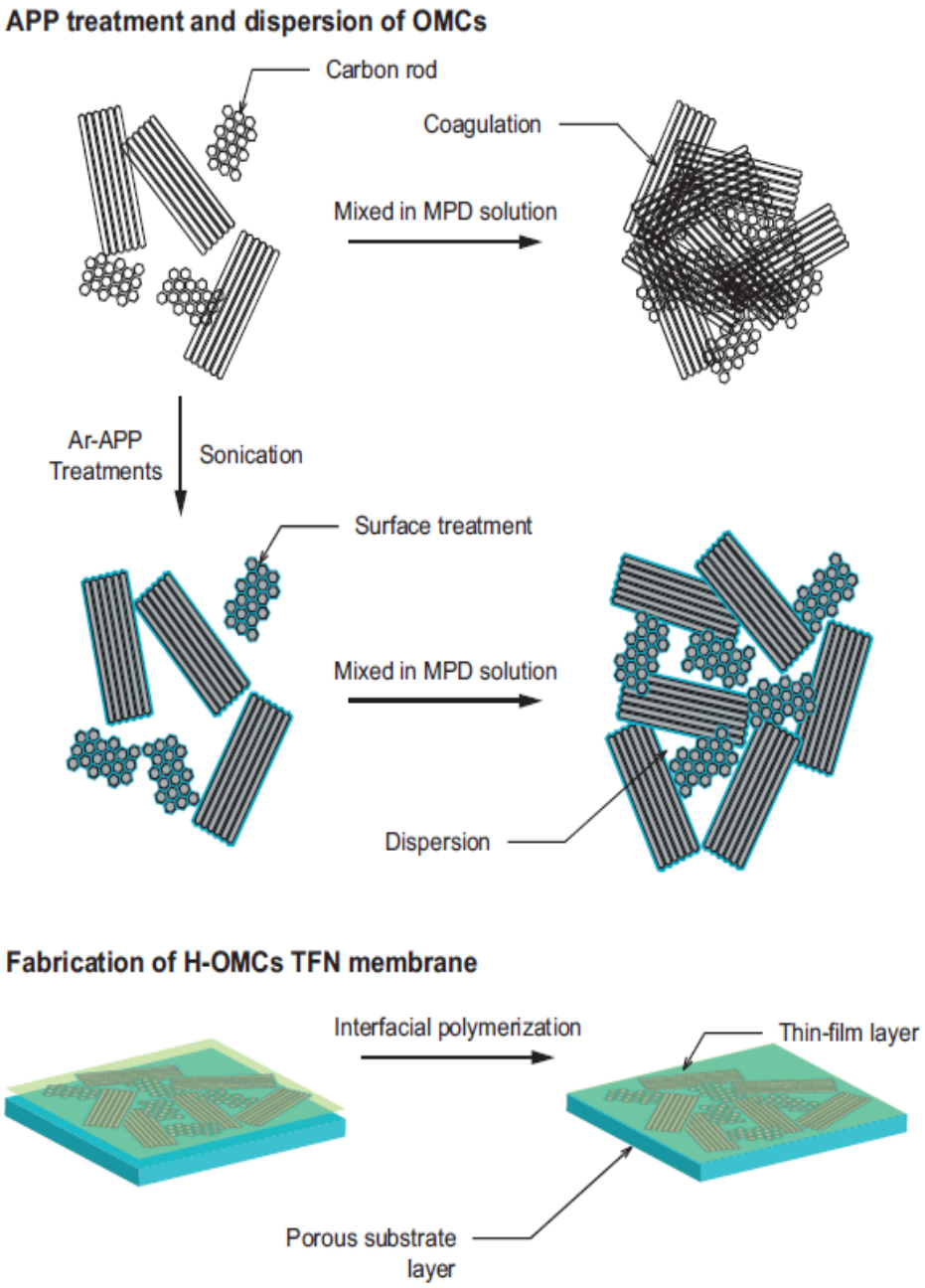

Figure 2.8 OMCs plus atmospheric pressure plasma (APP) treatment and TFN preparation using OMCs [37]

This membrane exhibiting controlled and improved performance with respect to water permeability and BSA adsorption. This displayed the effect of ordered structure in generating active pores for water permeation through the PA layer.

Monodispersed spherical mesoporous nanosilica PA thin film composite RO membranes were manufactured using IP technique. It was noted that the water flux was increased from 19 L/h.m^2 to 53 L/h.m^2 by increasing silica amount and solute rejection also increased by 96 %. So, we can conclude that such type of RO membranes can enhance the water flux in composite RO membranes [38]. Nanosilica loading and its effect on surface properties of TFC RO membranes is shown Figure 2.9.

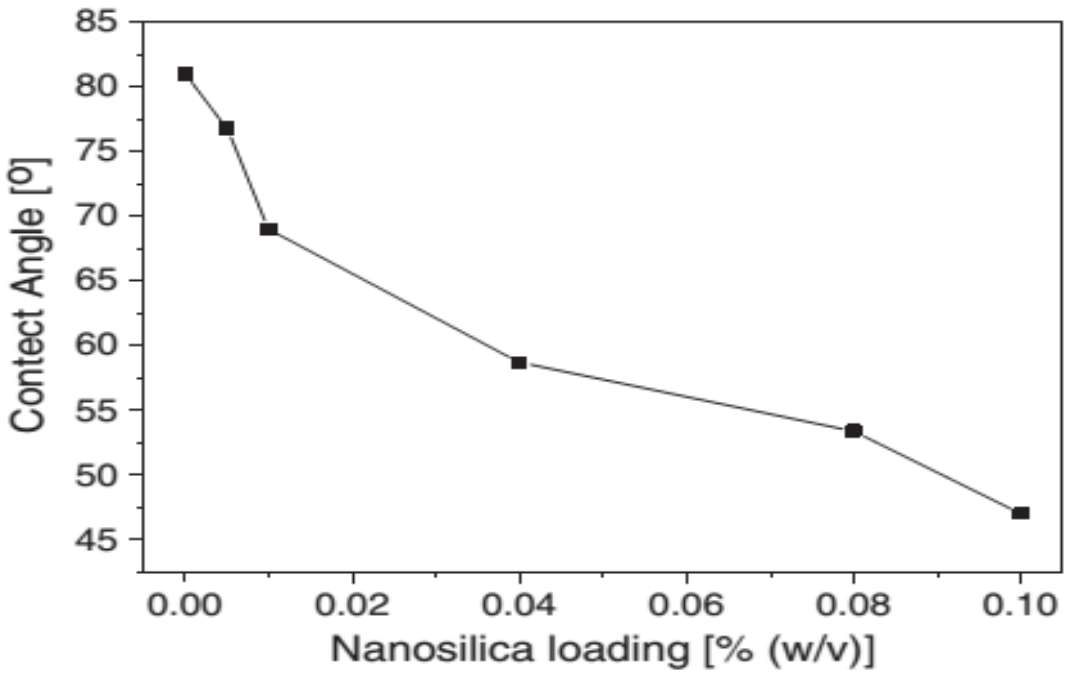

Figure 2.9 Nanosilica loading and its effect on surface properties of TFC RO membranes [38]

Wu et al functionalized mesoporous silica nanoparticles (mMSN) with amine groups using 3 aminopropyltriethoxysilane. The flux of modified membranes increased by an order of 1.5 to that of TFC membrane. The increased interaction between the functional groups and polymer matrix improved the water transport. Na_2SO_4 rejection was more than 80%. Addition of mMSN also enhanced the antifouling ability and long term stability of the membrane [39]. Figure 2.10 exhibiting the phenomena for mMSN preparation.

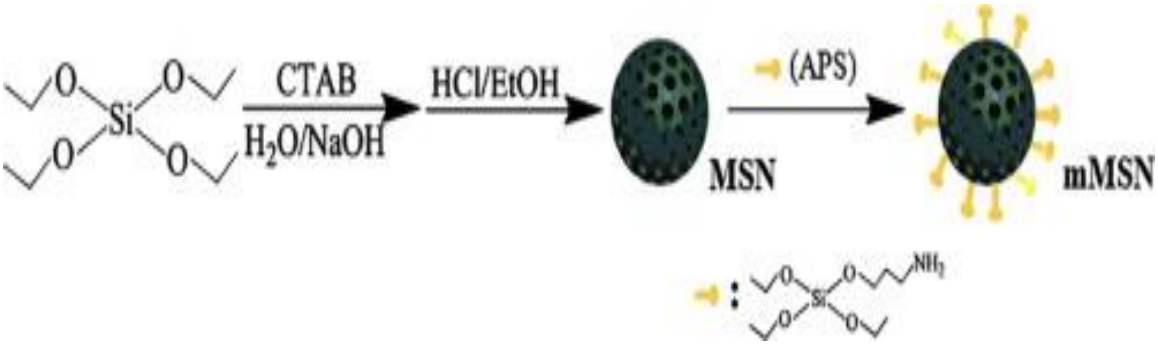

Figure 2.10 Schematic preparation of mesoporous silica nanoparticles (mMSN) [39]

In a very recent work, commercial RO membrane was modified with silver (Ag) nanofillers laminated with polyethyleneimine (Ag-PEI) and polyacrylic acid along with polyelectrolyte layer by layer (LBL) self-assembly as shown in Figure 2.11. Surface modification resulted in significant reduction of irreversible bacterial cell (Escherichia coli bacteria). Irreversible binding of silver nanoparticles to the membrane surface was achieved by the contraction of silver (Ag) salt with a reducing agent at the surface of the membrane. Except for slight reduction in water permeability (up to 17%), rest of the membrane properties remained unchanged. Addition of the nanoparticles imparted a very strong antibacterial property to the membrane. Use of silver nanoparticles for commercialization is still a matter of research due to severe leaching problem. Use of nanoparticles should be carefully considered due to their potential toxicity [40].

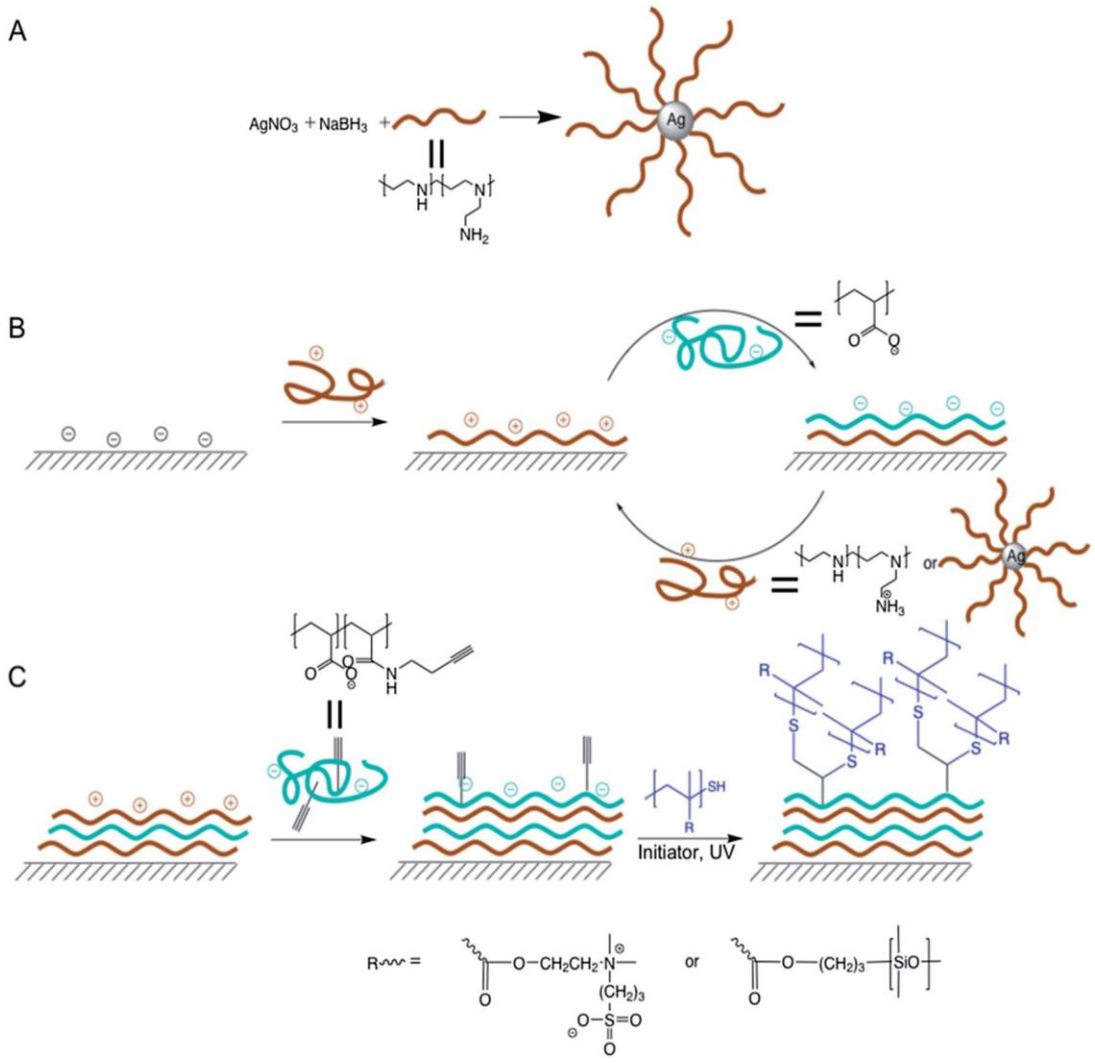

Figure 2.11 Preparation scheme for membrane modification, a) preparation of PEI coated agNPs, b) formation of LBL film,c) Grafting of the polymer brushes [40]

A new aromatic polyamide thin film nanocomposite RO (Nanofiltration) membrane was manufactured by incorporation of aminosilanized TiO_2 nanoparticles. The permeation and selectivity was improved by these generated membranes. The thermal stability of TFC membranes was also improved significantly by incorporation of TiO_2 nanoparticles as compared to TFC membranes. The salt rejection and water flux was also improved [41].

Titanate nanotubes (TNTs) and amin functionalized were used to manufacture titanate nanotubes (NH2- TNTs) for the fabrication of thin film nano composite reverse osmosis membranes. However, in these developed RO membranes, the water flux was increased from 19.11 L/m^2.h of thin film composite (TFC, control membrane) to 36.74 L/m^2.h using thin film nano-composite (TFN 0.05) and meanwhile the salt rejection increased from 94.05% to 96.53% just upon addition of 0.05% NH2-TNTs into the polyamide layer. Water flux was increased and alleviated the fouling rate by using TFN0.05 membranes [42].

It was noted that the membrane selectivity, membrane potential and membrane water contents were improved initially by employing nanoparticles of zeolite upto 8 wt% in casting solution and this trend start decreasing by more addition of additives concentration from 8 –16 wt%. However, membranes electrical conductivity and ionic flux was increased by using zeolite nanoparticles in casting solution. Electrochemical properties were also increased in modified membranes containing 8 wt% of zeolite nanoparticles as compare to other modified membranes [43].

The effect of diameter of carbon nano tubes (CNTs) and concentration on the characteristics and performance of mixed matrix membranes were noted. It was noted that the incorporation of CNTs on MMMs, the salt rejection and water flux was higher as compared to polyethersulfon (PES) membranes. Filtration performances were better than those MMMs planted with thinner CNTs (CNT1) rather than those planted with thicker CNTs (CNT2). Introduction of CNTs especially CNTs with 0.1 wt % concentration increased both water flux and salt rejection. Pure water flux of polyethersulfon/CNT1 membrane was approximately 60% higher than those of pristine PES membranes.

PES/CNT2 membranes with 0.1 wt% of CNT concentration, could offer maximum water flux of 38.91 $L/m^2.h$ and 87.25% of Na_2SO_4 rejection at 4 bar pressure. Filtration performance was reduced by high loading of CNTs [44].

In spite of the great performance of the TFN membranes relative to that of the asymmetric membranes in water desalination, the search for new materials with better performance that will enhance the properties of the selective layer still remains a high-priority research area over the years. Table 2.1 representing the membranes support with different type of incorporated nano particles, their operating conditions and outcomes.

Table 2.1 Membranes support with different nanoparticles, operating conditions and outcomes

Materials	Operating Conditions	Results/ Outcomes	References
Polysulfone support,0.1% MWCNT/PA polymer	Trans membrane pressure(TMP) (16 bar), Temperature (25 ^{0}C), Aquous NaCl solution(2000ppm), pH 7	Water flux = 28.05 LMH, Salt rejection > 90%, Cross flow configuration	[45]
Polysulfone support, 15 mg MW-CNT/g PA	TMP (3.9 MPa), Temperature (20 ^{0}C), aquous NaCl solution (4000 ppm)	0.71 LMH bar specific water, salt rejection 76%	[46]
0.1% MW-CNT as nanofiller in polyamide polymer	TMP (1.6 bar), Temperature (25 ^{0}C), NaCl salt solution (2000 ppm), terethalic acid (PTA) solution (2000 ppm) with pH 9	Pure water flux 71 LMH (NaCl solution), terephthalic acid (PTA) Rejection 98%	[47]
PES/0.5–4% MW-CNT	TMP was kept constant at 0.35 MPa (50 bar), Temperature	Cross flow setup was used.Fouling test with yeongsan river water,	[48]

	(21-23 ^{0}C)	95% water flux recovery after membrane cleaning. Upto 50% rejection of natural organic matters (NOM)	
Polyethersulfone support/ 0.045 % MW-CNTs	TMP (4bar), temperature 25 ± 1 ^{0}C, salt conc 2000 ppm for NaCl,$MgSO_4$, Na2SO_4 each, pH (7.0 ± 0.1)	Dear End filtration setup was used. Membrane effective area = 19.6 cm^2, pure water flux = 23.7 LMH, Na_2SO_4 rejection = 65%, $MgSO_4$ rejection = 45%, NaCl rejection = 20%, total 100% salt rejection	[49]
NaX nano-zeolite used as nanoparticles in interfacial polymerization reaction(PA)	TMP (12 bar) Temperature (25 ^{0}C), 2000 ppm of NaCl and $MgSO_4$ solution was used.	Pure water flux = 29.76 LMH	[30]
Polysulfone support was used with UF/specific zeolite 4A	TMP (0.1 MPa), Temperature (25 ^{0}C), bovine serum albumin (BSA) = 1000 mg/L and pepsin aqueous solutions	Pure water flux = 500 LMH, 97.0% BSA and 88.6% pepsin rejections	[50]
Polysulfone support was used. NaA zeolite nanoparticles used by interfacial polymerization/PA	TMP (1.24 MPa), Temperature (20 ^{0}C), Effective membrane area = 13.85 cm^2, 2000 ppm aqueous solution of PEG, 2000 ppm aqueous solutions of NaCl and $MgSO_4$.	Pure water flux = 3.8 ± 0.3 × 10^{-12} $mPa^{-1}.s^{-1}$, NaCl rejection = 93.9 ± 0.3	[24]

To the best of our knowledge, for the first time microporous carbide derived carbons (CDCs) nano carbon materials are used as nanofiller in TFN membranes for water desalination experiments. The microporous carbon nanoparticles prepared by chlorination of metal carbides at higher temperature (200-1200^{0}C) are known as Carbide – derived carbons (CDCs) [51].

Carbide derived carbon is a good candidate for the surface modification of the polyamide thin film composite RO membrane due to its tunable nano porous carbons which can be derived from metal carbides such as (SiC, TiC, Ti_2ALC, B_4C, Ti_3SiC_2, ZrC, WC, MO_2C, Fe_3C etc.) by selective removal of metal atoms using a halogen gas (chlorine gas) at high temperature (200^{0}C–1200^{0}C). This method provides highly porous carbon materials having good mechanical properties with good control over particle morphology [51] as shown in Figure 2.12.

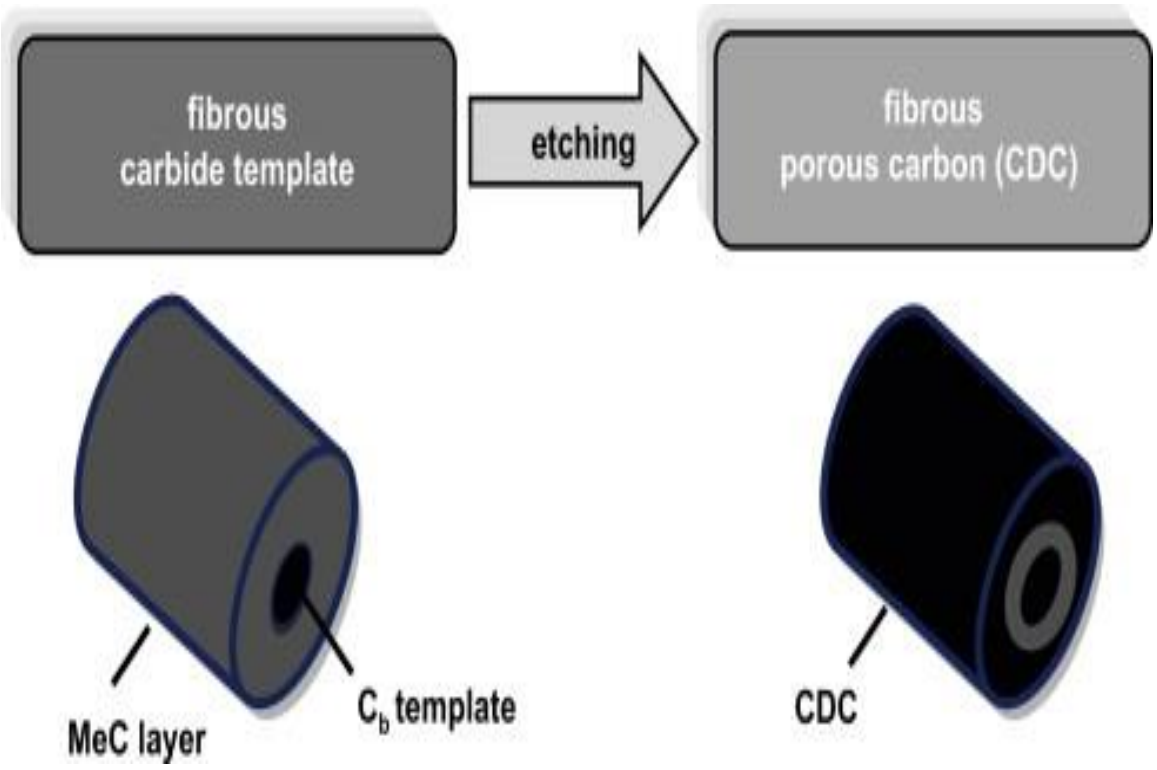

Figure 2.12 Schematic diagram of CDC processing by chlorination process [51]

Generally, the metal carbide reaction with chlorine to produce CDC can be written as [51].

$$M_eC + \frac{x}{2}Cl_2 \quad \rightarrow \quad M_eCl_x + C \qquad (2.\ 2)$$

Where M_e is metal.

In this reaction, the chlorine gas can be replaced by other halogens or their compounds. CDCs can also be formed by hydrothermal leaching and reaction of certain metal carbides with inorganic salts [52]. However, the halogenation method will produce highly porous carbon materials with good mechanical properties [53] as shown in Figure 2.13.

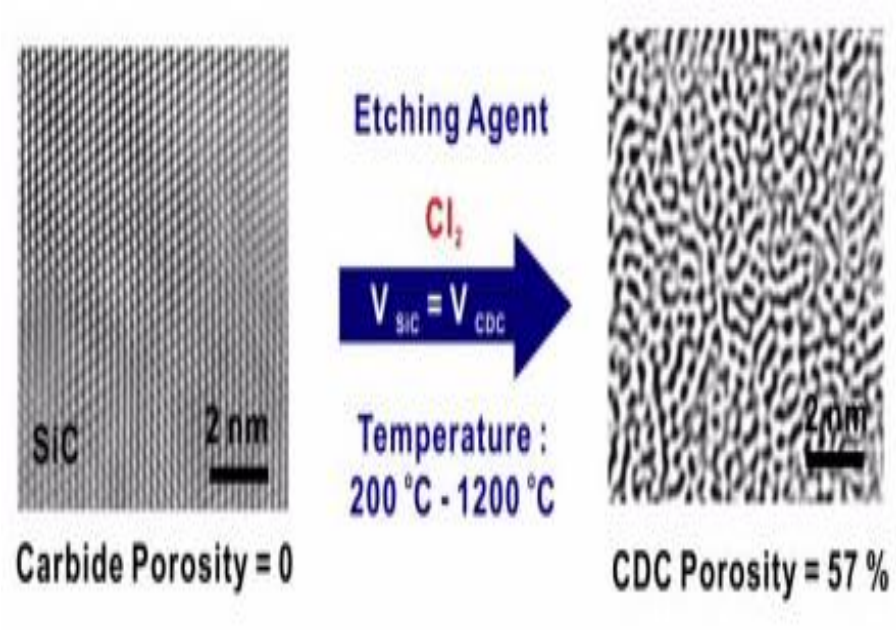

Figure 2.13 TEM micrographs of SiC halogenation to porous CDC [53]

The ordering in structure of CDC from amorphous to crystalline depends on chlorination temperature from lower to maximum temperature. At 600^0C, largely CDC shows amorphous nature, at 800^0C short range ordered structure and at 1200^0C long range ordered structure [54]. Figure 2.14 represents different type of structures from lower to higher temperature for TiC-CDC and ZrC-CDC.

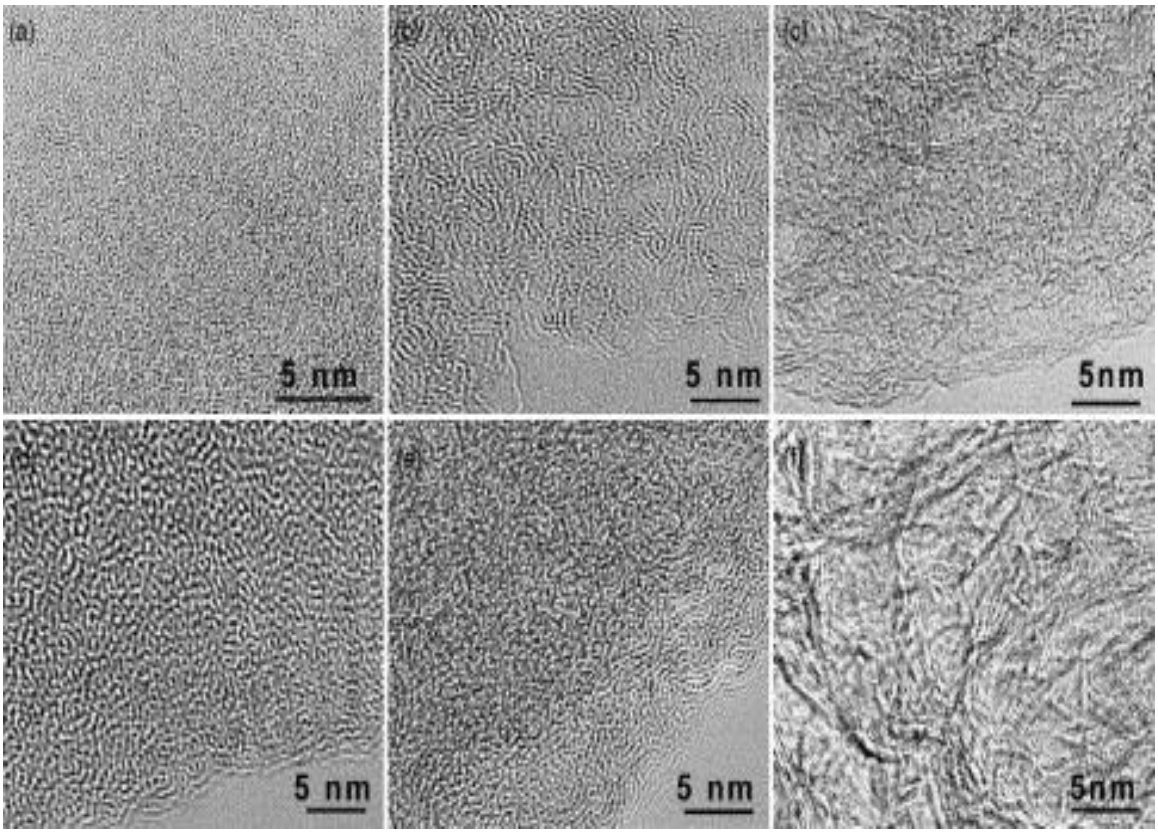

Figure 2.14 TEM images of TiC- DC prepared at (a) 600 °C, (b) 800 °C, (c) 1200 °C and ZrC- DC at (d) 600 °C, (e) 800 °C, (f) 1200 °C [54]

It allows a good control over properties such as pore size (0.5–3nm [55]), pore shape, surface chemistry, and surface area per unit mass (up to 3000m^2/g [55]) by changing the operating conditions, composition and structure of the carbide precursor [56]. For instance, pore size distribution of CDC of titanium carbide ,silicon carbide, Zirconium carbide and boron carbide at distinct temperature [57] is shown in Figure 2.15.

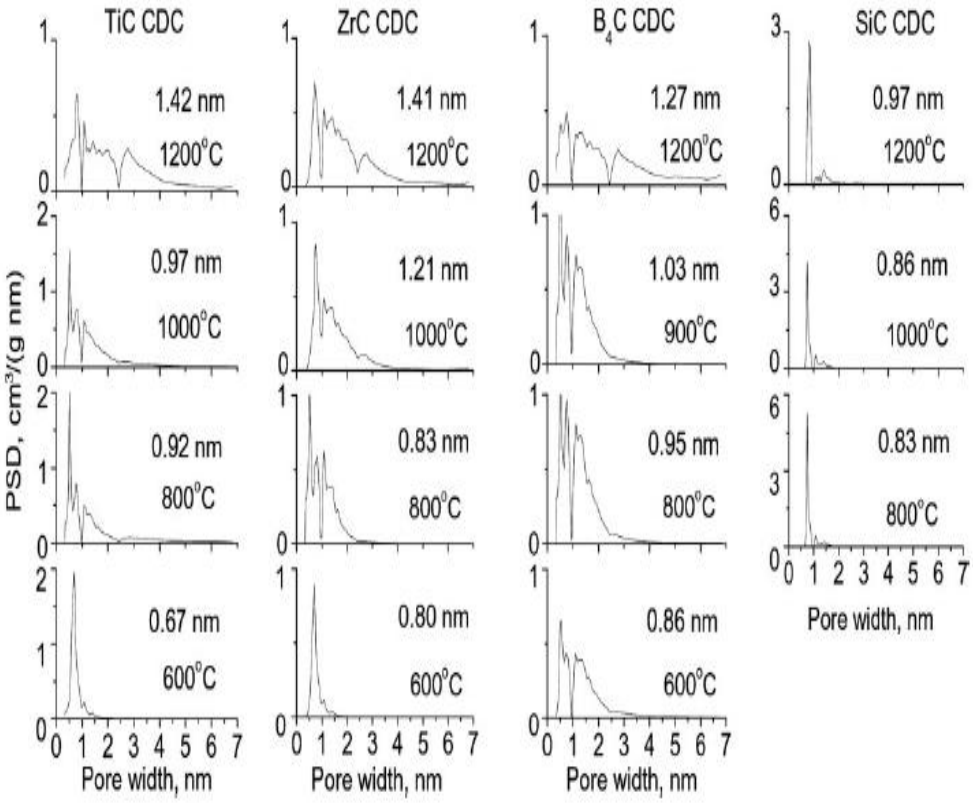

Figure 2.15 Pore size distributions of different carbides [57]

Figure 2.16 shows the nitrogen adsorption/desorption curves for TiC –CDC at 900 and 1200^0C and comparison of BET surface area with total pore volume with different chlorination temperature [55].

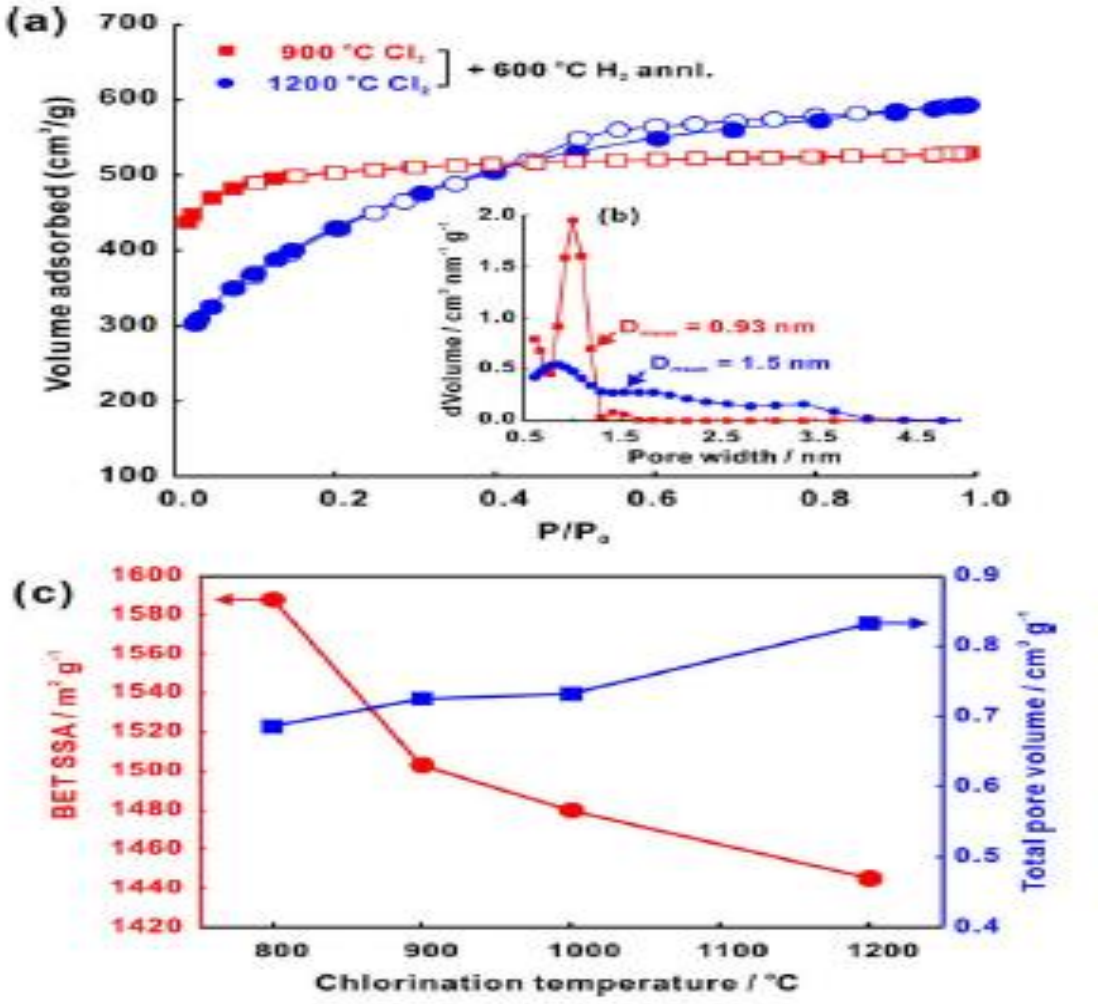

Figure 2.16 Nitrogen adsorption/desorption curves for TiC –CDC at 900 and 12000C and comparison of BET surface area with total pore volume with different chlorination temperature [55]

Following Table 2.2 presents a review about operating parameters such as temperature, pressure, chlorine gas flow rate and diluent, used to produce CDC from different metal carbide source having different particle size.

Table 2.2 Operating parameters for various Carbides sources for CDC production

Carbide Source	Particle Size	Temperature Range	Gas Used	Volumetric Flow Rate	Diluent	Pressure	Ref
SiC	1 um	600 –1000^{0}C	Chlorine gas		Argon gas (Ar)	Atm pressure (14.7 psi)	[58]
TiC	2um (Obtained from Alfa Aesar)	200-1200^{0}C	Chlorine Gas(Air gas UHP Grade)	10-15 cm^3/min, pass through 1 inch dia of tube for 3 h	(Ar, air Gas UHP Grade)	Atm pressure (14.7 psi)	[59]
B_4C	6 um	400–1200^{0}C	Chlorine gas	velocity of 10–15 cm^3/min for 3 h	Argon gas		[56]
Ti_3SiC_2	Large plate -like grains of 70–300lm in diameter and 5–30lm in thickness	200 –1200^{0}C	High purity Chlorine gas (BOC Gases, 99.5%)	flow rate of 10 SCCM for 3 h	High purity argon (BOC Gases, 99.9%) As reactive and purging gases	Atm pressure (14.7psi)	[60]
ZrC	8 um	200-1200^{0}C	Chlorine gas	10- 15 cm^3/min passed through a	Argon gas		[61]

				tube furnace 1 inch dia for 3h			
WC	Less than 10 um	700 –1100^{0}C	Chlorine gas	flow rate 50 ml/min	Argon Gas (500 ml /min)		[62]
Ti_2AlC	1 um	400-1200^{0}C	Chlorine gas (BOC Gases, 99.5%)	Cl_2 flow rate 10 sccm	High purity Argon gas (BOC Gases, 99.998%)		[63]
b-SiC	average diameter of 200 nm and an aspect ratio of ~300	700-1200^{0}C	Cl_2	flow rate of 15 sccm	To make air/oxygen free system, tube was purged with Ar(100 sccm) for 20 min.		[64]
Mo_2C	325 mesh powder 25gram quantity used	400 to 1200^{0}C	Cl_2 (AGA, 99.9999 %)	flow rate of Cl_2 was 50 ml/min	Argon gas (500 ml/min)		[65]
Fe_3C	(200/+270 mesh) 1grame quantity used	600^{0}C at a ramp rate of 5^{0}C /min	chlorine gas	flow rate of 25 ml /min	Ar flow (Airgas 99.999%) at a rate of 100 ml /min	ambient pressure	[66]

In addition, the halogenation method can produce various carbon nanostructures such as nanodiamonds, carbon nanotubes and carbon onions. Carbide derived carbon offers many

advantages in separation processes over polymers, zeolite, and porous carbon due to such significant characteristics [67].

CHAPTER 3

EXPERIMENTAL METHODOLOGY

The principles and methods of different experimental techniques employed to synthesize the carbide derived carbon (CDC) nanoparticles, membranes and characterization of all these materials are discussed in this chapter in detail. Different techniques were used to characterize the nanomaterials such as Scanning Electron Microscopy (FE-SEM), Nitrogen Adsorption/desorption which is used to determine the surface area (BET), pore size and pore size distribution of nanoparticles. Thermo-Gravimetric Analysis (TGA), Contact angle (CA) and Atomic Force Microscopy (AFM) were used.

3.1 Material

Polysulfone (average MW ~35,000 by LS) and dimethylformamide (DMF) were purchased from Sigma- Aldrich and employed for the membranes casting as a primary polymers respectively. Polyester support Novatexx 2484 was used as a basic support for polysulfone casting. Deionized water was used in immersion precipitation coagulation bath. Titanium Carbide nano powder (TiC, 99 + %, 1.2 μm, and cubic) was purchased from US Research nanomaterials, Inc, USA. Sulfuric Acid and n- hexane were purchased from Fisher Scientific Canada. Sodium chloride (NaCl), sodium hydroxide (NaOH), bovin serum albumin (BSA), m-phenylene diamine (MPD) and trimesoyl chloride (TMC) were purchased from Sigma Aldrich chemical company, USA. Some images of important stuff is shown in Figure 3.1.

(a)

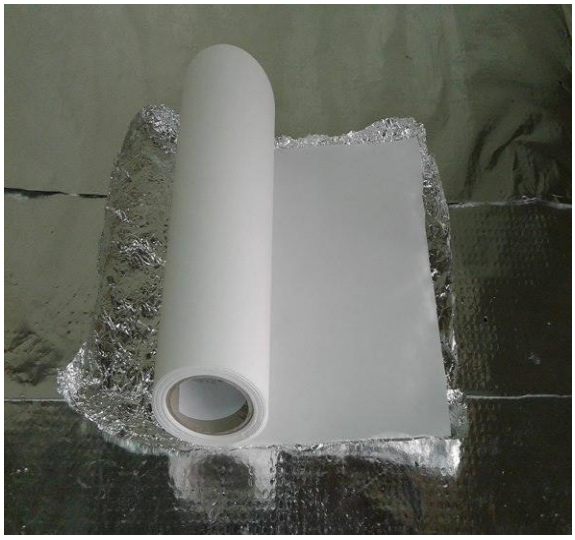

(b)

(c)

(d)

Figure 3.1 Important stuff used a) Polysulfone tablets, b) Polyester support Novatexx-2484 c) Casting blade, d) Deionized water source

3.2 Preparation of Carbide Derived Carbon (CDC) Nanoparticles

Titanium Carbide (TiC, 99+%) was placed in quartz tube with quartz boat. The furnace was heated to 700, 800 and 900^{0}C as final required temperature at a rate of 10^{0}C/min. Tubular quartz furnace was purged with Argon at room temperature to required final temperature to create air/oxygen free closed system. As the desired temperature was

reached, pure chlorine gas was started at a flow rate of (10-13cm^3/min) for 3 h with dilution of Argon gas. After chlorination, the post treatment was done for 1 h with Hydrogen gas and furnace was cooled down to room temperature with continuous Argon gas purge. Synthesis of carbide derived carbon from TiC powder (abbreviated in this work TiC-DC) is explained as following chemical reaction and setup is shown in Figure 3.2. Lab made CDC produced from TiC powder is shown in Figure 3.3.

$$2T_iC_{(s)} + 3Cl_{2(g)} \rightarrow 2T_iCl_{3(g)} + 2C_{(s)} \quad (3.1)$$

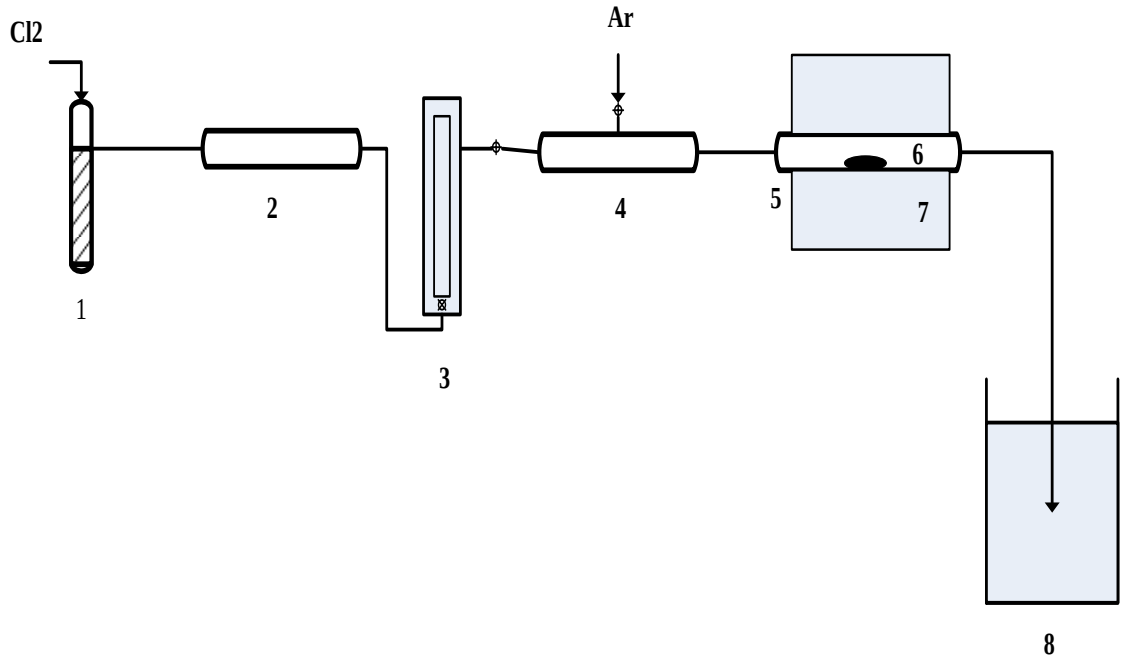

Figure 3.2 Practical Setup 1. Sulphuric acid, 2. Desiccant, 3. Flow meter, 4. Mixing column, 5. Quartz tube, 6. Sample, 7. Furnace, 8. Aqueous NaOH solution.

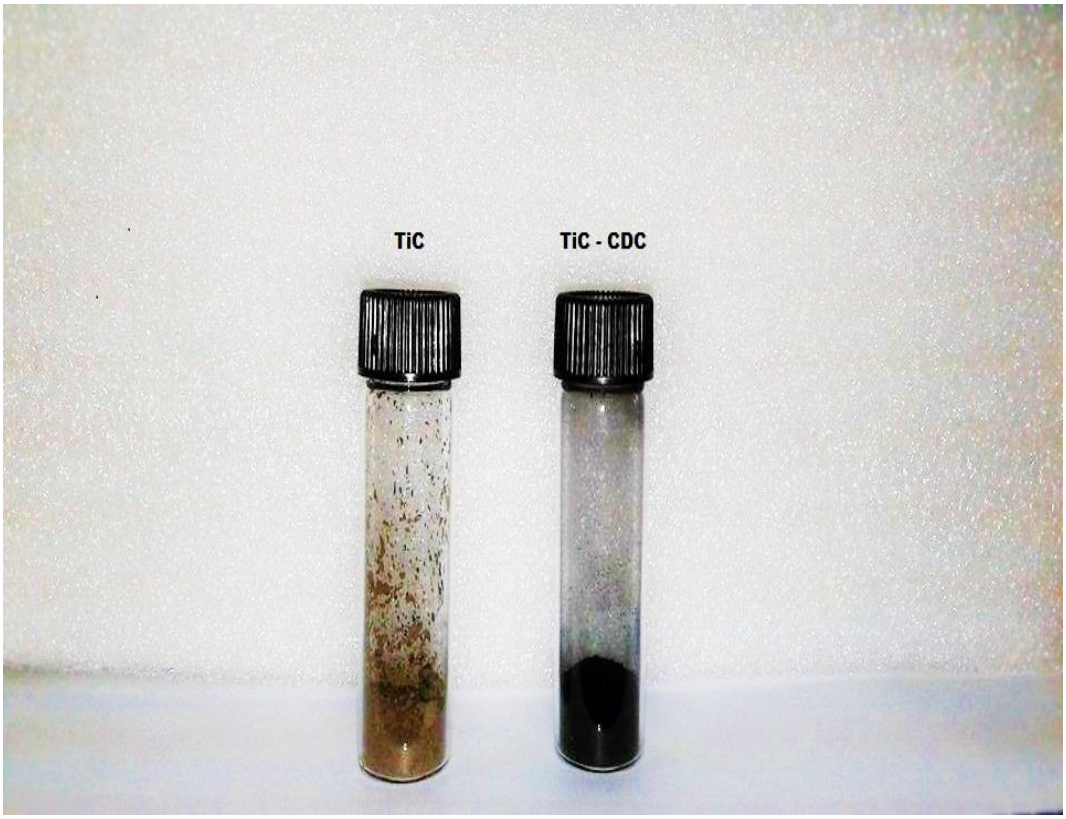

Figure 3.3 Lab made carbide derived carbon (CDC) from TiC powder at 800^{0}C

3.3 Preparation of TFC and TiC-DC-TFN Membranes

Polysulfone tablets were dried in vacuum oven at 100 0C over night to remove all trapped moisture inside the polysulfone tablets. The dried PSF tablets were put in dimethyformamide (DMF) solvent to prepared 20 wt % PSF solution. The casting solution was stirred for 24 h at 30^{0}C. The prepared solution was homogenous, colorless and without any agglomeration. Before casting the PSF support, 20 wt % PSF solution was degas for 1 h using degasser and placed in vacuum oven for 24 h to remove all trapped air/ bubbles inside the solution.

The solution was casted at room temperature on commercial polyester fabric support vortexx 2484 which was attached on a sticky thin flat sheet on glass plate. The casted

film was immediately immersed in deionized water bath at room temperature for 24 h to accomplish the phase inversion process. After 24 h the thin flat sheet was removed to get the pure polysulfone support.

Interfacial polymerization method was used for the preparation of TFC and TFN membranes. Polysulfone substrate was immersed for 5 min in MPD aqueous solution (2% w/v). The membrane was pulled out from MPD solution and the extra diamine solution was removed from the membrane surface by rolling once from one side with rubber roller. Then, PSF substrate was fixed into frame and TMC solution (0.15% w/v) was poured onto the surface for 1 min then rinsed with n-hexane for 30 s and placed in oven for 5 min at 60^0C and stored in DI water. For the preparation of TFN membranes, TiC-DC nanoparticles were completely dispersed in TMC solution (0.15 % w/v) in n-Hexane under ultrasonic treatment with 50 amplitude for 5 min at 25^0C and immediately poured onto the porous support to react for 1 min then rinsed with n-hexane and dried in oven for 5 min at 60^0C and stored in DI water.

Four TiC-DC nanoparticles concentrations were used to form TFN-TiC-DC membranes from 0.001, 0.002, and 0.003 to 0.0033 w/v % named as M1, M2, M3, M4 respectively and M0 for pristine PA membrane.

3.4 Separation Performance/ Filtration Experiments

Filtration experiments of TFN- TiC-CD membranes were evaluated in term of pure water, saline water (2000 ppm) and foulant (100 mg/L) in deionized water using a cross flow mode (Sterlitech CF-042 cross flow permeation cell with an effective membrane area of 42 cm^2 at constant trans membrane pressure (TMP) of 14.15 bar at ambient

temperature. Schematic and real equipment diagram is shown in Figure 3.4 and 3.5 respectively. The permeation flux was measured by using following formula

$$J_0 = \frac{V}{A \times \Delta t} \quad (3.2)$$

Where

J_0 = Volumetric Flux (L/m^2.h)

V = Volume of permeate (L)

Δt = Permeation time interval (h)

A = Effective membrane area (m^2)

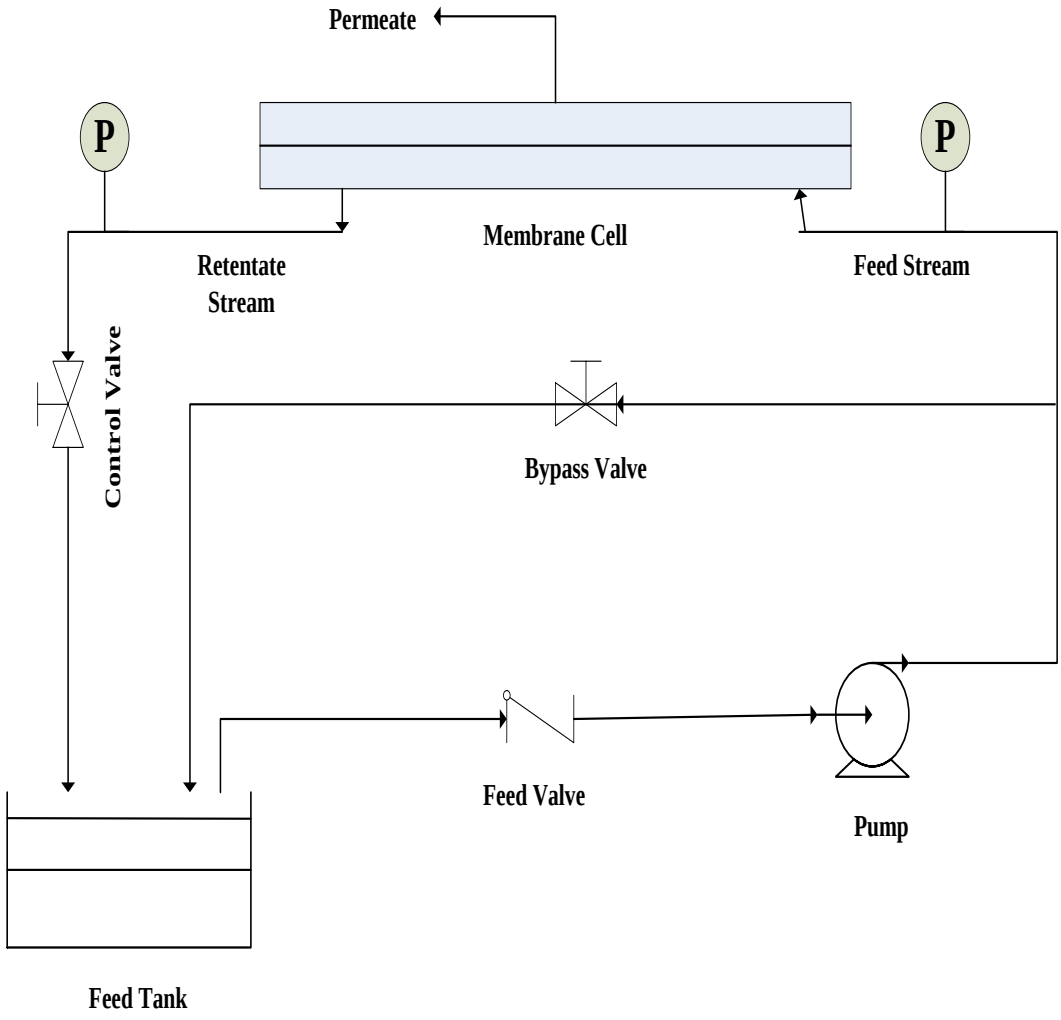

Figure 3.4 Schematic diagram of cross flow experimental setup.

Figure 3.5 Cross flow apparatus used to measure permeate flux.

3.5 Characterization

Characterization is very important part of this section. The detail of all the equipment's used for the characterizations is describe in this section.

3.5.1 Scanning Electron Microscopy (SEM)

To check the micro structural properties and surface morphology of materials, scanning electrons microscopy (SEM) technique is used extensively. SEM works on the principle of generating high energy of electron beam from electron gun. This beam of electron is condensed by condenser lens (may be one or two). Next, scanning coils are used to produce magnetic field and deflects electron beam back and forth. This electron bean focused on the specimen and scan the sample in required location.

The surface morphology of TiC-DC nanoparticles was perceived by using Field Emission Scanning Electron (FE-SEM) microscope (MIRA3, TESCAN) with increasing electron voltage of 15 KV. Gold layer of 10nm thickness was used for samples coating using Ion Sputter Q 150R S (Quorum Technologies) as shown in Figure 3.6 and 3.7 respectively.

Figure 3.6 Scanning electron microscope used for morphological analysis.

Figure 3.7 Coating machine used for sample coating before SEM analysis.

3.5.2 Nitrogen Adsorption/Desorption Measurements

The BET surface area was calculated from selected N_2 adsorption data within the range of relative pressure from 0 to 1. The pore volume $\boldsymbol{V_t}$ and adsorption isotherm were

determined as the volume of nitrogen adsorbed at a relative pressure of 0.99. The pore size distributions were obtained using DFT method from the adsorption branch using Quanta Chrome ® ASIQwin ™. Micropores volume $\boldsymbol{V_{micropore}}$ was obtained from t-plot method micropore analysis from v-t method section and mesopores volume $\boldsymbol{V_{mesopore}}$ was calculated by subtracting the micropores volume from total pore volume $\boldsymbol{V_t}$ using Quanta Chrome ® ASIQwin ™. Setup is shown in Figure 3.8.

Figure 3.8 Setup used to calculate nitrogen adsorption/desorption analysis.

3.5.3 Thermo Gravimetric Analysis (TGA)

Thermo gravimetric analysis is a method to measure the thermal stability of materials in which physical and chemical changes in the materials are determined as a function of increasing temperature upto certain level with constant heating rate. This method provides a curve with decreasing weight loss due to loss of material mass by decomposition phenomena with increasing temperature. A Netzsch model STA 449 F3

Jupiter ® TGA was used as shown in Figure 3.9 to check the thermal stability /degradation behavior of TFC and TiC-DC-TFN membranes.

Figure 3.9 Thermo gravimetric analyzer (TGA) used to check thermal stability of materials.

3.5.4 Atomic Force Microscope (AFM)

Atomic force microscope is also known as scanning probe microscope (SPM) in which scanning probe microscopes are arranged to measure the local properties of specimen for example, friction, height and magnetism with the usage of probe. The membrane surface roughness was studied by using Atomic Force Microscope (AFM) of Veeco Metrology Nano Scope IV with Dimension of 3100 SPM as shown in Figure 3.10.

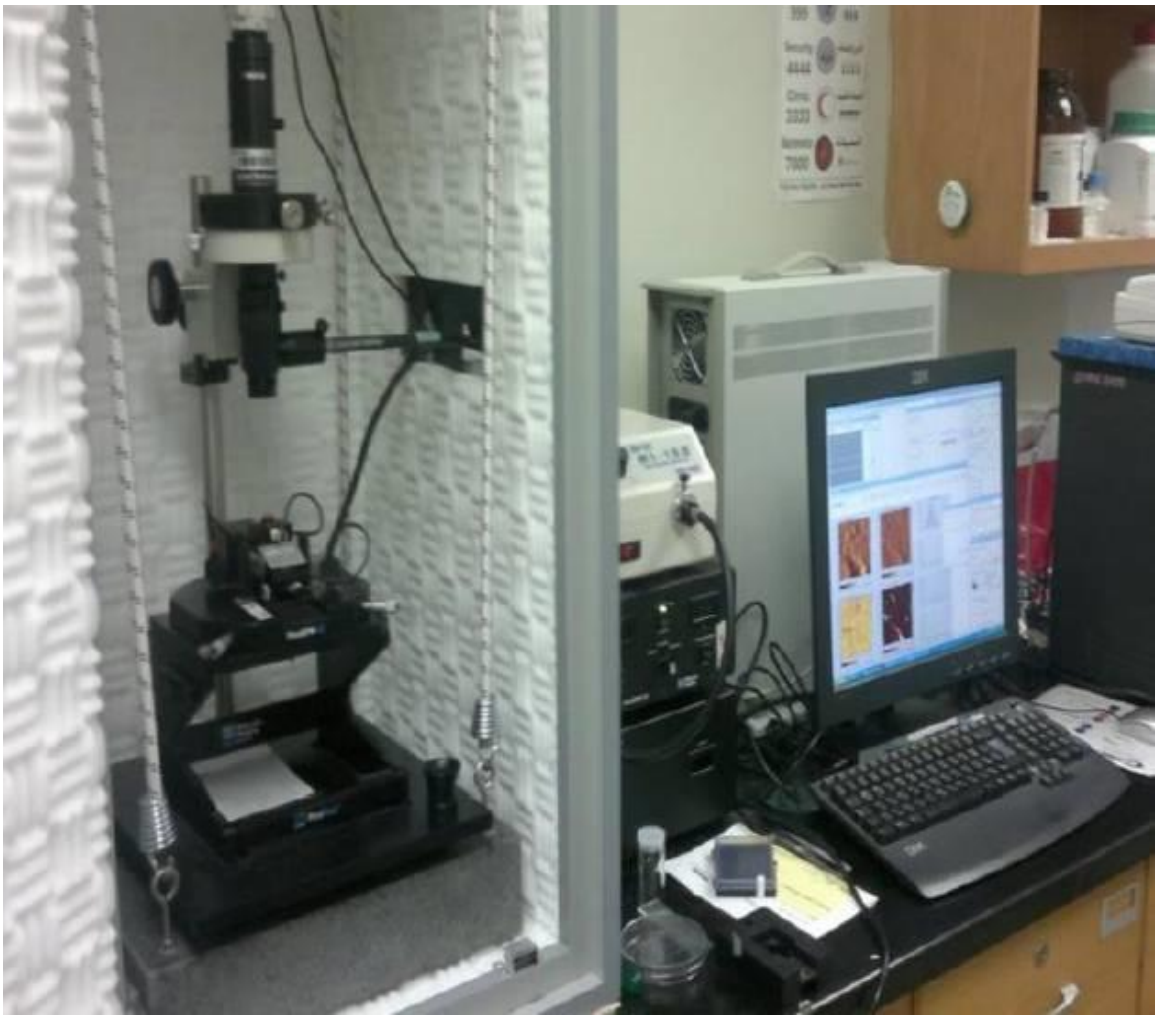

Figure 3.10 Atomic force microscope used to check membrane surface roughness.

3.5.5 Contact Angle Measurements

To check the hydrophobic / hydrophilic nature of membranes surface, contact angle measurements were done by a Drop Master, DM-501 device (Kyowa interface Science Co.).

Approximately 2 μL of DI water was dropped on the surface of membrane and contact angle was measured from different 7 surface positions and average value was taken. Contact angle measurement instrument is shown in Figure 3.11.

Figure 3.11 Contact angle measurement machine used to measure the contact angle.

CHAPTER 4

RESULTS AND DISCUSSIONS

This chapter consist of all experimental findings and a comprehensive discussion on all results. This chapter includes the discussion on three main parts. In first part, whole discussion is about the properties of untreated and treated TiC such as adsorption isotherms, pore volume, pore size distribution (PSD), Specific surface area (SSA) and SEM images.

Second part of the discussion is about characterizations of TFC and TFN-TiC-DC membranes such as their flux permeation with pure, saline and foulant water. Thermo gravimetric behavior of TFN-TiC –DC membranes with different compositions of nanofillers. Surface wettability and surface roughness estimations of bare and modified membranes were done by measuring their surface contact angle and AFM and linked with flux permeation trends.

Last part of the discussion deals with the antifouling performance of mixed matrix membrane like specific flux ratio j/j_0, pore blocking model, washing and fouling cycles and calculation about flux recovery ratio, total resistance, reversible and irreversible resistance.

4.1 Characterization of Carbide Derived Carbon (CDC) nanoparticles

4.1.1 Scanning Electron Microscope Analysis

The surface morphologies of the untreated titanium carbide powder (TiC) and TiC-DC adsorbents were observed using FE-SEM. The reason to start chlorination of precursor carbide from 700^0C to onward is to produce more crystalline and ordered shape carbide[68]. The micrographs of precursor carbide(TiC) and derived carbons is presented in Figure 4.1 which shows the untreated TiC and Titanium carbide derived carbon (TiC-DC) at 700, 800 and 900^0C. Precursor carbide and CDCs produced at different temperature look alike and exhibiting preservation of particles shape with slight shrinkage and some etching signs [68]. In the micrographs, CDCs of TiC exhibiting faceted surfaces [68] and particles structure [56] with average particle size of 0.1–0.3 μm and is scattered with allover micropores.

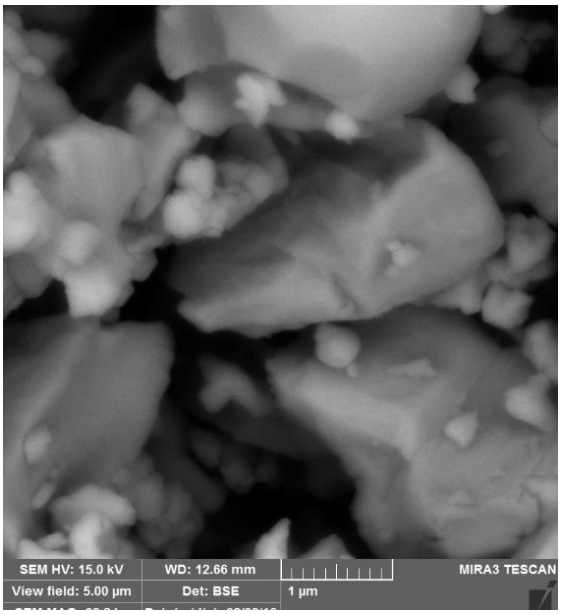
SEM HV: 15.0 kV
WD: 12.66 mm
MIRA3 TESCAN
View field: 5.00 µm
Det: BSE
1 µm

(a)

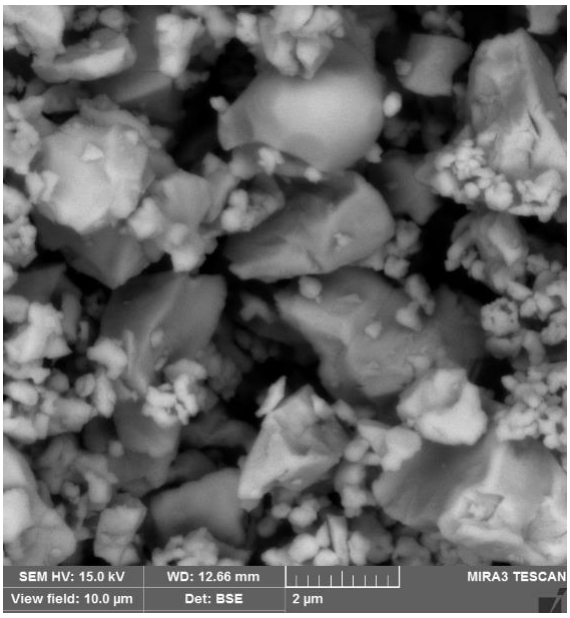
SEM HV: 15.0 kV
WD: 12.66 mm
MIRA3 TESCAN
View field: 10.0 µm
Det: BSE
2 µm

(b)

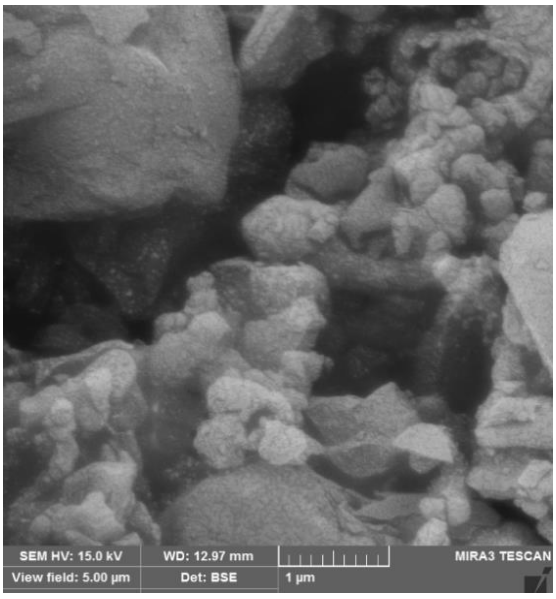
SEM HV: 15.0 kV
WD: 12.97 mm
MIRA3 TESCAN
View field: 5.00 µm
Det: BSE
1 µm

(c)

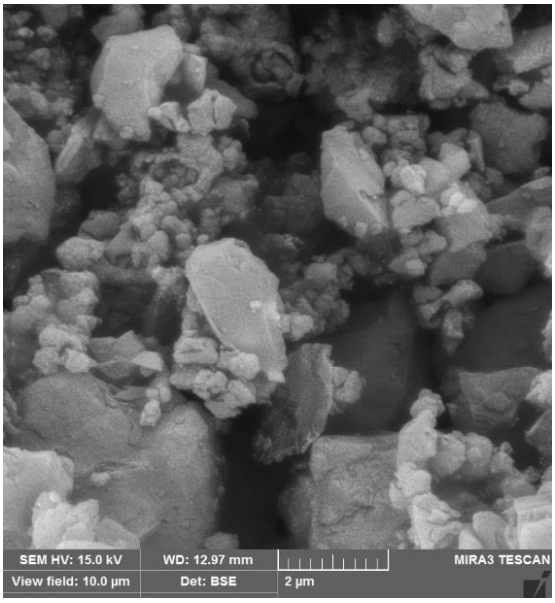
SEM HV: 15.0 kV
WD: 12.97 mm
MIRA3 TESCAN
View field: 10.0 µm
Det: BSE
2 µm

(d)

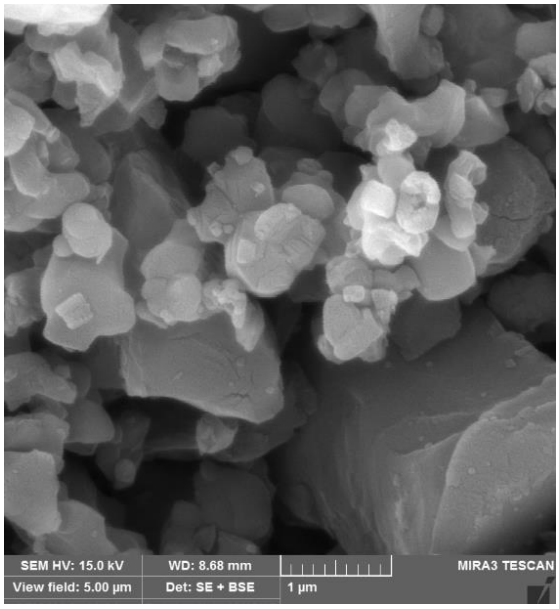

(e)

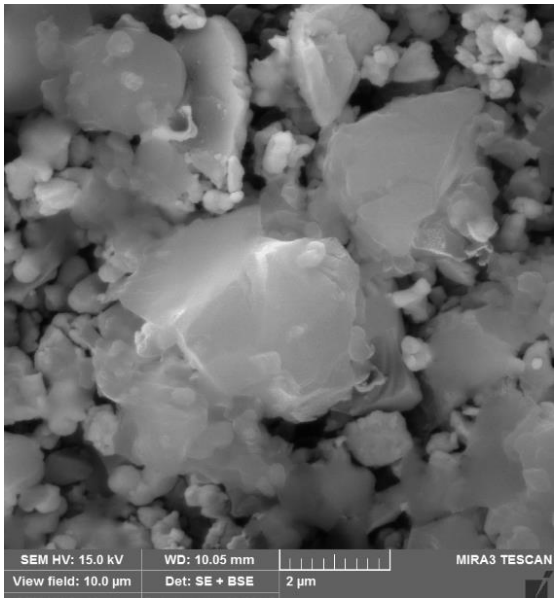

(f)

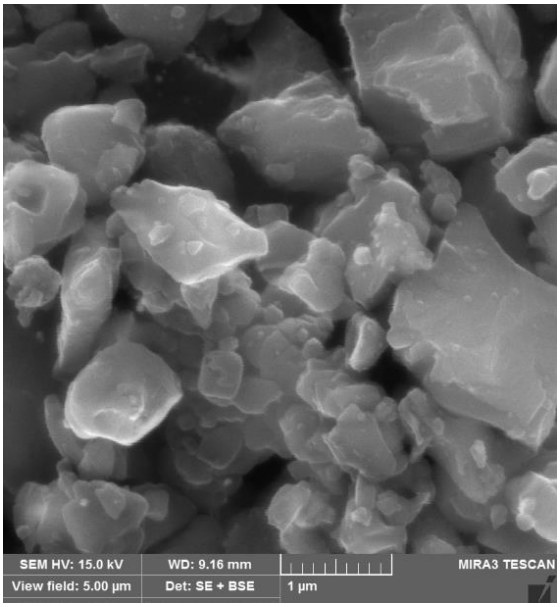

(g)

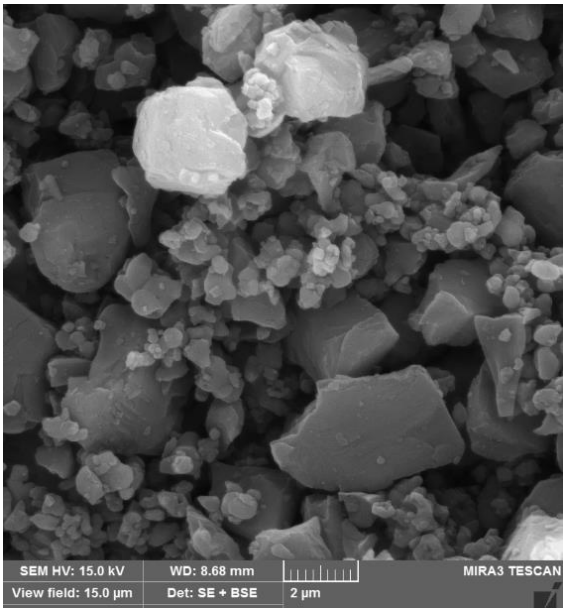

(h)

Figure 4.1 SEM images of untreated TiC powder (a and b) and TiC-DC at 700^0C (c and d), 800^0C (e and f) and 900^0C (g and h).

4.1.2 Transmission Electron Microscopy (TEM)

Transmission electron microscopy (TEM) is a microscopy technique in which a beam of electrons is transmitted through an ultra-thin specimen, interacting with the specimen as it passes through it. From Figure 4.2, it can be seen that maximum beam of electrons are passing throug carbide specimen which is strong sign of microporosity nature of lab made carbide[68].

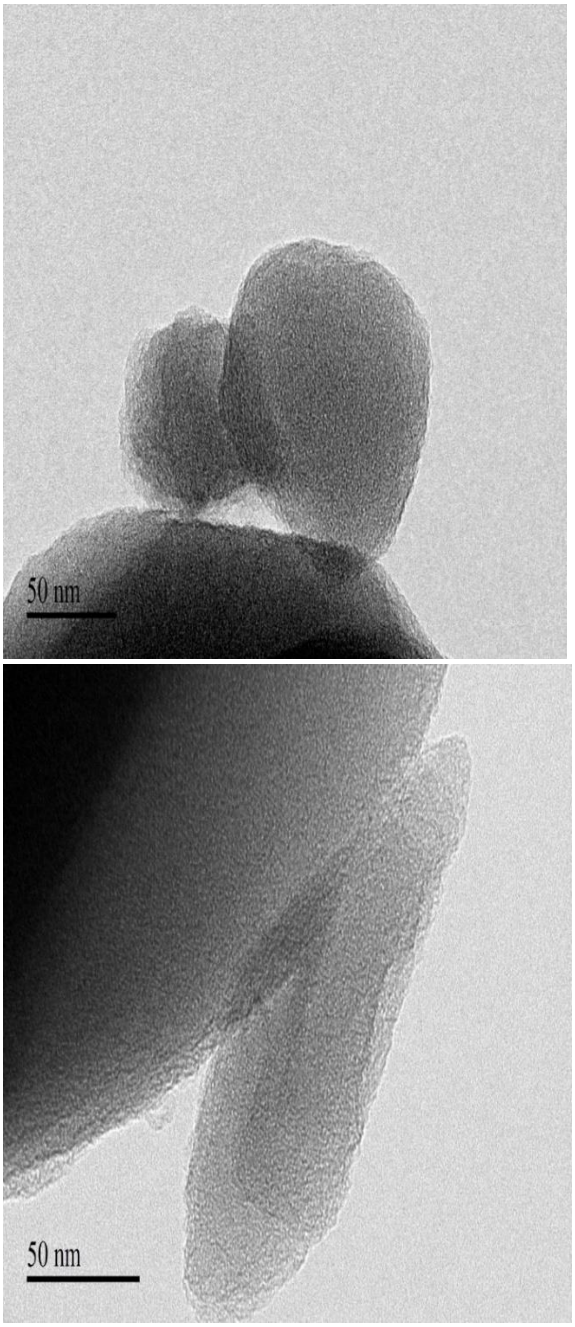

Figure 4.2 TEM images of the lab made TiC-DC at 800^{0}C.

Temperature has a great influence on the crystalinity of the carbide. As the temperature is increased from lower to high, carbide tends to produce from amorphous to crystalline nature nanoparticles [68]. From Figure 4.3, it can be seen clearly that increasing

temperature from 700^0C to 900^0C, carbide nanoparticles are converting from amorphous to crystalline nature with more ordered structure.

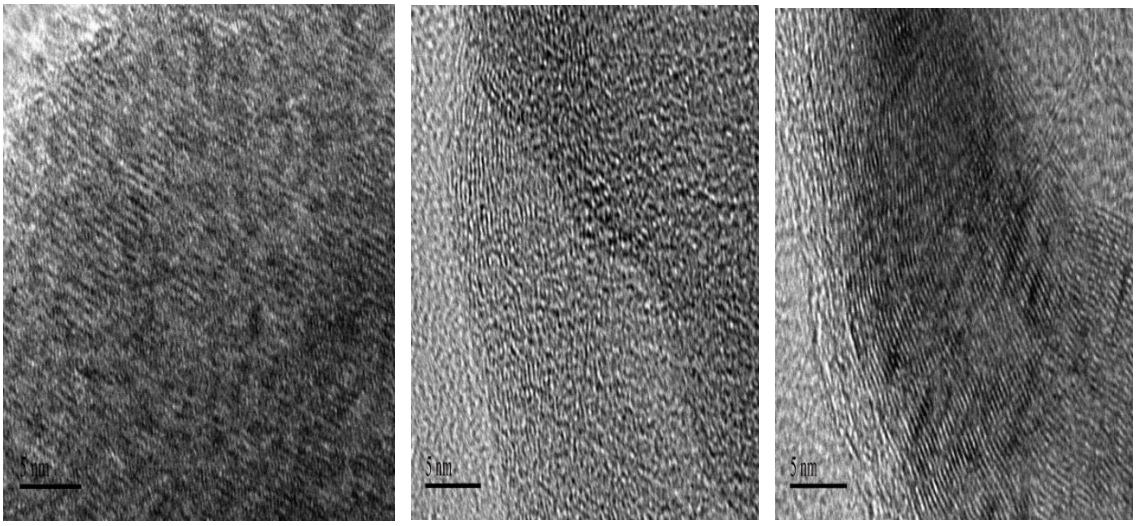

(a) (b) (c)

Figure 4.3 TEM images of TiC-DC at (a) 700^0C, (b) 800^0C, (c) 900^0C.

4.1.3 Nitrogen Adsorption/Desorption Measurement

Nitrogen adsorption measurement of untreated TiC powder and lab made TiC-DC at different three temperatures at 77 K are shown in Figure 4.4. As it can be observed that TiC powder before chlorination shows no significant steep increase which shows negligible adsorption of nitrogen for untreated TiC powder. On the other hand, there are different level of steep increase in adsorbed nitrogen volume at 700, 800 and 900^0C at low relative pressure (p/p_0 less than 0.01) which conformed that these three TiC-DC samples have pure microporous structure and according to international union of pure and applied chemistry (IUPAC), it is a strong evidence of type I isotherm [69]. The existence of significant steep increase in nitrogen adsorption isotherm at low relative pressure indicates the existence of narrow pore size distribution (Figure 4.5). As the

chlorination temperature increased from 700 to 800^{0}C, the amount of adsorbed nitrogen increased which shows the formation of more micropores nanoparticles. As the temperature enhanced from 800 to 900^{0}C, there is a crash of porous structure of nanoparticles which reduced the micro porosity of nanoparticles which can be seen from Table 4.1

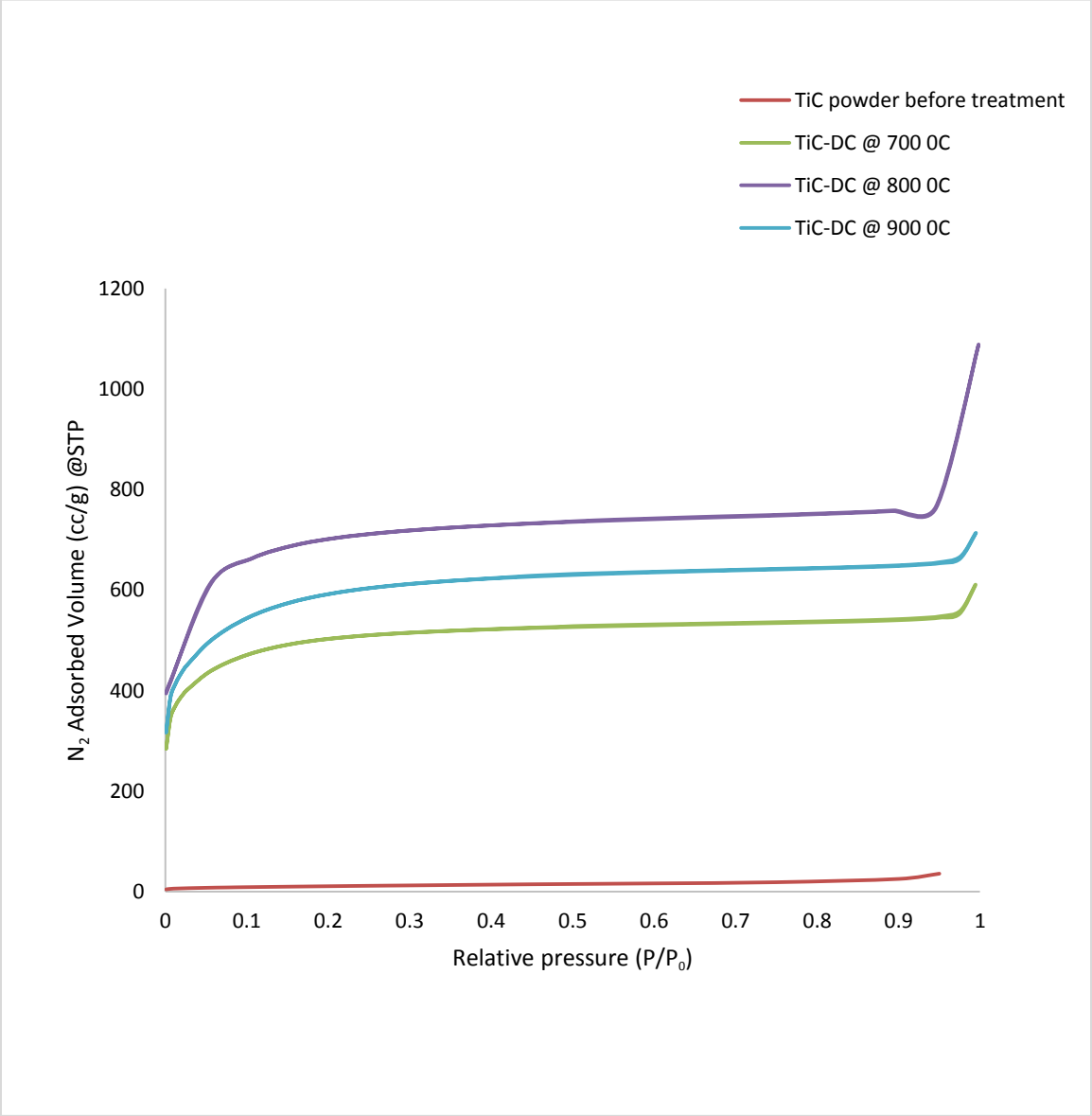

Figure 4.4 Adsorption Isotherms of untreated TiC and TiC-DC at 700, 800 and 900^{0}C.

Table 4. 1 Different structural properties of lab made TiC-DC at 700, 800 and 900^{0}C

T(℃)	$A_{micropore}$ m^2/g	$A_{external\ surface}$ m^2/g	V_{total} cm^3/g	V_{micro} cm^3/g	V_{meso} cm^3/g
$TiC_{untreated}$	7.664	31.360	0.051	0.002	0.049
700	1716.091	162.146	0.788	0.658	0.130
800	1827.716	323.918	1.216	0.873	0.343
900	1935.468	216.165	0.921	0.761	0.160

In above Table 4.1, we can see the variation of porosity with increasing temperature. We can see that from 700 to 800^{0}C, the micro porosity is increased from 0.658 to 0.873 cm^3/g but as we increase the temperature from 800 to 900^{0}C, particles collosion with each other due to high energy, reduced the micro porosity from 0.873 to 0.761 cm^3/g.

The formation of porous carbon having a density lower than that of graphite is done by removing the metal from metal carbide. During 1960s, Carbide derived carbon (CDC) were generated as a byproduct of metal chloride manufacturing process according to following equation (4.1)

$$\boldsymbol{M_eC + \frac{x}{2}Cl_2 \quad \rightarrow \quad M_eCl_x + C} \qquad (4.1)$$

Where M_e is representing metal. Unfortunately, in those days CDCs were considered as waste and undesired product and just thrown inside reactor to enhance the rate of production for chlorine [70]. Carbide derived carbon (CDC) pore size is affected by the special arrangement of atoms in carbon molecule in the metal carbide, manufacturing temperature, chlorine molecules size, catalyst particles existence and the influence of post treatment which is optional like activation or purification [70]. It is well known practice that CDC nanoparticles become more porous by increasing the chlorination temperature upto 900^0C which enhance the apparent surface area (S.A) and total volume of the micropore [71]. It is significant to mention that adsorption of nitrogen directly shows the important modification in carbon nanoparticles porous structure with different temperature range[71]. Figure 4.5 shows the Pore size distributions of untreated TiC and lab made TiC-DC by using mathematically model based on Density Functional Theory (DFT) method to nitrogen adsorption. Pore size distribution (PSD) achieved by employing slit shape pore model which indicates the existence of narrow micropores (0.4-0.7 nm) and significant changes in microporous structures like pore volume and pore size. From Figure 4.5, it is observed that increasing the TiC-DC production temperature from 0 to 900^0C, leads to pore enlargement and wider pore size distributions. Maximum pore size distribution is shown in TiC-DC produced at 800^0C in range from 0.4 to 0.7 nm and approximately same trend is seen for Ti-DC produced at 900^0C and lower from 700^0C and negligible for untreated TiC powder. Samples post treatments/ annealing were done with H_2 for 1 h at same production temperature to remove all the residual chlorine trapped on the nanoparticles surface during the CDCs production time which enhance the specific surface area of the nanoparticles and also micropore volume.

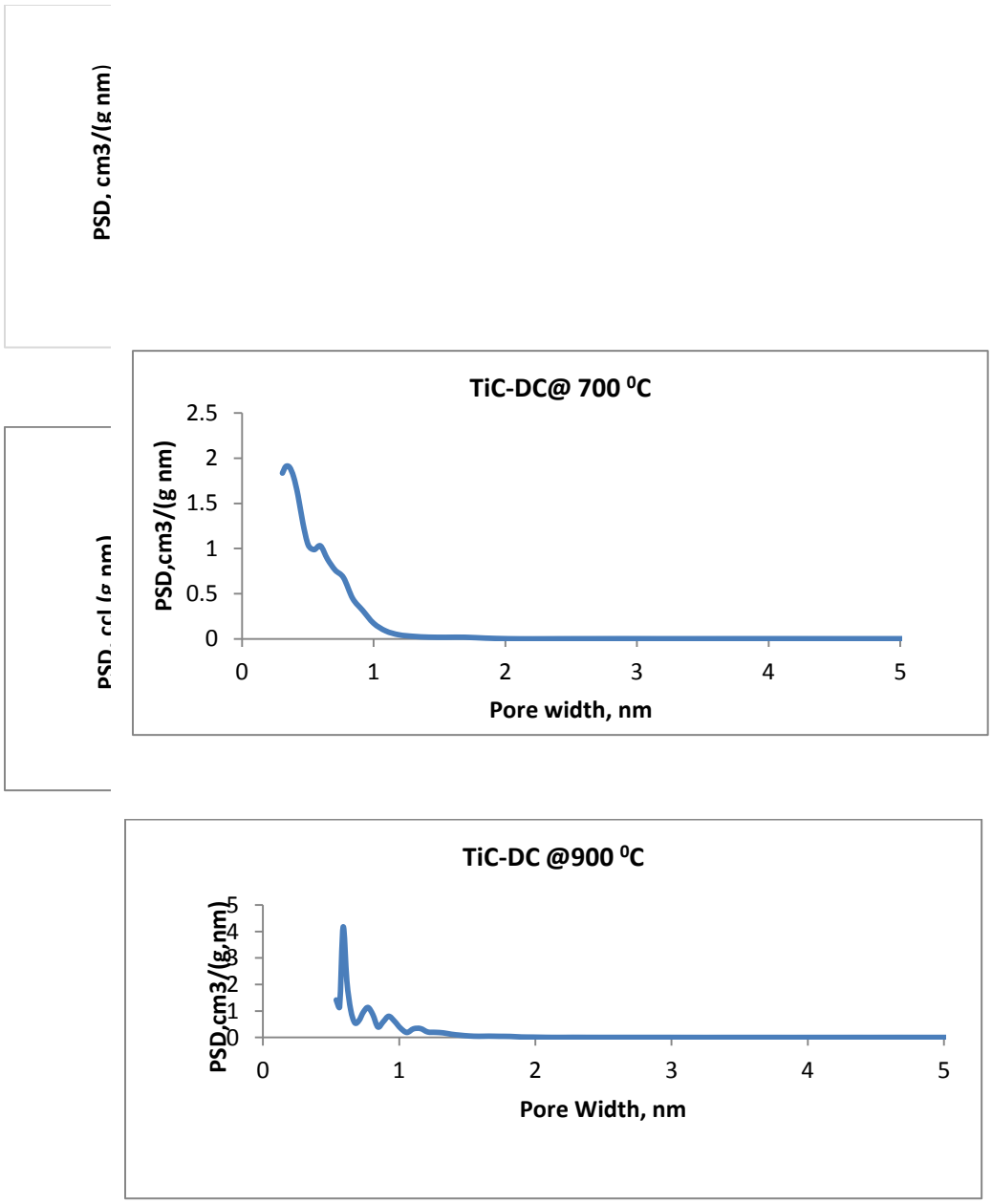

Figure 4.5 Pore size distributions (PSD) of untreated TiC and TiC-DC at 700, 800 and 900^{0}C.

Porosity analysis of untreated TiC and lab made TiC-DC was carried out with the usage of nitrogen as adsorbate using Quanta Chrome ® ASIQwin TM . Nitrogen adsorption result shows that according to BET surface area analysis as the chlorination temperature increased from 0 to 800^{0}C, specific surface area (SSA) increased from 38.780m^2/g

(untreated TiC powder) to 2637.669 m^2/g, but SSA dropped to 2196.093m^2/g as the chlorination temperature reached 900^0C. Same trend can be seen in surface areas according to Langmuir method as shown in Table 4.2.

Table 4. 2 SSA of untreated TiC powder and TiC-DC at 700, 800 and 900 0C

Temperature (^0C)	BET Surface area (m^2/g)	Langmuir Surface area(m^2/g)
TiC powder before treatment	38	128
TiC – DC at 700^0C	1878	2420
TiC – DC at 800^0C	2637	3651
TiC – DC at 900^0C	2196	2902

4.2 Characterization of TiC-DC-TFN Membranes

4.2.1 Surface Morphologies of Lab Casted Psf Support, TFC and TiC-DC-TFN

Figure 4.6 shows the smooth and defect free lab made polysulfone support by using 20(w/v%) of polysulfone tablets and dimethylformamide (DMF) as solvent. Lab de-ionized water was used as a coagulation bath at ambient temperature (~ 24^0C). Unlike the smooth porous PSF surface, the SEM images of a pristine TFC (Figure 4.7a) was bumpy and rough, having layer of tightly packed,

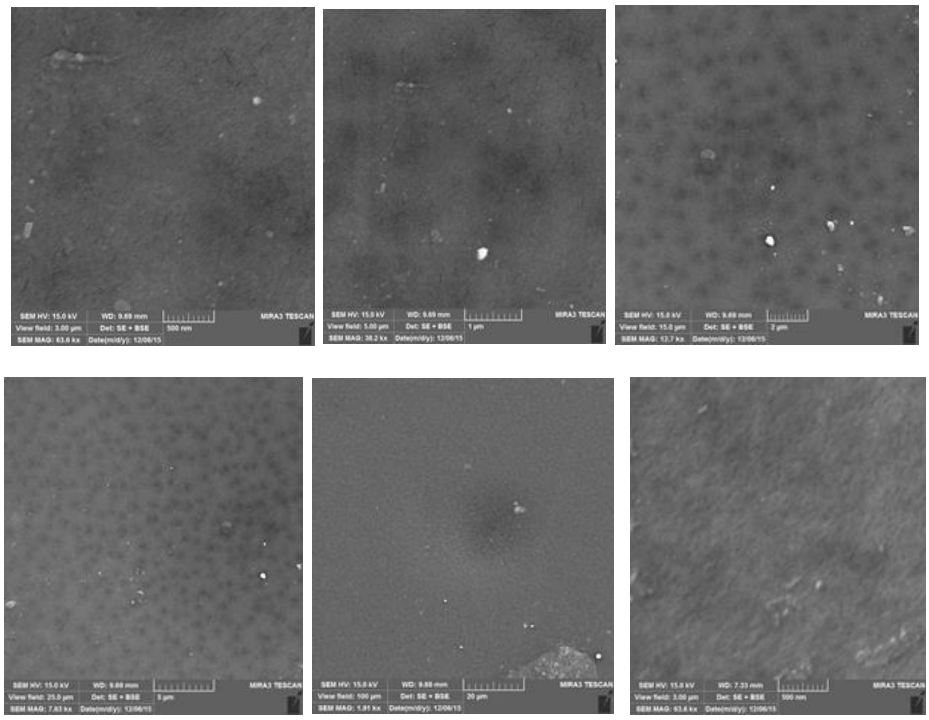

Figure 4.6 SEM Images of lab made PSF support.

Strewed ear shaped polyamide ridges and represents the typically hill and valley structure formed in aromatic PA RO membranes [72], [73]. A less conspicuous hill and valley structure with rippleless surface was observed with increasing the lab made TiC-DC loading up to M3 which reflects that membranes surface getting more smoother by

addition of nanoparticles upto certain point, which is proved by AFM and contact angle measurements also (Figure 4.11-4.12). At higher TiC-DC loading (M4) more nanofillers can be seen on the membrane surface which are responsible for decreasing a little bit contact angle and smoothness on the membrane surface due to high concentration and unequal distribution of nanoparticles. According to Ingo et al.[74] no ZIF-8 nanoparticles were seen on membrane surface in SEM images but in this work nanoparticles can be seen easily in the membrane surface incorporated via interfacial polymerization method. Figure 4.8 demonstrates the morphologies of the cross sectional images of TiC-DC- TFN membranes. As it is well known statement that TFN membrane is described / identified by a thin selective layer of polyamide supported on the porous PSF substrate [75]. From cross sectional, SEM images it is obvious to figure out a thin dense polyamide layer at top of PSF support membrane having fingure like porous structures. Furthermore, it can be noticed that TiC-DC nanoparticles are completely incorporated within the PA layer whitout any apparent agglomeration or segregation.TiC-DC nanoparticles are obvious on porous support due to absorption when the porous support was engaged with aquous phase containg nanofillers [39].

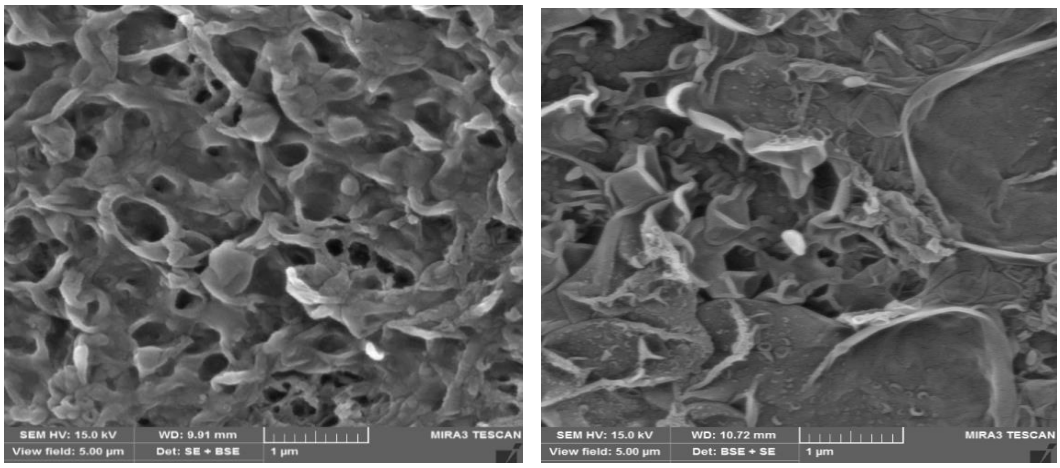

(a) (b)

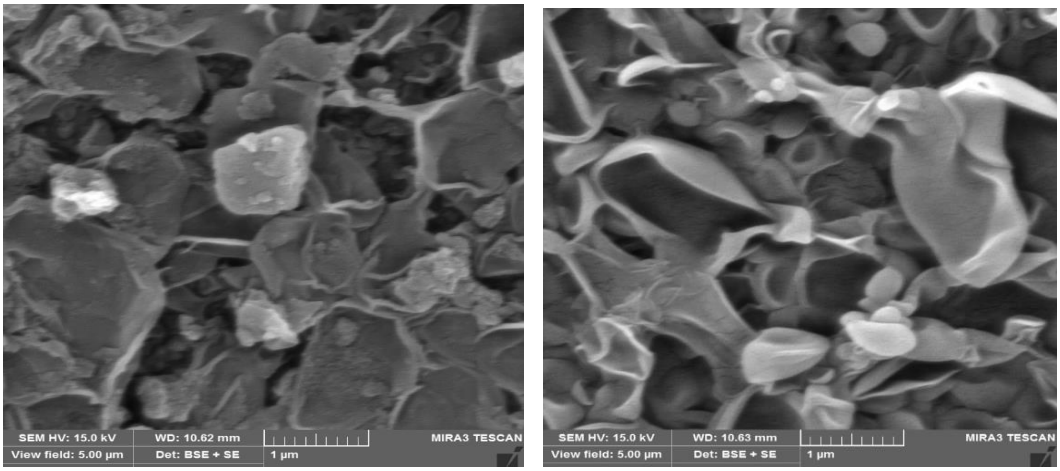

(c) (d)

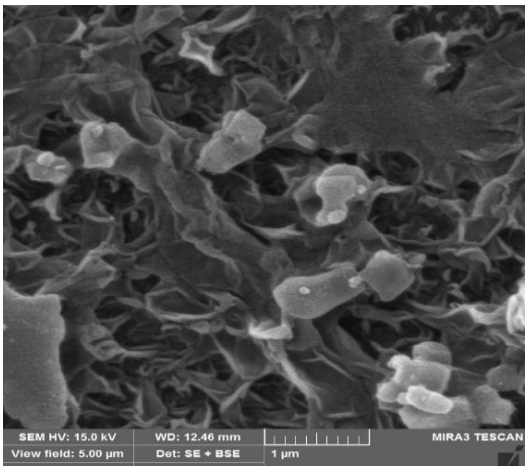

(e)

Figure 4.7 Surface SEM images of (a) lab casted TFC and (b-e) TFN membranes prepared with 0.001, 0.002, 0.003 and 0.0033 (w/v %) TiC-DC nanoparticles respectively.

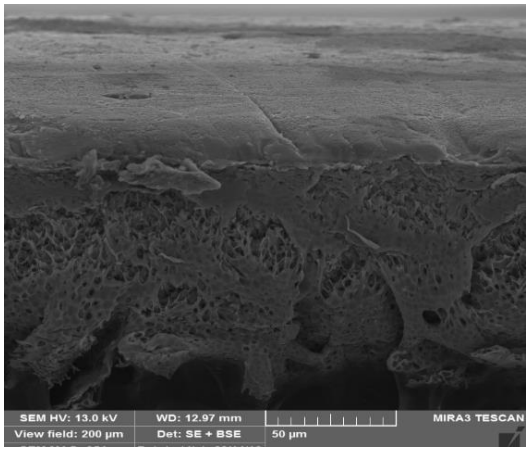

(a)

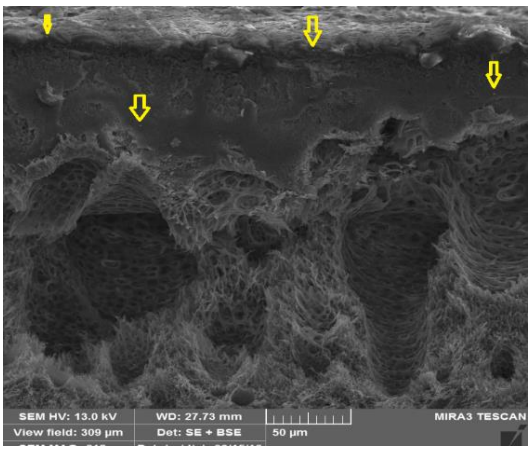

(b)

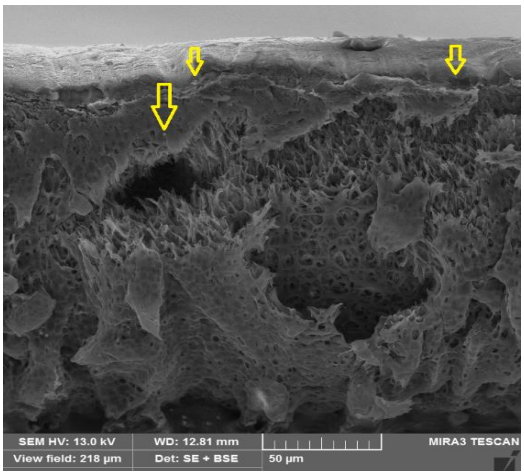

(c)

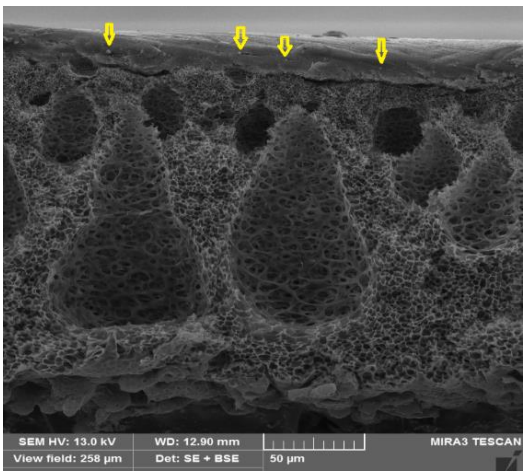

(d)

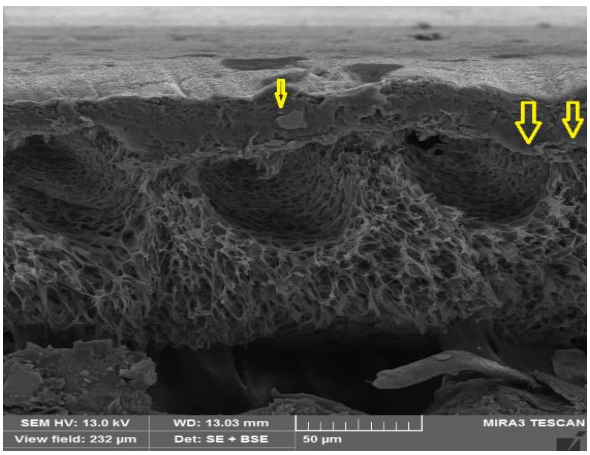

(e)

Figure 4.8 Cross sectional images of (a) lab casted TFC and (b-e) TFN membranes prepared with 0.001, 0.002, 0.003 and 0.0033 (w/v %) TiC-DC nanoparticles respectively.

4.2.2 Thermal Gravimetric Analysis (TGA)

Figure 4.9 and 4.10 represents the thermal degradation behavior of the PA and TFN-TiC-DC with different loading under nitrogen atmosphere. It can be noticed that the thermogravemetric curves of TiC-DC- TFN membranes demonstrated a slight shift as compared to M0 proving that the thermal strength/stability of the TFN-TiC-DC membranes is enhanced by the addition of TiC-DC nanoparticles [76]. A very imperceptible weight loss at 250^0C can be related to the removal of any trapped organic solvent merged with membrane surface during manufacturing process. The second weight loss at approximately 350^0C was attributed to degradation of the polymer matrix [77]. Initial degradation behavior starts from M0 and weight% loss starts at 350^0C as compared to other membranes with nanofiller loading which start degradation from 360 to 380^0C with sequence in loading. A big variation in weight % loss can be seen between 400 to 450^0C and 500 to 500^0C. Maximum loss in weight % is reported by M0 and minimum loss is noted in M4. The enduring masses after TGA analysis are 16%, 19%, 20%, 23% for M0, M1, M2, M3 and M4 respectively. It can be observed that after TGA analysis, the increment in the enduring mass confirms the presence of the added TiC-DC nanoparticles in the prepared membranes. However, from TGA analysis, it can be observed that incorporation of nano particles in membranes surface make them more thermally stable [78].

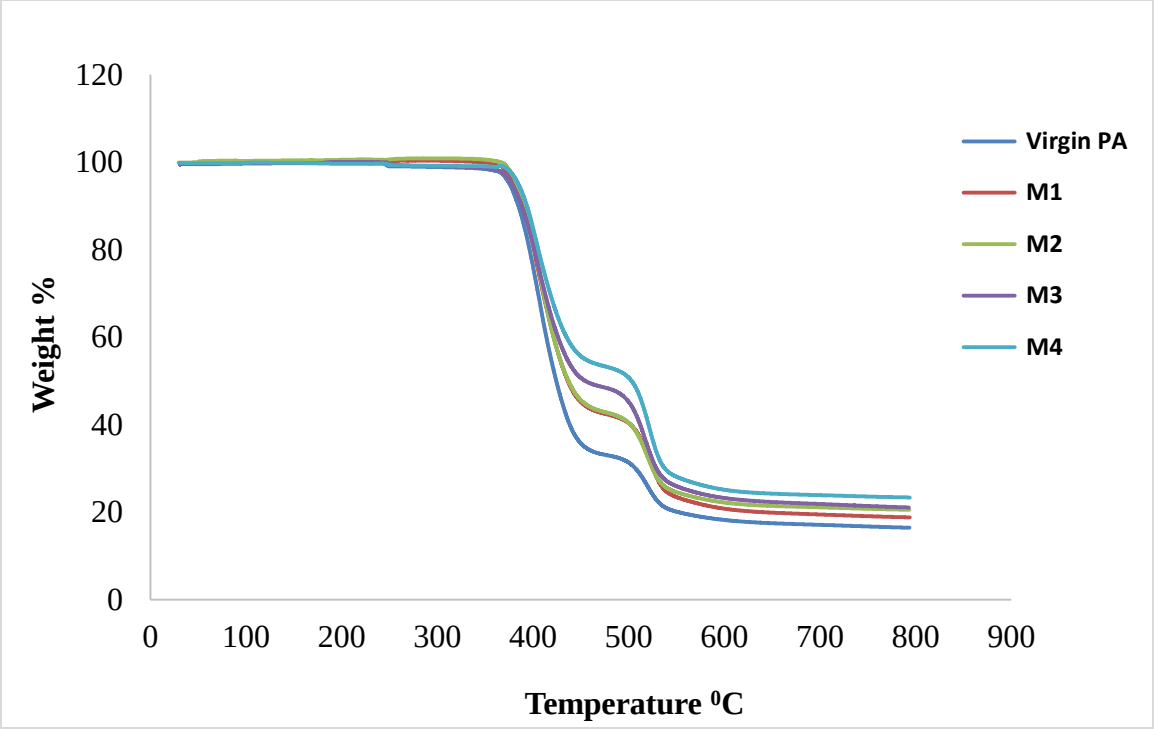

Figure 4.9 TGA analysis of lab made bare PA and TFN-TiC-DC with different w/v% loading.

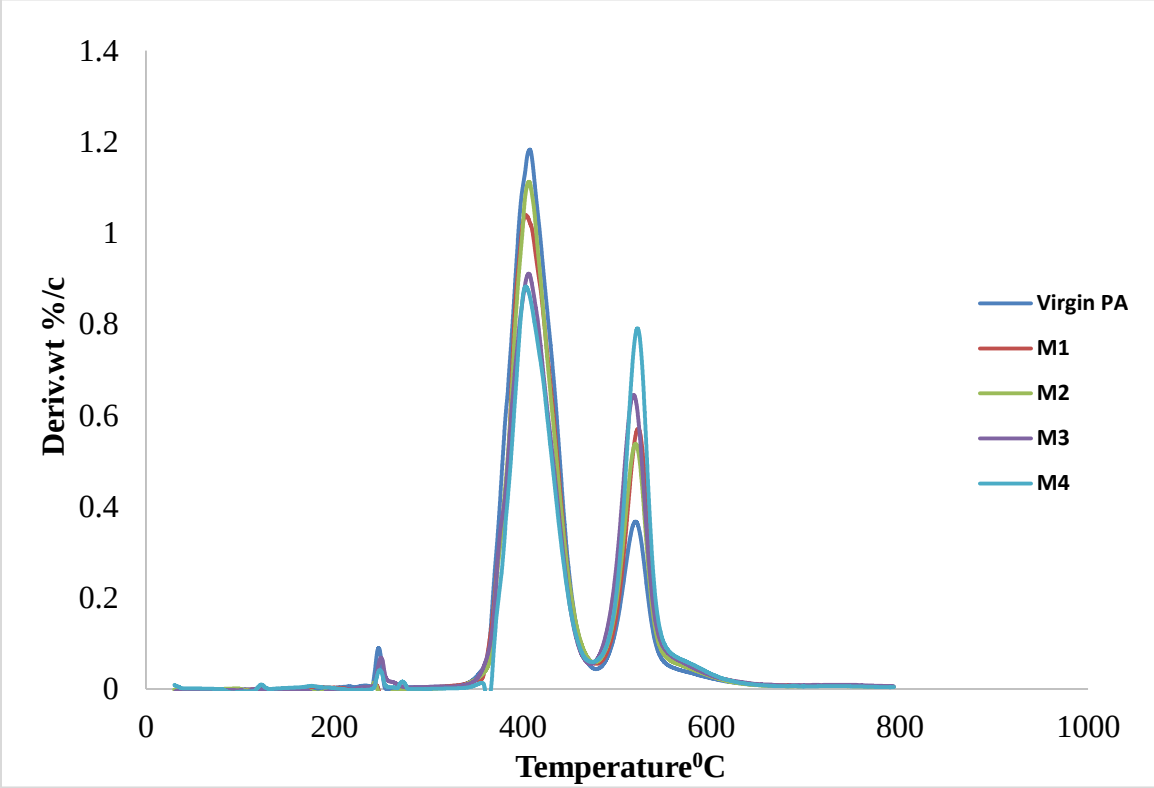

Figure 4.10 TGA analysis of lab made bare PA and TiC-DC-TFN with different w/v% loading.

4.2.3 Atomic Force Microscope (AFM)

Figure 4.11 shows the three dimensional surface AFM images of bare PA and TFN-TiC-DC with different loading of nanoparticles at a scan size of 10 µm × 10 µm. Membranes surface roughness was measured by probing two different random positions on the membrane surface. Light and dark areas in the AFM images are representing the highest and the lowest/valley locations on the membranes surface [73]. A lowest surface roughness (Rq, 0.13 µm) was noticed for M3 as compared to M0 (Rq, 0.31 µm). There is a gradually decreasing trend in surface roughness from M0 to M3 which is also conformed from direct contact angle measurements (Figure 4.12) for these membranes showing smoother surfaces. Surface roughness for highest nanoparticles loading membrane (M4) shows both, a little bit higher surface roughness and contact angle as compare to best one (M3) due to higher concentration of nanoparticles which are responsible for agglomeration on the membrane surface.

(a)

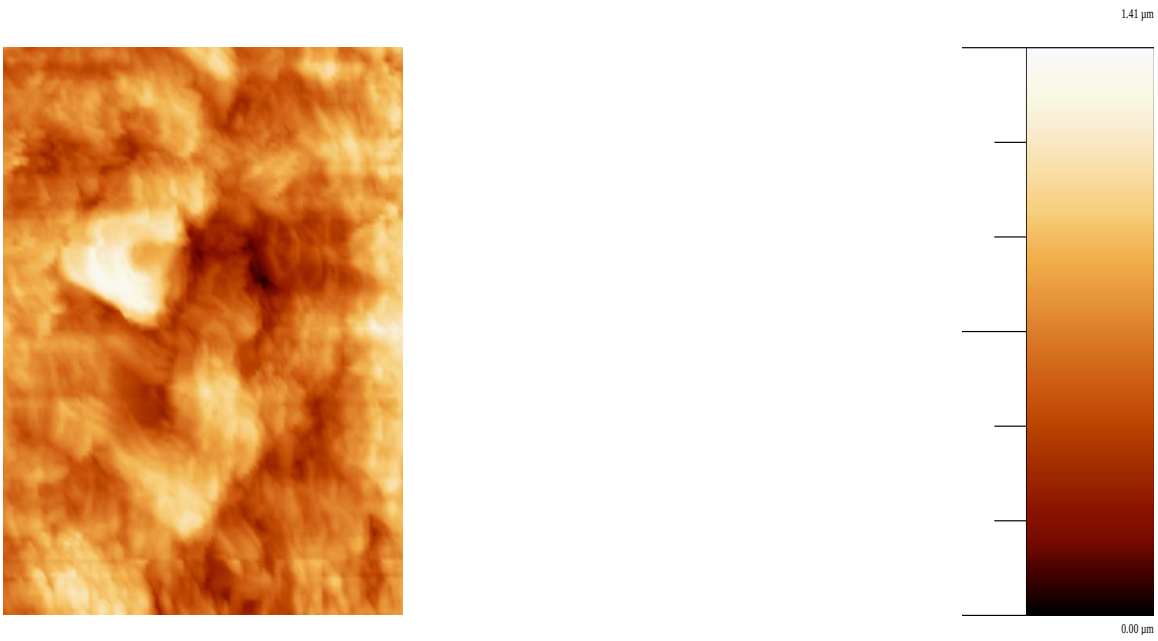

(b)

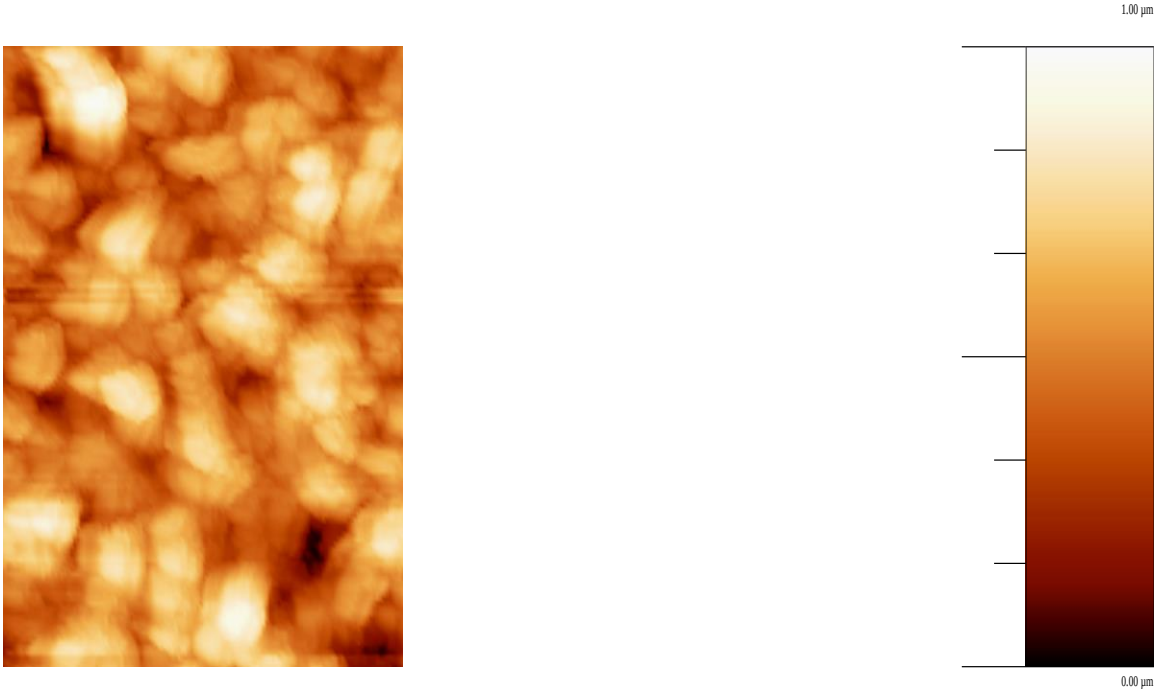

(c)

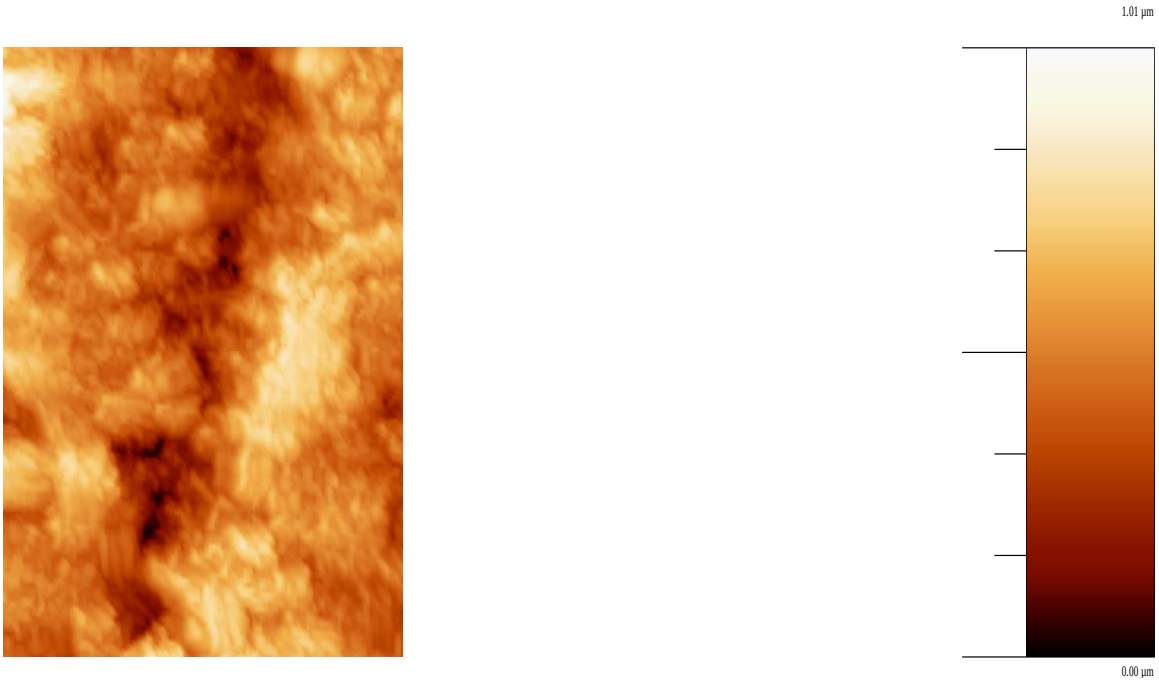

(d)

(e)

Figure 4.11 AFM images of lab made bare PA (a) and TFN-TiC-DC (b-e) with 0.001, 0.002, 0.003, 0.0033 w/v% loading respectively.

4.2.4 Contact Angle Measurements

Figure 12 shows the direct water contact angle on the surface of TiC-DC-TFN mixed matrix membrane. It can be observed that water contact angle is (77.7^0) for M0, on the other hand as the concentration of TiC-DC increases from M1 to M3, there is decline in contact angle from 64.9^0 to 39.8^0 respectively which shows that nanoparticles are interconnecting the membranes pores and making the surface more smoother and hydrophilic. Higher loading upto a certain concentration reduces the water contact angle. This phenomena can be linked to reduction of crosslinking extent on the surface of PA structure; higher carboxylic acid groups disclosed on the PA surface tends to lower the water contact angle on the TFN mixed matrix membrane. The higher the hydrophilic surfaces of PA membranes, the lower organic fouling tendency for these membranes [79].

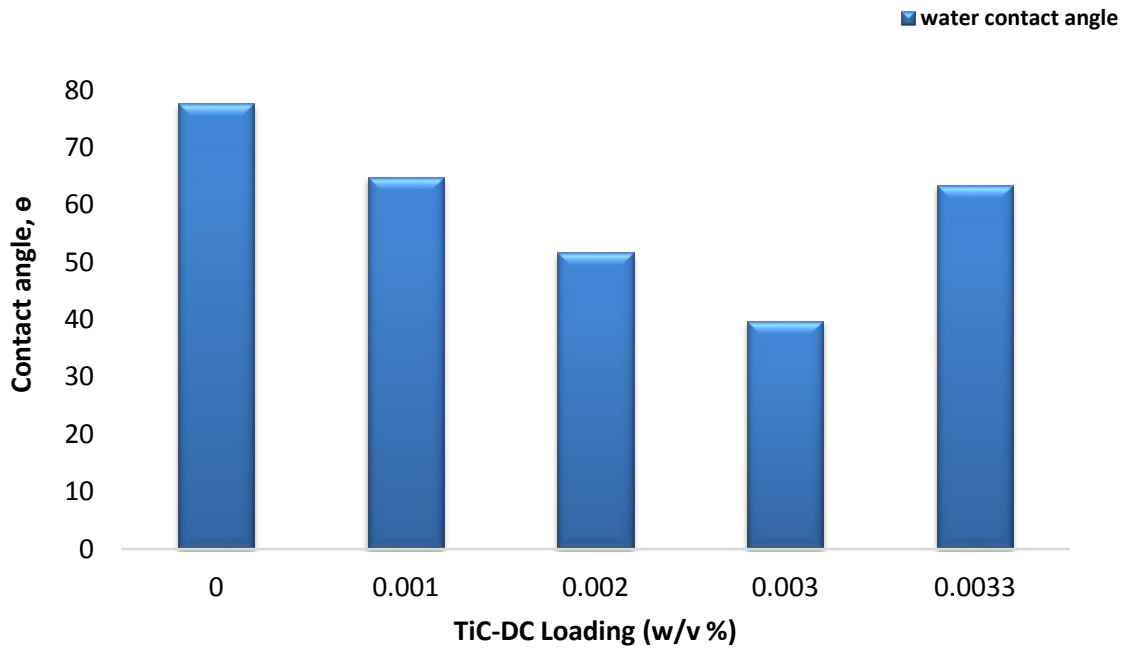

Figure 4.12 Static water contact angle of TiC-DC-TFN membranes vs different nanofiller loading concentrations.

4.2.5 Pure and Saline Water Flux Measurements

Mixed matrix membranes enhance the properties of polymer matrix with the addition of nanoparticles as fillers, which lead to develop a good improvement in selectivity, permeability, thermal and chemical stability, moreover enhance the fouling resistance of the composites [24]–[27], [80]. Nano size particles changed the membrane performance to a good extent. Polymer structure is modified by addition of carbon fillers to enhance the water flux. Figures 4.13 and 4.14 show the effect of TiC-DC loadings on the pure and saline water permeance. From the Figure 4.13, it can be observed that the M0 had average pure water flux of 14.35 $L/m^2.h$ and by adding microporous carbon nanofillers the pure water flux increased from 14.35 to 21.61 $L/m^2.h$ upto M3 and next decreased due to higher concentration of TiC-DC loading. This phenomena can be interpreted that the hydrophilicity and porosity of lab made membrane enhanced by addition of TiC-DC nanoparticles which would raise the membranes water flux [76]. So, in our case the optimum loading point is M3. Addition of more nanoparticles (M4) tends to reduce the water flux as compared to M3 membrane. This trend is due to unequal distribution and agglomeration of the TiC-DC on the membrane surface which is responsible for pores blocking on the membranes surface [76]. For salt water permeance, it can be observed that, for M0, the saline water flux is 11.84 $L/m^2.h$ but it start increasing from 15.42 to 17.2 $L/m^2.h$ with increasing TiC-DC loading from M1 to M3 respectively. Membrane surface morphology and the hydrophilicity are two main factors which can play a big role for permeation flux. Membrane surface hydrophilicity is proportional to the flux permeation. Water contact angle has direct relation with membrane hydrophilicity. Lower water contact proves that the membrane surface is also hydrophilic in nature [49], [81]. It

can be seen (Figure 4.12, Table 4.2) that contact angle decreases with increasing the TiC-DC loading upto M3, which shows surface hydrophilicity with loading concentration.

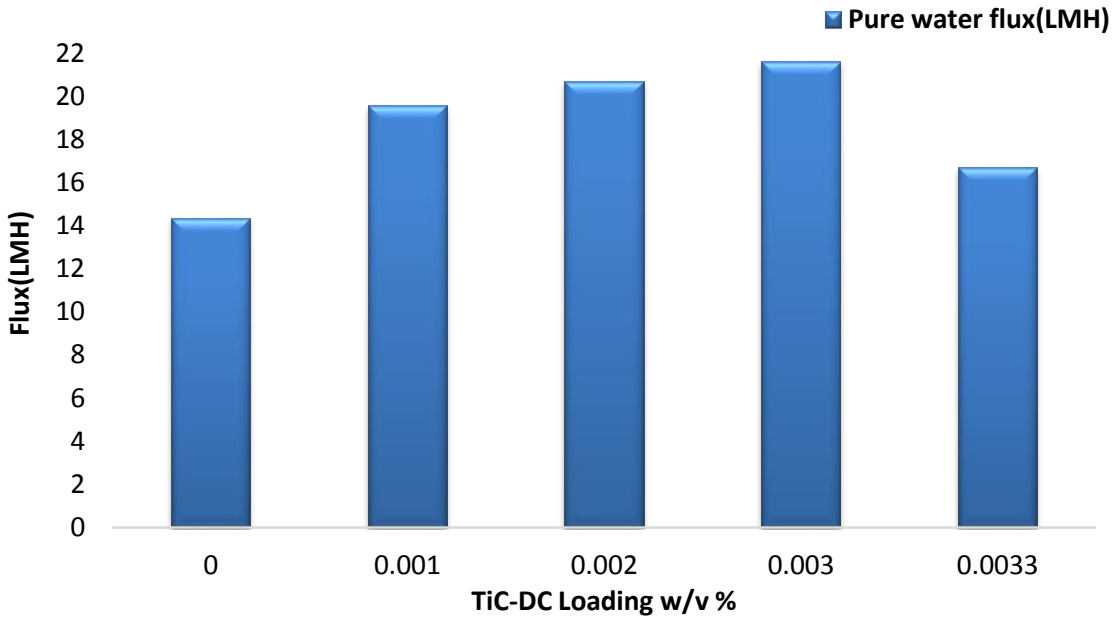

Figure 4.13 Pure water flux of pristine PA with different TiC-DC concentrations.

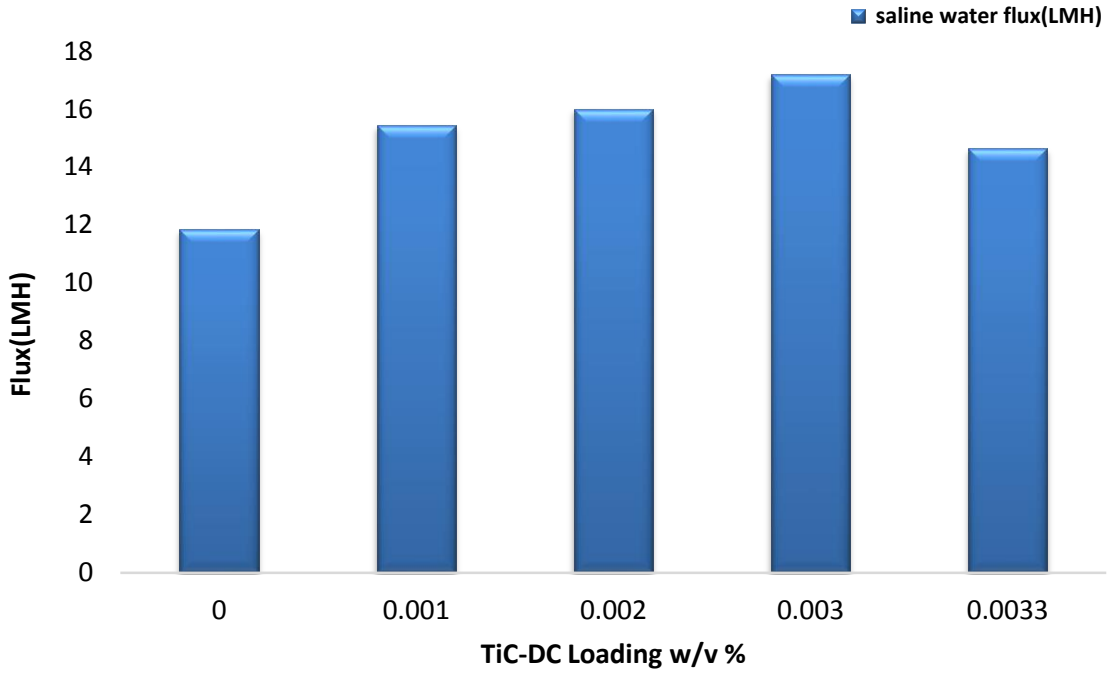

Figure 4.14 Saline water flux of pristine PA with different TiC-DC concentrations.

The apparent and true salt rejection performance of mixed matrix membrane is shown in Figure 4.15 by using a concentration of 2000 ppm of monovalent ion pair (NaCl). Reverse osmosis membranes works on the principle of solution diffusion transport mechanism. There is strong link between water flux j_w and applied pressure on membrane surface and concentration gradient across the membrane [12], [82], [83]. This mechanism is described by equation

$$j_w = A(\Delta p - \Delta\pi) \tag{4. 2}$$

Where $\boldsymbol{A}$ is water permeance (LMH/bar), $\boldsymbol{\Delta p}$ is pressure difference across the membrane (bar). $\boldsymbol{\Delta\pi}$ is osmotic pressure differential across the membrane (bar).

Mathematically we can describe the salt flux (Js) across the RO membrane by the following mathematical equation

$$j_s = B\left(c_{j0} - c_{jl}\right) \tag{4. 3}$$

Where $\boldsymbol{j_s}$ is salt flux, $\boldsymbol{B}$ is the permeability constant for salt, $\boldsymbol{c_{j0}}$ and $\boldsymbol{c_{jl}}$ are salt concentration (mg/L) on feed and permeate sides of the membranes respectively.

Usually in reverse osmosis membranes salt concentration in the permeation solution is very low as compared to salt concentration in feed solution, so we can neglect $\boldsymbol{c_{jl}}$ from equation (4.3) which gives a simple equation (4.4)

$$j_s = B\left(c_{j0}\right) \tag{4. 4}$$

From both equation (4.3) and (4.4), we can see the dependence and independence of water and salt flux on pressure respectively. Membranes selectivity can be measured by its salt rejection coefficient R, defines as [12]

$$R_{app} = \left(1 - \frac{c_{jl}}{c_{j0}}\right) \times 100 \quad (4.5)$$

Where $\boldsymbol{R}$ is rejection coefficient [12].

Concentration polarization has great influence on the direct calculated salt rejection values and actual/true salt rejection. Computed values of rejection are lower than true salt rejection of the membrane because of concentration polarization which enhances the concentration of salt on the membrane surface more than bulk solution concentration [12], [84]–[86]. To calculate the true salt rejection of RO membranes, a model correlating the salt concentration at the surface of membrane and simply computed bulk concentration is used in this work.

To calculate pure water flux for pure water feed (i.e ... $\Delta\pi = 0$), equation 4.2 can be simplified as

$$j_{w(pw)} = A(\Delta P) \quad (4.6)$$

Saline water flux can be measured as

$$j_{w(NaCl)} = A\left[\Delta p - \left(\Delta\pi_{so(m)} - \pi_{sl}\right)\right] \quad (4.7)$$

Where $\Delta\boldsymbol{\pi_{so(m)}}$ is osmotic pressure $\pi = 2cRT$ [84] at the membrane surface and $\boldsymbol{\pi_{sl}}$ is osmotic pressure in the permeate. If A is constant, then equations 4.8 and 4.9 canbe solved to give [87] equation 4.10.

$$\Delta\pi_{so(m)} = \pi_{sl} + \Delta p \times \left(1 - \frac{J_{w(NaCl)}}{j_{w(pw)}}\right) \quad (4.8)$$

This equation is used to calculate the salt concentration at membrane surface. so, true rejection can be computed as [87]

$$R_{true} = \left(1 - \frac{\pi_{sl}}{\Delta\pi_{so(m)}}\right) \times 100\% \qquad (4.9)$$

The apparent and true salt rejection performance of virgin PA and TFN TiC-DC with different loading of nanofillers is shown in Figure 4.15 and Table 4.2. The apparent NaCl rejection for M0 is 91.5 % after 2 hours of salt filtration with pH of 7.0 in cross flow mode. The rejection was enhanced from 92.5 to 96% with increasing the loading of nanoparticles from M1 to M3. Significant improvement in pure water flux without loss in rejection has been associated to preferential flow channels provided by TiC-DC pores for water (2.7 Å) [35]. These pores are large enough to allow passage of water molecules but are too small for solute transport (8–9 Å) [37]. The decrease in salt rejection for M4 is due to high concentration of the nanoparticles which are responsible for agglomeration on the membrane surface. Moreover, these agglomerated particles create blockage on some part of membrane surface and somewhere create voidage which lead to reduce the water flux and rejection also [12], [48], [49], [88].

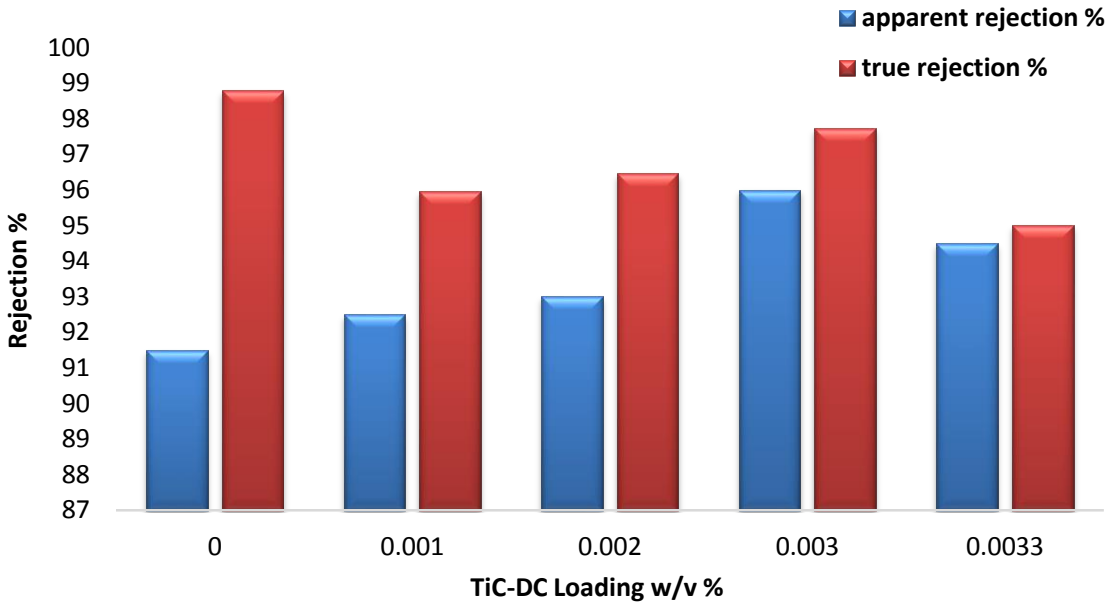

Figure 4.15 Apparent and true salt rejection of bare PA and TFN with different TiC-DC loading.

Table 4. 3 Over view of all membranes characterizations and performance

Membrane	J_{pw}, L/m^2hr	J_{saline}, L/m^2hr	$J_{foulant}$, L/m^2hr	R_{app} (%)	R_{true} (%)	Contact angle, θ	$S_{roughness}$ $R_q(\mu m)$
M0	14.35	11.84	10.86	91.5	98.79	77.7	0.55 ± 0.2
M1	19.57	15.43	11.77	92.5	95.95	64.9	0.22 ± 0.01
M2	20.71	16.00	12.69	93	96.47	51.7	0.16 ± 0.01
M3	21.61	17.20	14.96	96	97.72	39.8	0.15 ± 0.01
M4	16.71	14.63	11.70	94	95.02	63.5	0.25 ± 0.05

4.3 Antifouling Properties of TiC-DC-TFN Membrane

4.3.1 Mixed Matrix Membrane Action against BSA

Effect of concentration of TiC-DC concentration on the flux achievement was aslo inspected using 100 mg/L BSA solution. After 0–120 min running of membrane in cross flow mode, initial and final water flux values were taken. From Figure 4.16 it can be observed that permeate flux decreased in first 110 min then became constant. The decrease in flux for protein ultrafiltration is associated to membrane fouling. Some protein molecules tend to attached and adsorbed on the surface of the membrane and pore walls and tend to reduce the flux [76]. After 110 min M3 showed the higher permeation flux than all others membranes which is the best membrane for all results.

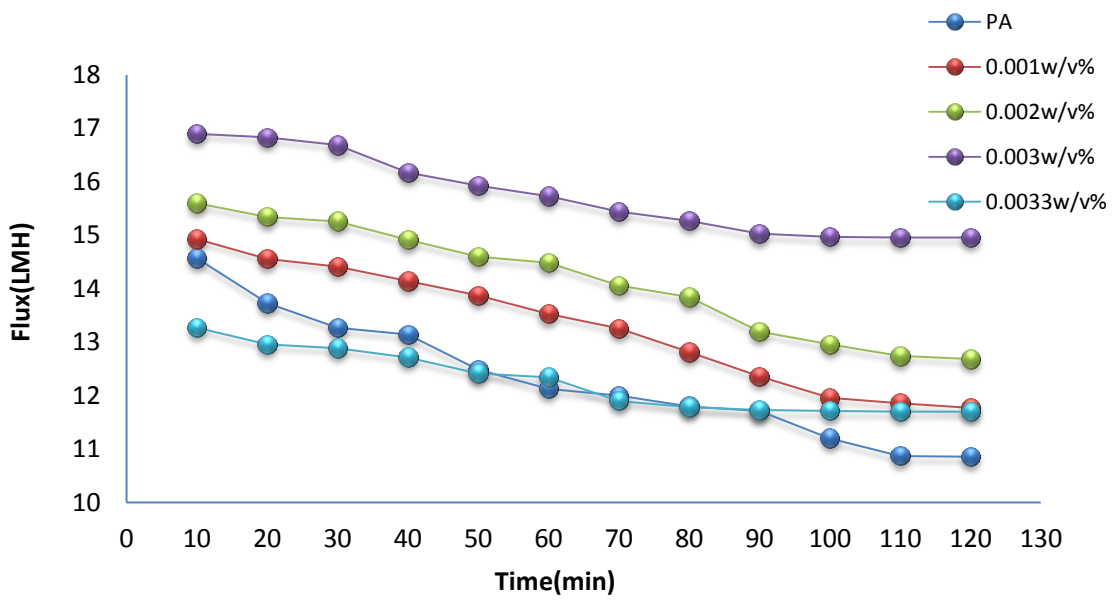

Figure 4.16 Time dependent flux of bare PA and TiC-DC-TFN membranes using 100 mg/L BSA solution.

Figure 4.17 exhibits pure water and BSA solution permeance performance with different nanofillers loading. If we just look at the flux of membranes with nanoparticles loading vs M0 while using BSA solution, it can be seen that all membranes with different loading performed better than M0, apparently due to improved hydrophilicity of the mixed matrix membranes. It is very eminent that higher hydrophilicity decreases the fouling of organic foulants, which results in increasing the anti-fouling resistance and flux achievement [89]. The smoothening of the membrane surface roughness as seen from the AFM data (Figure 4.11) and contact angle data (Figure 4.12) may also participates to upgrade the flux of mixed matrix membranes because it is well known that more surface roughness, produces large membranes fouling [89]–[91].

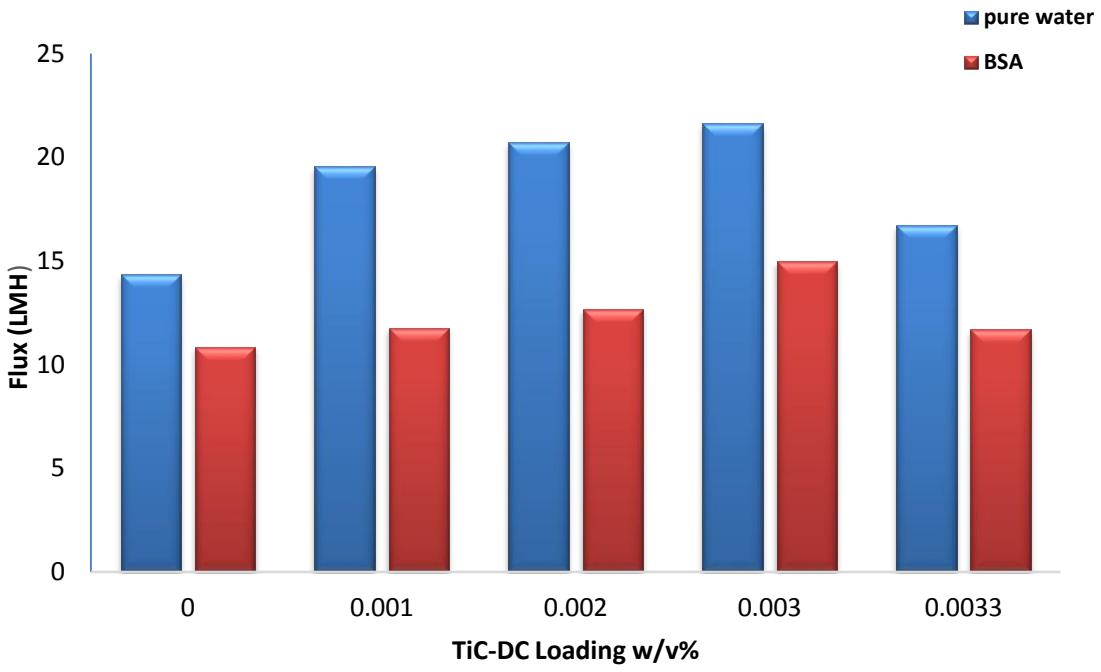

Figure 4.17 Pure water and BSA Fluxes comparison with different TiC-DC loadings.

4.3.2 Membranes Fouling Mechanism by Pore Blocking Model

A decreasing trend in permeate flow is due to pore blocking mechanism which can be describe mathematically by following equation

$$d^2t/dV^2 = k\left(\frac{dt}{dv_p}\right)^n \qquad (4.\ 10)$$

Where t is filtration time, V_p is permeate volume, k and n are experimental constants and n is a dimensionless number that is related to fouling mechanism [92][93][94].

For internal pore blocking $n = 1.5$ and flux equation can be written as

$$j_{n=1.5} = \frac{4j_0}{\left[2+t\times k_s\sqrt[2]{A_m j_0}\right]^2} \qquad (4.\ 11)$$

Where A_m is membrane area, j_0 is the initial flux and k_s is the fouling constant by internal pore blocking.

Experimental data and pore blocking model data trend is shown in (Figure 4.18) which shows that M0, M1 and M4 almost overlapping the modeling trend line which confirms the internal pore blocking for these membranes and lower flux permeation is also a strong evidence for these membranes as compare to M2 and M3 (Table 4.3). On the other hand M2 and M3 exhibiting a little bit deviation from modeling line which shows less internal pore blocking for these membranes and also higher flux (Figure 4.17). Linear equations and correlation coefficient (R2) of all membranes representing internal pore blocking model mechanism is shown in Table 4.4.

Table 4. 4 Internal pore blocking model mechanism for different TiC-DC loading

Membrane	Linear Equation	Correlation coefficient ($\mathbf{R^2}$)
M_0	$j^{-1/2} = 0.0004 \times t + 0.2623$	0.9741
M_1	$j^{-1/2} = 0.0003 \times t + 0.254$	0.9814
M_2	$j^{-1/2} = 0.0003 \times t + 0.2486$	0.9771
M_3	$j^{-1/2} = 0.0002 \times t + 0.2743$	0.9697
M_4	$j^{-1/2} = 0.0002 \times t + 0.2743$	0.9214

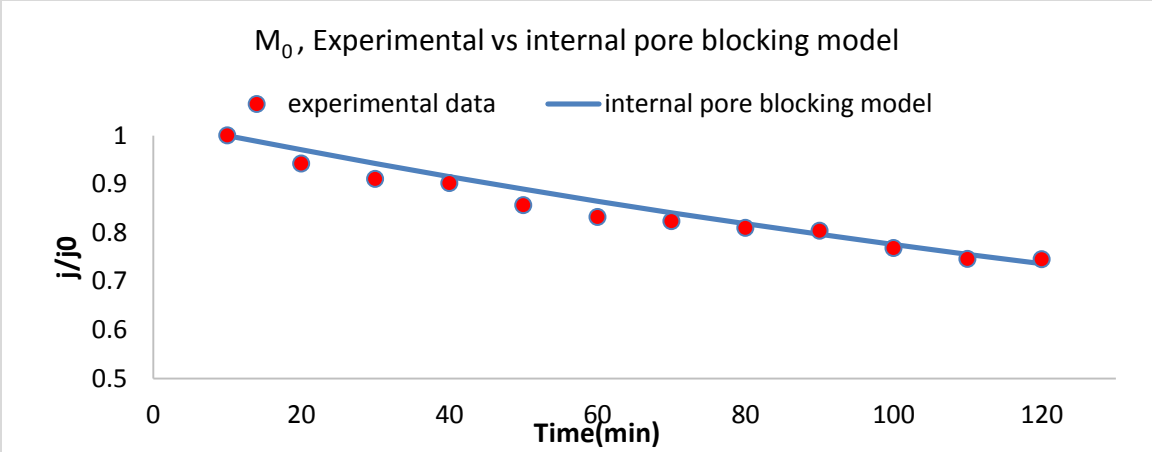
M0 , Experimental vs internal pore blocking model
experimental data
internal pore blocking model
j/j0
1
0.9
0.8
0.7
0.6
0.5
0
20
40
60
80
100
120
Time(min)

(a)

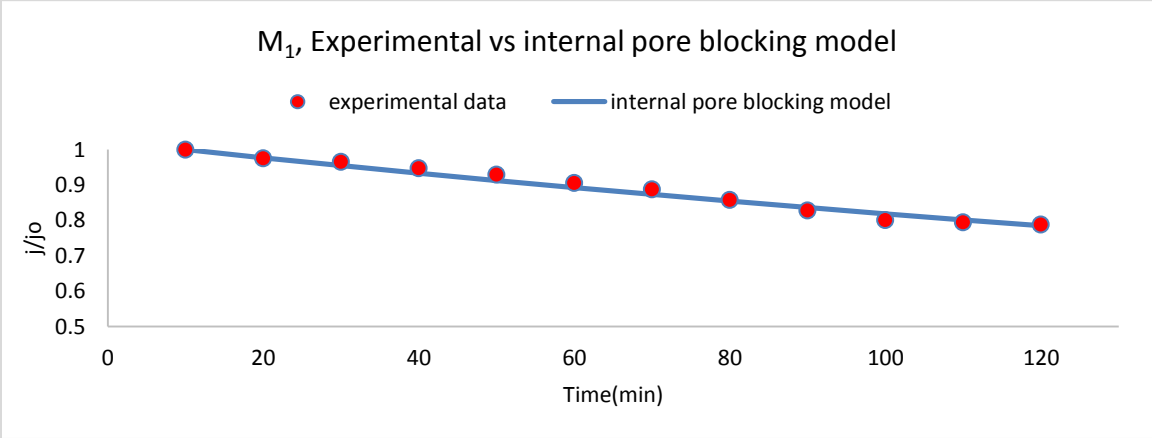
M1, Experimental vs internal pore blocking model
experimental data
internal pore blocking model
j/jo
1
0.9
0.8
0.7
0.6
0.5
0
20
40
60
80
100
120
Time(min)

(b)

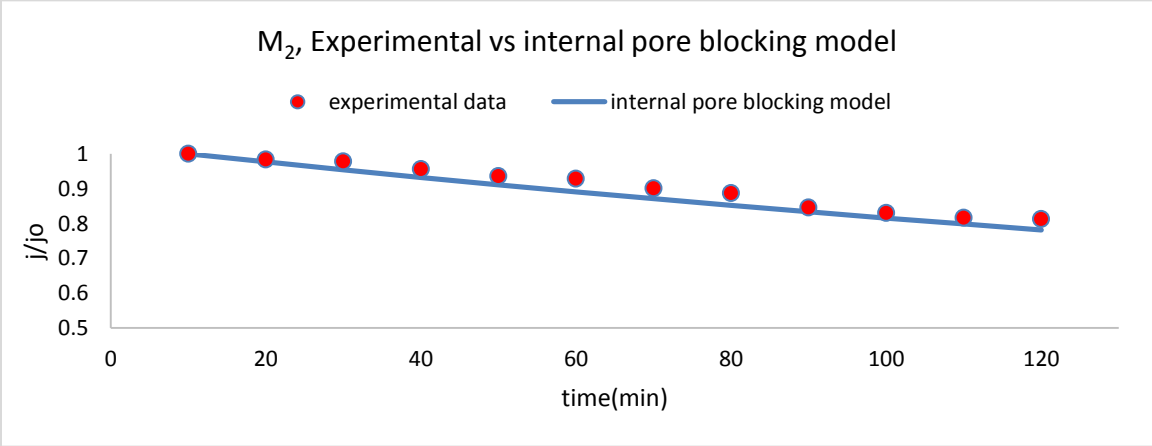
M2, Experimental vs internal pore blocking model
experimental data
internal pore blocking model
j/jo
1
0.9
0.8
0.7
0.6
0.5
0
20
40
60
80
100
120
time(min)

(c)

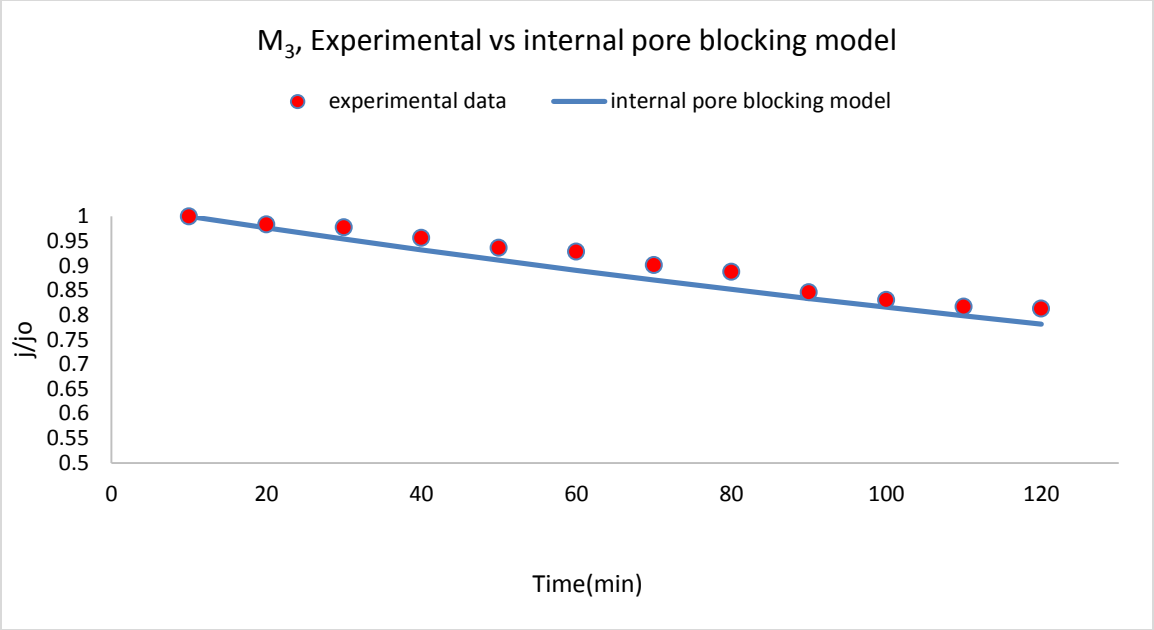

(d)

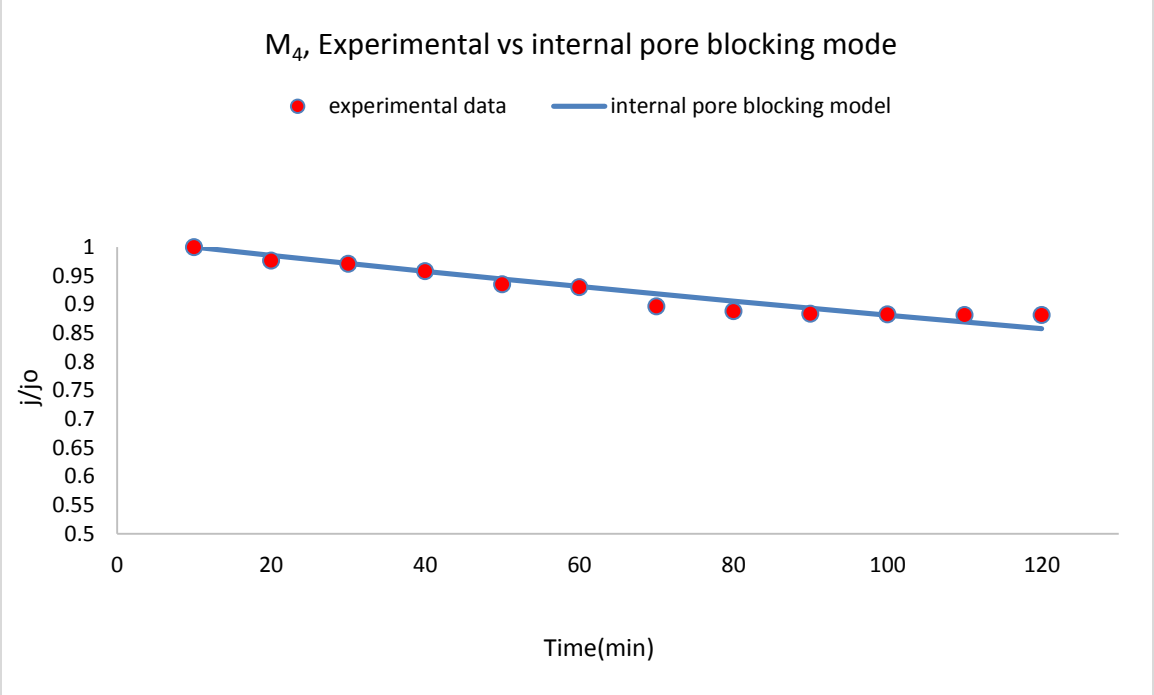

(e)

Figure 4.18 Experimental vs internal pore blocking model trend for M0 and mixed matrix membranes.

4.3.3 Reaction of Lab Made TiC-DC-TFN Membranes against BSA Solution

Figure 4.19 and 4.20 shows the antifouling properties for the lab made PA and TiC-DC-TFN with different loading of nanoparticles using (100 mg/L) BSA solution. Figure 4.19 representing that the fouling experiments were conducted for 2 h and specific flux ratio (j/j0) was calculated to check the flux loss in term of percentage (Figure 4.20). It can be seen that for M0 the flux loss is 25.5% and this trend is decreasing with the increasing loading of nanoparticles in the membranes. The minimum flux loss is reported by M3 which is 11.5%. This effect can be related to filling mechanism of nanoparticles inside the defects/large pores on the membranes surface and reduce the space inside the membranes pores and decrease the tendency of natural organic matters/protein particles to settle down inside the pores [95]. Lower water contact angle with increasing concentration of nanoparticles (Figure 4.12) is an evidence for the membranes surface smoothness which shows that membranes getting more hydrophilic surface with nanoparticles loading [49].

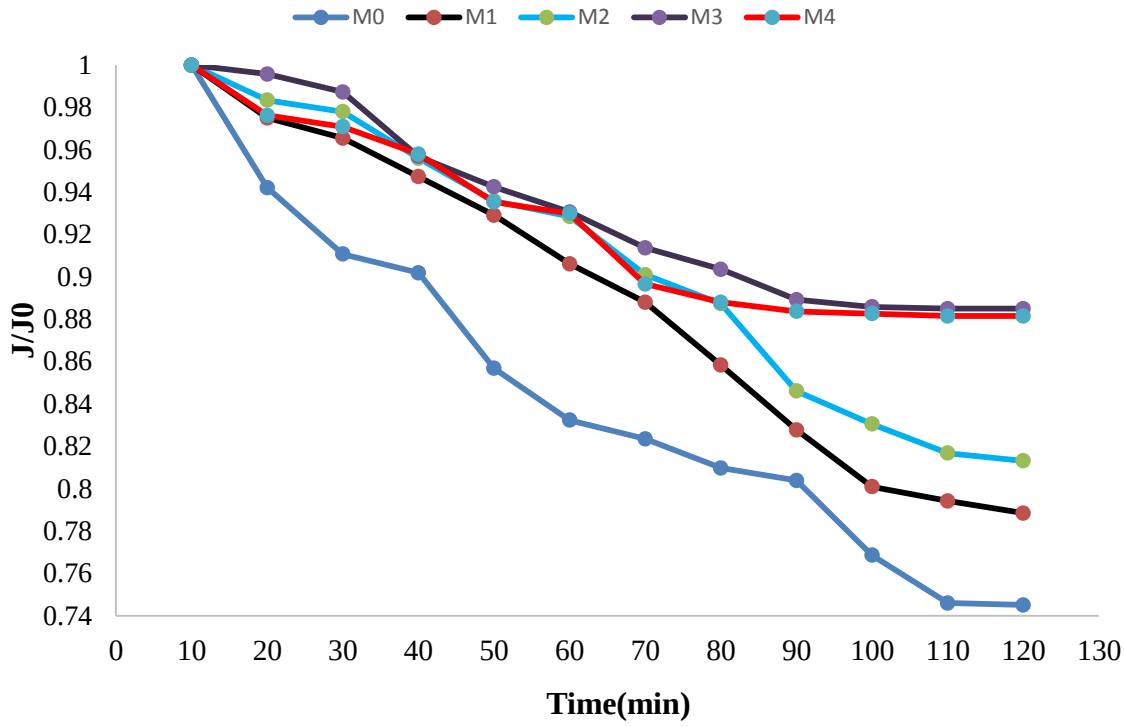

Figure 4.19 Anti-fouling trends of membranes with different loading against BSA solution.

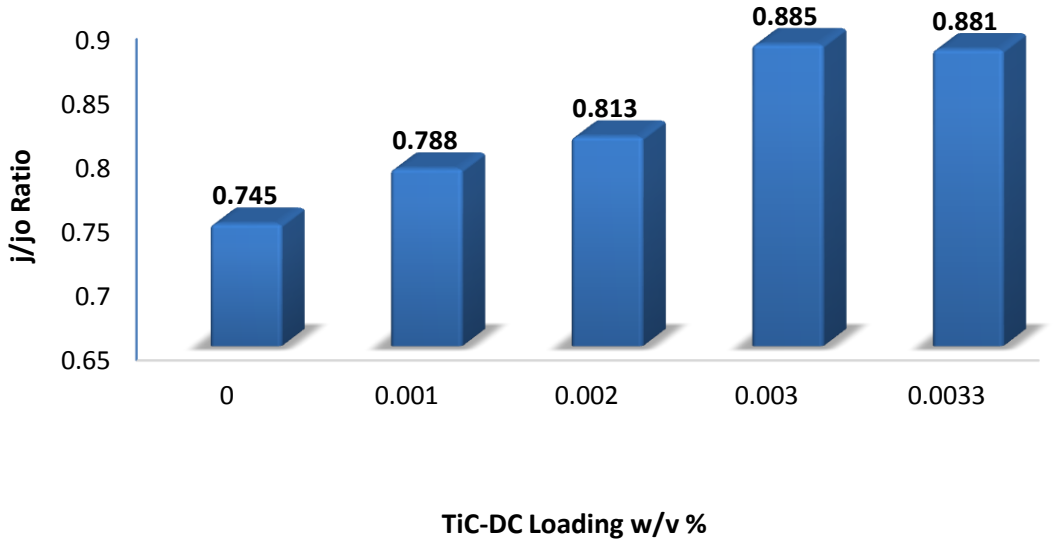

Figure 4.20 j/j0 vs TiC-DC loading, antifouling properties of membrane.

4.3.4 Antifouling Performance of Best Membrane (M3)

Figure 4.21 represents the cleaning phenomena and flux recovery of best membrane (M3). Membrane was fouled with BSA solution (100 mg BSA /L DIW at 7 pH) and flux j_1 was measured after filtration of BSA solution for 2 h. After that, fouled membrane was washed with 6g NaOH /12L of deionized water for 30 min and water flux j_2 was measured. Three cycles were performed and antifouling characteristics of best membrane was calculated for each cycle by using different parameter like flux recovery ratio (FRR), irreversible (Rir), reversible (Rr) and total fouling resistance (Rt) [96].

$$FRR\% = \frac{j_2}{j_0} \times 100 \quad (4.\ 12)$$

$$R_r\% = \frac{(j_2 - j_1)}{j_0} \times 100 \quad (4.\ 13)$$

$$\boldsymbol{R_{ir}\% = \frac{(j_0 - j_2)}{j_0} \times 100} \quad (4.\ 14)$$

$$R_t\% = \frac{(j_0 - j_1)}{j_0} \times 100 \quad (4.\ 15)$$

Where jo is the initial water flux, j1 is the BSA filtration flux, j2 is fouled membrane water flux after its washing with aqueous solution of sodium hydroxide (6g NaOH/12L DIW). Figure 4.22 shows the different resistance percentages for M3. It can be seen that flux recovery ratio was 97.06%, 91.74%, 86.09% for first, second and third washing cycle respectively. Upgraded anti-fouling properties of TiC-DC-TFN membranes can be associated to their improved hydrophilicity and surface roughness. Decreased hydrophobic interaction membrane surface and the BSA molecules is due to revised hydrophilicity and membrane surface smoothness might participate to increase the antifouling characteristics of the lab made TiC-DC-TFN membranes [41].

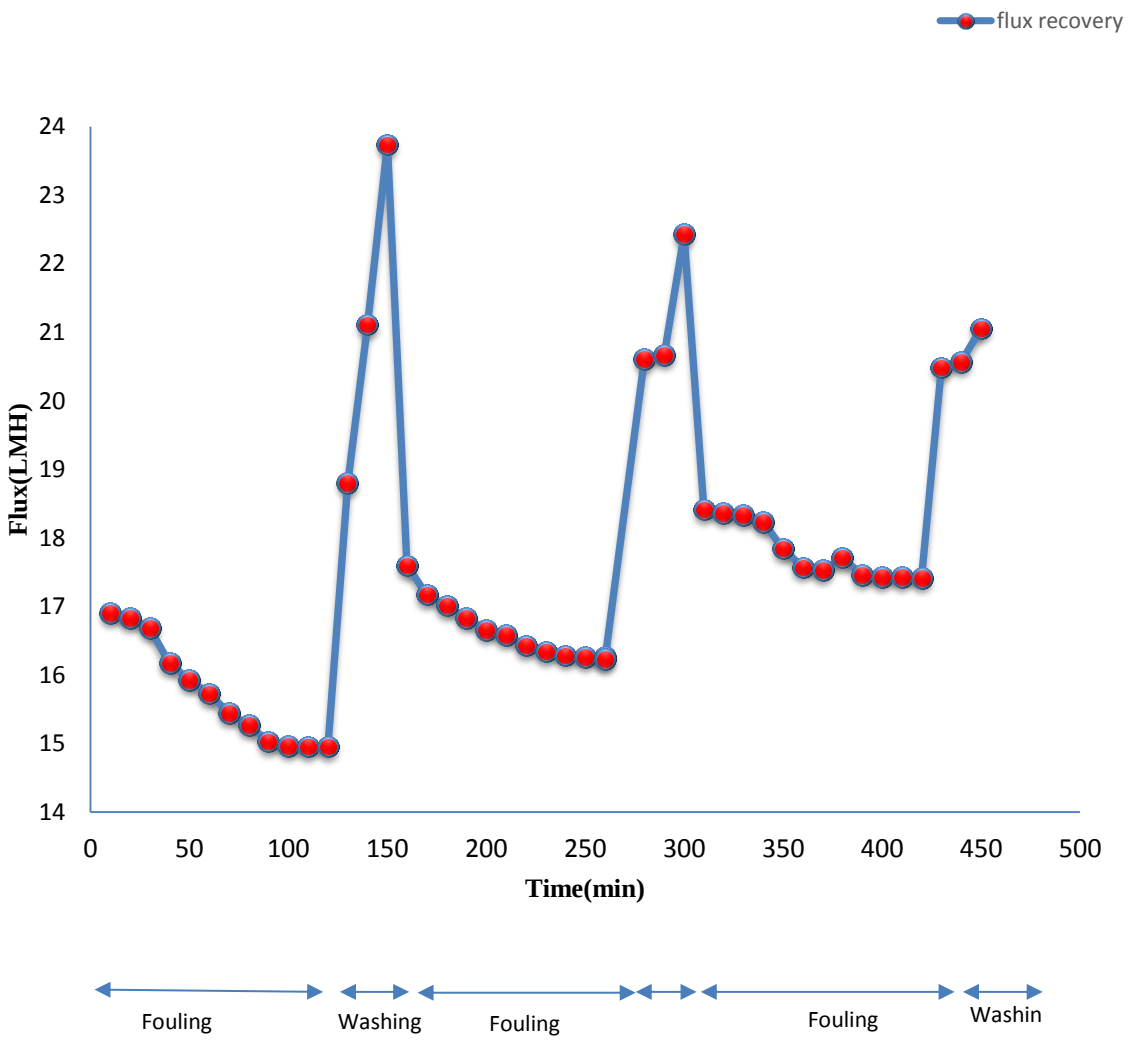

Figure 4.21 Cleaning phenomena and flux recovery of best membrane (M3).

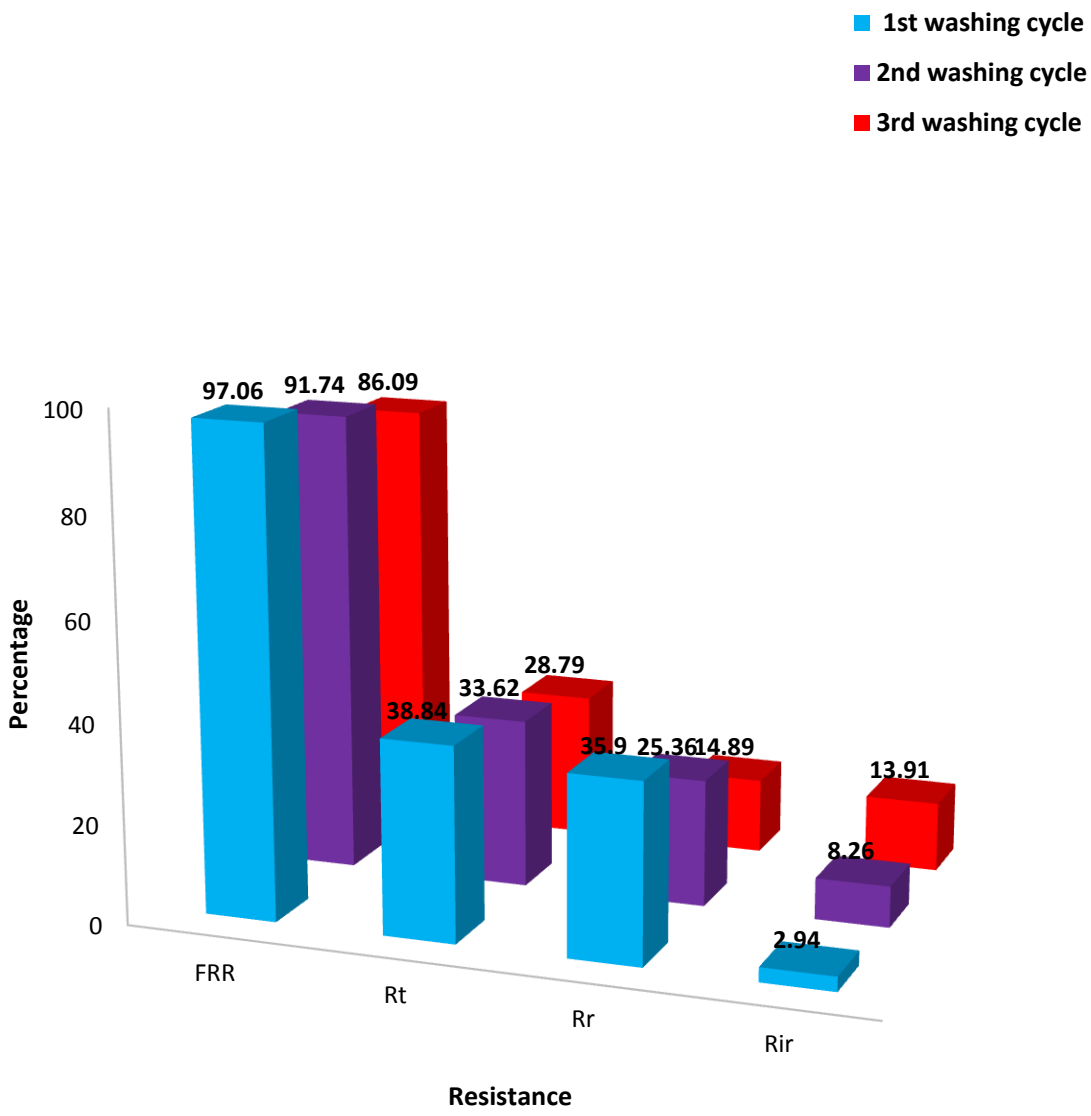

Figure 4.22 Flux recovery and fouling resistances for (M3) membrane.

CHAPTER 5

CONCLUSIONS AND RECOMMENDATIONS

This chapter consist of the following conclusions of the study.

- The hydrophilicity of TiC-DC-TFN membrane (M_3) surface was much higher (49%) than that of the virgin polyamide (PA) membrane (M_0).
- Desalination experiments showed that the permeate flux increased 51%, 45% and 38% as compared to the PA membrane under pure water conditions, brackish water conditions and fouling conditions respectively.
- PA membrane lost 26% of its initial flux while TiC-DC-TFN membrane (M_3) lost only 11% after 2 hours of operation.
- Membrane cleaning with dilute NaOH solution was able to recover 97% of the original water flux.
- This study showed that the CDC nanoparticles can significantly enhance the performance of the polyamide membrane.

The proposed future recommendations are the followings.

- To prepare an inorganic CDC membrane.
- To test the long term stability of the membrane and check the nano particle leaching.
- To covalently bond the nano particles to the polyamide layer.

References

[1] P. Gleick, *Water in crisis: a guide to the world's fresh water resources.* 1993.

[2] A. M. Boulay, C. Bouchard, C. Bulle, L. Deschênes, and M. Margni, "Categorizing water for LCA inventory," *Int. J. Life Cycle Assess.*, vol. 16, no. 7, pp. 639–651, 2011.

[3] V. Lazarova, Y. Emsellem, J. Paille, K. Glucina, and P. Gislette, "Water quality management of aquifer recharge using advanced tools.," *Water Sci. Technol.*, vol. 64, no. 5, pp. 1161–8, 2011.

[4] I. Bremere, M. Kennedy, A. Stikker, and J. Schippers, "How water scarcity will effect the growth in the desalination market in the coming 25 years," *Desalination*, vol. 138, no. 1–3, pp. 7–15, 2001.

[5] M. Hajeeh and A. Al-Othman, "Application of the analytical hierarchy process in the selection of desalination plants," *Desalination*, vol. 174, no. 1, pp. 97–108, 2005.

[6] D. Colombo, M. De Gerloni, and M. Reali, "An energy-efficient submarine desalination plant," *Desalination*, vol. 122, no. 2–3, pp. 171–176, 1999.

[7] M. Elimelech and W. A. Phillip, "The Future of Seawater Desalination: Energy, Technology, and the Environment," *Science (80-.).*, vol. 333, no. 6043, pp. 712–717, 2011.

[8] S. Jenkins, "Membranes on Polyolefins Plants Vent Recovery," *Chem. Eng.*, 2013.

[9] N. Schmeling, R. Konietzny, D. Sieffert, P. Rölling, and C. Staudt, "Functionalized copolyimide membranes for the separation of gaseous and liquid mixtures," *Beilstein J. Org. Chem.*, vol. 6, pp. 789–800, 2010.

[10] A. Tiraferri, "Membrane-based water treatment to increase water supply," pp. 1–13, 2014.

[11] G. R. Xu, J. N. Wang, and C. J. Li, “Strategies for improving the performance of the polyamide thin film composite (PA-TFC) reverse osmosis (RO) membranes: Surface modifications and nanoparticles incorporations,” *Desalination*, vol. 328, pp. 83–100, 2013.

[12] R. W. Baker, *Membrane Technology and Applications*. 2004.

[13] J. Ferry, “Ultrafilter Membranes and Ultrafiltration.,” *Chem. Rev.*, 1936.

[14] E. Bash, *No Title No Title*, vol. 1. 2015.

[15] J. Henis and M. Tripodi, “A novel approach to gas separations using composite hollow fiber membranes,” *Sep. Sci. Technol.*, 1980.

[16] K. P. Lee, T. C. Arnot, and D. Mattia, “A review of reverse osmosis membrane materials for desalination-Development to date and future potential,” *J. Memb. Sci.*, vol. 370, no. 1–2, pp. 1–22, 2011.

[17] H. Bechhold, “Kolloidstudien mit der Filtrationsmethode,” *Zeitschrift für Elektrochemie und Angew.*, 1907.

[18] C. Reid and E. Breton, “Water and ion flow across cellulosic membranes,” *J. Appl. Polym. Sci.*, 1959.

[19] R. E. Larson, J. E. Cadotte, and R. J. Petersen, “The FT-30 seawater reverse osmosis membrane--element test results,” *Desalination*, vol. 38, no. C, pp. 473–483, 1981.

[20] M. Murakami, *Managing water for peace in the middle east; alternative strategies*. 1995.

[21] P. Gorgojo, M. F. Jimenez-Solomon, and A. G. Livingston, “Polyamide thin film composite membranes on cross-linked polyimide supports: IMPROVEMENT of RO performance via activating solvent,” *Desalination*, vol. 344, pp. 181–188, 2014.

[22] L. Y. Ng, A. W. Mohammad, C. P. Leo, and N. Hilal, “Polymeric membranes

incorporated with metal/metal oxide nanoparticles: A comprehensive review," *Desalination*, vol. 308, pp. 15–33, 2013.

[23] S.-T. Hwang, "Inorganic membranes and membrane reactors," *Korean J. Chem. Eng.*, vol. 18, no. 6, pp. 775–787, 2001.

[24] B. H. Jeong, E. M. V Hoek, Y. Yan, A. Subramani, X. Huang, G. Hurwitz, A. K. Ghosh, and A. Jawor, "Interfacial polymerization of thin film nanocomposites: A new concept for reverse osmosis membranes," *J. Memb. Sci.*, vol. 294, no. 1–2, pp. 1–7, 2007.

[25] G. L. Jadav and P. S. Singh, "Synthesis of novel silica-polyamide nanocomposite membrane with enhanced properties," vol. 328, pp. 257–267, 2009.

[26] J. Yin, E. S. Kim, J. Yang, and B. Deng, "Fabrication of a novel thin-film nanocomposite (TFN) membrane containing MCM-41 silica nanoparticles (NPs) for water purification," *J. Memb. Sci.*, vol. 423–424, pp. 238–246, 2012.

[27] A. Peyki, A. Rahimpour, and M. Jahanshahi, "Preparation and characterization of thin film composite reverse osmosis membranes incorporated with hydrophilic SiO2 nanoparticles," *Desalination*, vol. 368, pp. 152–158, 2014.

[28] A. Khalid, A. A. Al-Juhani, O. C. Al-Hamouz, T. Laoui, Z. Khan, and M. A. Atieh, "Preparation and properties of nanocomposite polysulfone/multi-walled carbon nanotubes membranes for desalination," *Desalination*, vol. 367, pp. 134–144, 2015.

[29] M. G. Buonomenna, "Nano-enhanced reverse osmosis membranes," *Desalination*, vol. 314, pp. 73–88, 2013.

[30] M. Fathizadeh, A. Aroujalian, and A. Raisi, "Effect of added NaX nano-zeolite into polyamide as a top thin layer of membrane on water flux and salt rejection in a reverse osmosis process," *J. Memb. Sci.*, vol. 375, no. 1–2, pp. 88–95, 2011.

[31] B. Hofs, R. Schurer, D. J. H. Harmsen, C. Ceccarelli, E. F. Beerendonk, and E. R. Cornelissen, "Characterization and performance of a commercial thin film

nanocomposite seawater reverse osmosis membrane and comparison with a thin film composite," *J. Memb. Sci.*, vol. 446, pp. 68–78, 2013.

[32] H. Huang, X. Qu, X. Ji, X. Gao, L. Zhang, H. Chen, and L. Hou, "Acid and multivalent ion resistance of thin film nanocomposite RO membranes loaded with silicalite-1 nanozeolites," *J. Mater. Chem. A*, vol. 1, pp. 11343–11349, 2013.

[33] M. L. Lind, A. K. Ghosh, A. Jawor, X. Huang, W. Hou, Y. Yang, and E. M. V. Hoek, "Influence of Zeolite Crystal Size on Zeolite-Polyamide Thin Film Nanocomposite Membranes," *Langmuir*, vol. 25, no. 17, pp. 10139–10145, Sep. 2009.

[34] M. Lind, D. E. Suk, and T. Nguyen, "Tailoring the structure of thin film nanocomposite membranes to achieve seawater RO membrane performance," *Sci. Technol.*, 2010.

[35] N. Ma, J. Wei, R. Liao, and C. Y. Tang, "Zeolite-polyamide thin film nanocomposite membranes: Towards enhanced performance for forward osmosis," *J. Memb. Sci.*, vol. 405–406, pp. 149–157, 2012.

[36] J. Yin, Y. Yang, Z. Hu, and B. Deng, "Attachment of silver nanoparticles (AgNPs) onto thin-film composite (TFC) membranes through covalent bonding to reduce membrane biofouling," *J. Memb. Sci.*, 2013.

[37] E. Kim and B. Deng, "Fabrication of polyamide thin-film nano-composite (PA-TFN) membrane with hydrophilized ordered mesoporous carbon (H-OMC) for water purifications," *J. Memb. Sci.*, vol. 375, no. 1–2, pp. 46–54, 2011.

[38] M. Bao, G. Zhu, L. Wang, M. Wang, and C. Gao, "Preparation of monodispersed spherical mesoporous nanosilica-polyamide thin film composite reverse osmosis membranes via interfacial polymerization," *Desalination*, vol. 309, pp. 261–266, 2013.

[39] H. Wu, B. Tang, and P. Wu, "Optimizing polyamide thin film composite

membrane covalently bonded with modified mesoporous silica nanoparticles," *J. Memb. Sci.*, vol. 428, pp. 341–348, 2013.

[40] M. S. Rahaman, H. Thérien-Aubin, M. Ben-Sasson, C. K. Ober, M. Nielsen, and M. Elimelech, "Control of biofouling on reverse osmosis polyamide membranes modified with biocidal nanoparticles and antifouling polymer brushes," *J. Mater. Chem. B*, vol. 2, no. 12, pp. 1724–1732, 2014.

[41] V. Vatanpour, S. S. Madaeni, R. Moradian, S. Zinadini, and B. Astinchap, "Fabrication and characterization of novel antifouling nanofiltration membrane prepared from oxidized multiwalled carbon nanotube/polyethersulfone nanocomposite," *J. Memb. Sci.*, vol. 375, no. 1–2, pp. 284–294, 2011.

[42] D. Emadzadeh, W. J. Lau, M. Rahbari-Sisakht, A. Daneshfar, M. Ghanbari, A. Mayahi, T. Matsuura, and A. F. Ismail, "A novel thin film nanocomposite reverse osmosis membrane with superior anti-organic fouling affinity for water desalination," *Desalination*, vol. 368, pp. 106–113, 2015.

[43] S. M. Hosseini, S. Rafiei, A. R. Hamidi, A. R. Moghadassi, and S. S. Madaeni, "Preparation and electrochemical characterization of mixed matrix heterogeneous cation exchange membranes filled with zeolite nanoparticles: Ionic transport property in desalination," *Desalination*, vol. 351, pp. 138–144, 2014.

[44] L. Wang, X. Song, T. Wang, S. Wang, Z. Wang, and C. Gao, "Fabrication and characterization of polyethersulfone/carbon nanotubes (PES/CNTs) based mixed matrix membranes (MMMs) for nanofiltration application," *Appl. Surf. Sci.*, vol. 330, pp. 118–125, 2015.

[45] H. Zhao, S. Qiu, L. Wu, L. Zhang, H. Chen, and C. Gao, "Improving the performance of polyamide reverse osmosis membrane by incorporation of modi fi ed multi-walled carbon nanotubes," *J. Memb. Sci.*, vol. 450, pp. 249–256, 2014.

[46] H. A. Shawky, S. R. Chae, S. Lin, and M. R. Wiesner, "Synthesis and

characterization of a carbon nanotube/polymer nanocomposite membrane for water treatment," *Desalination*, vol. 272, no. 1–3, pp. 46–50, 2011.

[47] L. Zhang, G. Shi, S. Qiu, and L. Cheng, "Preparation of high-flux thin film nanocomposite reverse osmosis membranes by incorporating functionalized multi-walled carbon nanotubes," *Desalin. Water*, 2011.

[48] E. Celik, H. Park, H. Choi, and H. Choi, "Carbon nanotube blended polyethersulfone membranes for fouling control in water treatment," *Water Res.*, vol. 45, no. 1, pp. 274–282, 2011.

[49] V. Vatanpour, M. Esmaeili, and M. H. D. A. Farahani, "Fouling reduction and retention increment of polyethersulfone nanofiltration membranes embedded by amine-functionalized multi-walled carbon nanotubes," *J. Memb. Sci.*, vol. 466, pp. 70–81, 2014.

[50] F. Liu, B. R. Ma, D. Zhou, Y. H. Xiang, and L. X. Xue, "Breaking through tradeoff of Polysulfone ultrafiltration membranes by zeolite 4A," *Microporous Mesoporous Mater.*, vol. 186, pp. 113–120, 2014.

[51] J. Tascón, *Novel carbon adsorbents*. 2012.

[52] J. Torop, V. Palmre, M. Arulepp, T. Sugino, K. Asaka, and A. Aabloo, "Flexible supercapacitor-like actuator with carbide-derived carbon electrodes," *Carbon N. Y.*, vol. 49, no. 9, pp. 3113–3119, 2011.

[53] "Nanoporous carbide-derived carbon with tunable pore size," *Nat. Mater.*, 2003.

[54] J. Chmiola, G. Yushin, R. Dash, and Y. Gogotsi, "Effect of pore size and surface area of carbide derived carbons on specific capacitance," *J. Power Sources*, vol. 158, no. 1, pp. 765–772, 2006.

[55] S. H. Yeon, I. Knoke, Y. Gogotsi, and J. E. Fischer, "Enhanced volumetric hydrogen and methane storage capacity of monolithic carbide-derived carbon,"

Microporous Mesoporous Mater., vol. 131, no. 1–3, pp. 423–428, 2010.

[56] R. K. Dash, A. Nikitin, and Y. Gogotsi, "Microporous carbon derived from boron carbide," *Microporous Mesoporous Mater.*, vol. 72, no. 1–3, pp. 203–208, 2004.

[57] G. Yushin, R. Dash, J. Jagiello, J. E. Fischer, and Y. Gogotsi, "Carbide-derived carbons: Effect of pore size on hydrogen uptake and heat of adsorption," *Adv. Funct. Mater.*, vol. 16, no. 17, pp. 2288–2293, 2006.

[58] S. Welz, M. J. McNallan, and Y. Gogotsi, "Carbon structures in silicon carbide derived carbon," *J. Mater. Process. Technol.*, vol. 179, no. 1–3, pp. 11–22, 2006.

[59] R. Dash, J. Chmiola, G. Yushin, Y. Gogotsi, G. Laudisio, J. Singer, J. Fischer, and S. Kucheyev, "Titanium carbide derived nanoporous carbon for energy-related applications," *Carbon N. Y.*, vol. 44, no. 12, pp. 2489–2497, 2006.

[60] G. N. Yushin, E. N. Hoffman, A. Nikitin, H. Ye, M. W. Barsoum, and Y. Gogotsi, "Synthesis of nanoporous carbide-derived carbon by chlorination of titanium silicon carbide," *Carbon N. Y.*, vol. 43, no. 10, pp. 2075–2082, 2005.

[61] R. K. Dash, G. Yushin, and Y. Gogotsi, "Synthesis, structure and porosity analysis of microporous and mesoporous carbon derived from zirconium carbide," *Microporous Mesoporous Mater.*, vol. 86, no. 1–3, pp. 50–57, 2005.

[62] I. Tallo, T. Thomberg, K. Kontturi, A. J??nes, and E. Lust, "Nanostructured carbide-derived carbon synthesized by chlorination of tungsten carbide," *Carbon N. Y.*, vol. 49, no. 13, pp. 4427–4433, 2011.

[63] E. N. Hoffman, G. Yushin, M. W. Barsoum, and Y. Gogotsi, "Synthesis of Carbide-Derived Carbon by Chlorination of Ti_2AlC," *Chem. Mater.*, vol. 17, no. 9, pp. 2317–2322, May 2005.

[64] Z. G. Cambaz, G. N. Yushin, Y. Gogotsi, K. L. Vyshnyakova, and L. N. Pereselentseva, "Formation of carbide-derived carbon on ??-silicon carbide whiskers," *J. Am. Ceram. Soc.*, vol. 89, no. 2, pp. 509–514, 2006.

[65] A. Jänes, T. Thomberg, H. Kurig, and E. Lust, “Nanoscale fine-tuning of porosity of carbide-derived carbon prepared from molybdenum carbide,” *Carbon N. Y.*, vol. 47, no. 1, pp. 23–29, 2009.

[66] M. C. Mangarella, J. L. Ewbank, M. R. Dutzer, F. M. Alamgir, and K. S. Walton, “Synthesis of embedded iron nanoparticles in Fe3C-derived carbons,” *Carbon N. Y.*, vol. 79, no. 1, pp. 74–84, 2014.

[67] F. Group, *HANDBOOK*. 2006.

[68] Sigita, *Synthesis and Characterisation of Carbide Derived Carbons*. 2008.

[69] K. Sing, “Reporting physisorption data for gas/solid systems with special reference to the determination of surface area and porosity (Recommendations 1984),” *Pure Appl. Chem.*, 1985.

[70] M. . b Sevilla and R. . Mokaya, “Activation of carbide-derived carbons: A route to materials with enhanced gas and energy storage properties,” *J. Mater. Chem.*, vol. 21, no. 13, pp. 4727–4732, 2011.

[71] A. Silvestre-Albero, S. Rico-Franc??s, F. Rodr??guez-Reinoso, A. M. Kern, M. Klumpp, B. J. M. Etzold, and J. Silvestre-Albero, “High selectivity of TiC-CDC for CO2/N2 separation,” *Carbon N. Y.*, vol. 59, pp. 221–228, 2013.

[72] M. Porter, “Handbook of industrial membrane technology,” 1989.

[73] F. A. Pacheco, I. Pinnau, M. Reinhard, and J. O. Leckie, “Characterization of isolated polyamide thin films of RO and NF membranes using novel TEM techniques,” *J. Memb. Sci.*, vol. 358, no. 1–2, pp. 51–59, 2010.

[74] J. Duan, Y. Pan, F. Pacheco, E. Litwiller, Z. Lai, and I. Pinnau, “High-performance polyamide thin-film-nanocomposite reverse osmosis membranes containing hydrophobic zeolitic imidazolate framework-8,” *J. Memb. Sci.*, vol. 476, pp. 303–310, 2015.

[75] A. Rahimpour, M. Jahanshahi, N. Mortazavian, S. S. Madaeni, and Y. Mansourpanah, “Preparation and characterization of asymmetric polyethersulfone and thin-film composite polyamide nanofiltration membranes for water softening,” *Appl. Surf. Sci.*, vol. 256, no. 6, pp. 1657–1663, 2010.

[76] J. Huang, G. Arthanareeswaran, and K. Zhang, “Effect of silver loaded sodium zirconium phosphate (nanoAgZ) nanoparticles incorporation on PES membrane performance,” *Desalination*, vol. 285, pp. 100–107, 2012.

[77] N. A. H. M. Nordin, A. F. Ismail, A. Mustafa, R. S. Murali, and T. Matsuura, “The impact of ZIF-8 particle size and heat treatment on CO 2 /CH 4 separation using asymmetric mixed matrix membrane,” *RSC Adv.*, vol. 4, no. 94, pp. 52530–52541, 2014.

[78] W. J. Koros, “Evolving beyond the thermal age of separation processes: Membranes can lead the way,” *AIChE J.*, vol. 50, no. 10, pp. 2326–2334, 2004.

[79] L. Zou, I. Vidalis, D. Steele, A. Michelmore, S. P. Low, and J. Q. J. C. Verberk, “Surface hydrophilic modification of RO membranes by plasma polymerization for low organic fouling,” *J. Memb. Sci.*, vol. 369, no. 1–2, pp. 420–428, 2011.

[80] S. Kulprathipanja, H. Estates, R. W. Neuzil, D. Grove, N. N. Li, and A. Heights, “United States Patent: Separation of Fluid by Means of Mixed Matrix Membranes,” *US Pat.*, pp. 1–7, 1988.

[81] P. Le-Clech, V. Chen, and T. A. G. Fane, “Fouling in membrane bioreactors used in wastewater treatment,” *J. Memb. Sci.*, vol. 284, no. 1–2, pp. 17–53, 2006.

[82] D. R. Paul, “Reformulation of the solution-diffusion theory of reverse osmosis,” *J. Memb. Sci.*, vol. 241, no. 2, pp. 371–386, 2004.

[83] J. G. Wijmans and R. W. Baker, “The solution-diffusion model: a review,” *J. Memb. Sci.*, vol. 107, no. 1–2, pp. 1–21, 1995.

[84] R. F. Probstein, “Phiscochemical Hydrodynamics,” pp. 190–195, 1994.

[85] U. Merten, H. Lonsdale, and R. Riley, “Boundary-layer effects in reverse osmosis,” *Chem. Fundam.*, 1964.

[86] T. Sherwood, P. Brian, and R. Fisher, “Salt concentration at phase boundaries in desalination by reverse osmosis,” *Ind.*, 1965.

[87] I. Sutzkover, D. Hasson, and R. Semiat, “Simple technique for measuring the concentration polarization level in a reverse osmosis system,” *Desalination*, vol. 131, no. 1–3, pp. 117–127, 2000.

[88] E. Celik, L. Liu, and H. Choi, “Protein fouling behavior of carbon nanotube/polyethersulfone composite membranes during water filtration,” *Water Res.*, vol. 45, no. 16, pp. 5287–5294, 2011.

[89] V. Kochkodan and N. Hilal, “A comprehensive review on surface modified polymer membranes for biofouling mitigation,” *Desalination*, vol. 356, pp. 187–207, 2015.

[90] E. M. Vrijenhoek, S. Hong, and M. Elimelech, “Influence of membrane surface properties on initial rate of colloidal fouling of reverse osmosis and nanofiltration membranes,” *J. Memb. Sci.*, vol. 188, no. 1, pp. 115–128, 2001.

[91] V. Kochkodan, D. J. Johnson, and N. Hilal, “Polymeric membranes: Surface modification for minimizing (bio)colloidal fouling,” *Adv. Colloid Interface Sci.*, vol. 206, pp. 116–140, 2014.

[92] H. Huang, T. Young, and J. Jacangelo, “Unified membrane fouling index for low pressure membrane filtration of natural waters: principles and methodology,” *Environ. Sci.*, 2007.

[93] K. J. Hwang, C. Y. Liao, and K. L. Tung, “Analysis of particle fouling during microfiltration by use of blocking models,” *J. Memb. Sci.*, vol. 287, no. 2, pp. 287–293, 2007.

[94] S. Chellam and W. Xu, “Blocking laws analysis of dead-end constant flux microfiltration of compressible cakes,” *J. Colloid Interface Sci.*, vol. 301, no. 1,

pp. 248–257, 2006.

[95] V. Freger, J. Gilron, and S. Belfer, “TFC polyamide membranes modified by grafting of hydrophilic polymers: An FT-IR/AFM/TEM study,” *J. Memb. Sci.*, vol. 209, no. 1, pp. 283–292, 2002.

[96] Y. Wang, T. Wang, Y. Su, F. Peng, H. Wu, and Z. Jiang, “Remarkable reduction of irreversible fouling and improvement of the permeation properties of poly (ether sulfone) ultrafiltration membranes by blending with pluronic,” *Langmuir*, 2005.

Vitae

Name	:Anwar Ul Haq Khan
Nationality	:Pakistani
Date of Birth	:9/29/1989
Email	:anwarulhaq01@gmail.com
Address	:Chak # 214-RB Jaranwala Road Faisalabad, Pakistan.
Academic Background	:B.Sc. Chemical Engineering, Institute of Chemical Engineering & Technology, University of the Punjab, Lahore Pakistan
Patent	Carbide Derived Carbon (CDC)/ Polyamide mixed matrix membrane (Submitted).
Journal Publication	**Anwar Ul Haq Khan**, Isam Al-jundi, Water desalination using carbide derived carbon (CDC)/ Polyamide mixed matrix RO membrane, Separation and purification technology (Submitted).
Conference Publication	A new fouling-resistant Mixed Matrix Membrane for water Desalination, (16AK) Advanced Membrane Technology VII (Ireland).